Improving Regional Biogenic VOC Emission Estimates Using an Airborne PTRMS Eddy Flux Measurement System

Contract No. #09-339
Prepared for the California Air Resources Board

Principal Investigator
Professor Allen H. Goldstein
Department of Environmental Science, Policy and Management
University of California Berkeley
137 Mulford Hall
University of California
Berkeley, CA 94720-3114
(510) 643-3788
ahg@berkeley.edu

Co-Investigators and Sub-contractors:
Dr. Alex Guenther and Dr. Thomas Karl
National Center for Atmospheric Research
Atmospheric Chemistry Division
1850 Table Mesa Drive
Boulder, Colorado 80305

Roy Woods and Haf Jonsson
CIRPAS
Hangar 507
3200 Imgin Road
Marina, California 93933

Contributing Researchers
Dr. Pawel K. Misztal, Postdoc, UC Berkeley

11 February, 2014

DISCLAIMER

The statements and conclusions in this Report are those of the contractor and not necessarily those of the California Air Resources Board. The mention of commercial products, their source, or their use in connection with material reported herein is not to be construed as actual or implied endorsement of such products.

ACKNOWLEDGEMENTS

We thank our colleagues at the California Air Resources Board for useful collaboration on using the airborne fluxes for improvement of California biogenic inventories. In particular, we acknowledge modeling work and suggestions from Jeremy Avise and Klaus Scott, and encouragement and support from our project manager Ash Lashgari.

We acknowledge the Naval Postgraduate School CIRPAS aircraft team Haf Jonsson, Roy Woods, and Nava Roy for help in instrument integration and flight preparation as well as the mission pilots Marko Jaakkola and Bryce Kujatat from ZIVKO Aeronautics for their dedicated help in flight preparation, planning, and execution.

We acknowledge Abhinav Guha and Robin Weber (UC Berkeley) for their contributions to the successful campaign. We also acknowledge Prof. Maggi Kelly at GIF, UC Berkeley for suggestions regarding geospatial treatment of landcovers.

We would like to thank Andrew Turnipseed and Tiffany Duhl (NCAR) for performing GC analyses of VOC sample cartridges collected on the aircraft and at Tonzi Ranch, and Steve Shertz (NCAR) for engineering support.

Glossary of Symbols and Acronyms

AEC	Airborne Eddy Covariance
AvDEC	Airborne virtual Disjunct Eddy Covariance
ARB	California Air Resources Board
BEF	Basal Emission Factor
BER	Basal Emission Rate
BVOC	Biogenic Volatile Organic Compound
CABERNET	California Airborne BVOC Emission Research in Natural Ecosystem Transects
CLM	Community Land Model
CLM4.0	Community Land Model v. 4.0
CWT	Continuous Wavelet Transformation
EC	Eddy Covariance
EF	Emission Factor
FFT	Fast Fourier Transformation
FRAP	Fire Resource and Assessment Program
GC/MS	gas chromatography/mass spectrometry
IRT Nad	Infra-Red Temperature airborne scanner
IVOC	intermediate-volatility organic compound
MW	molecular weight
NOAA	National Oceanic and Atmospheric Administration
O_3	ozone
OH	hydroxide radical
PAR	Photosynthetically Active Radiation
PFT	Plant Functional Type
PTR-MS	Proton Transfer Reaction Mass Spectrometry
REA	Relaxed Eddy Accumulation
RH	relative humidity
SOA	secondary organic aerosol
SoCAB	South Coast Air Basin

SJVAB	San Joaquin Valley Air Basin
TAS	true air speed
USEPA	United States Environmental Protection Agency
vDEC	virtual Disjunct Eddy Covariance
VOC	Volatile Organic Compound
WRF	Weather Research and Forecasting model
WRF-Chem	WRF coupled with Chemistry

Proposed Tasks and Work Described in this Report

The work done for each of the 5 tasks identified in the contract is briefly summarized below:

Task 1. Field campaign planning

The initial step in field campaign planning was to utilizing improved landcover databases (Gap Analysis Program (GAP) landcover database) and Emission Factors for isoprene in the old California ARB BEIGIS model and the NCAR MEGAN 2.0 model for elucidating areas where isoprene flux flight measurements would be the most useful, focusing on where the models disagree and where there are the most suitable terrains for testing the airborne flux technique (flat homogenous terrains and high emissions). Satellite derived landcover products, including the National Land Cover Dataset (NLCD), and plant species distribution data developed by UC-Berkeley, including oak distribution data, and MODIS LAI products were also compared. The flight tracks were planned to overlap with above-canopy BVOC measurement towers operating in California. More than 12 regions were selected for airborne VOC flux measurements and some tracks were chosen to overlap on different days.

Task 2. Field Measurements

VOC eddy covariance (EC) measurements were conducted on aircraft during June 2011 with 40 hours of flight time divided into 8 different days to quantify and improve regional BVOC emissions information. Area emissions were characterized over racetrack patterns of ~30 km (with each side of the racetrack being ~15 km) resulting in reliable emission measurements resolving spatial scales appropriate for BVOC emission model verification. To account for all footprints encountered in the campaign and for compatibilities with the models the datasets were averaged to 2 km^2 resolution. The flight tracks were designed mainly to measure isoprene emissions from the areas in California with substantial Oak tree densities. We

covered a wide range of oak landscapes including those with low, moderate and high plant densities. Additional locations in California were also sampled to characterize emissions from croplands and conifer forests.

Task 3. Data Reduction

Eddy covariance fluxes were calculated from raw wind and concentration measurements. Two mathematical methods were used to reduce the raw data to actual emission fluxes. The first method is based on conventional Fast Fourier Transformation (FFT), which computes an average flux over an entire flight leg (approx. 15 km or longer). The second method is based on wavelet transformation, which computes an instantaneous correlation between two quantities over a chosen bandwith and results in highly resolved flux over discrete shorter length scales.

Task 4. Data Analysis

The measured fluxes were mapped onto landcover maps and isoprene emissions were directly correlated with modeled emissions. Using the CARB BEIGIS VOC emission model we performed linear regression analysis to evaluate the level of agreement between measured and modeled isoprene emissions above different landcover types. For the areas in California dominated by oak woodlands isoprene seemed the most important VOC, while monoterpene fluxes were too small to measure, so the tracer ratio for specific monoterpenes and related compounds could not be applied. However, methanol fluxes which are assumed to account for approximately half of oxygenated VOC emissions by mass were directly measured.

Task 5. Final Reports

This report is submitted in fulfillment of Task 5.

In addition, multiple papers and posters have been presented at various workshops, meetings and seminars. The peer-reviewed publications using the CABERNET data to date include:

1) Peischl, J., Ryerson, T. B., Holloway, J. S., Trainer, M., Andrews, A. E., Atlas, E. L., Blake, D. R., Daube, B. C., Dlugokencky, E. J., Fischer, M. L., Goldstein, A. H., Guha, A., Karl, T., Kofler, J., Kosciuch, E., Misztal, P. K., Perring, A. E., Pollack, I. B., Santoni, G. W., Schwarz, J. P., Spackman, J. R., Wofsy, S. C., and Parrish, D. D.: Airborne observations of methane emissions from rice cultivation in the Sacramento Valley of California, Journal of Geophysical Research: Atmospheres, 117, D00V25, 10.1029/2012jd017994, 2012.

2) Karl, T., Misztal, P. K., Jonsson, H. H., Shertz, S., Goldstein, A. H., and Guenther, A. B.: Airborne flux measurements of BVOCs above Californian oak forests: Experimental investigation of surface and entrainment fluxes, OH densities and Dahmköhler numbers, J Atmos Sci, 10.1175/jas-d-13-054.1, 2013.
3) Misztal, P. K., T. Karl, R. Weber, H. H. Jonsson, A. B. Guenther, and A. H. Goldstein, Airborne flux measurements of Biogenic Volatile Organic Compounds over California, Atmospheric Chemistry and Physics Discussions, Submitted MS No acp-2014-84, 2014.

TABLE OF CONTENTS

Disclaimer....ii
Acknowledgments....iii
Glossary of Symbols and Acronyms.... v
Proposed Tasks and Work Described in This Report....vi
Table of Contents....viii
List of Figures....xii

ABSTRACT....XVI

1 EXECUTIVE SUMMARY 1

2 INTRODUCTION 2

3 METHODS AND THEORY 8

3.1 Study region 8
3.2 Climatology during field campaign.... 9
3.3 Flight track planning 9
3.3.1 RF 1 – June 8.... 11
3.3.2 RF 2 – June 9.... 12
3.3.3 RF 3 – June 10.... 12
3.3.4 RF 4 – June 14.... 12
3.3.5 RF 5 – June 15.... 13
3.3.6 RF 6 – June 16.... 13
3.3.7 RF 7 – June 20.... 13
3.3.8 RF 8 – June 21.... 14
3.3.9 Racetrack flight planning 14
3.4 Aircraft 15
3.5 Our Measurement Approach: airborne eddy covariance flux measurements 17
3.5.1 Proton Transfer Reaction Mass Spectrometry (PTR-MS) 17
3.5.2 Airborne eddy covariance (AEC) 21
3.5.2.1 Area source emission measurements 23
3.5.2.2 Corrections related to aircraft motion 24
3.5.3 Airborne virtual Disjunct Eddy Covariance (AvDEC).... 24
3.5.4 Fast Fourier Transform (FFT) 26

3.5.5 Continuous Wavelet Transform (CWT) ... *27*
3.5.6 Flux footprints ... *29*
3.5.7 Error analysis (quality of fluxes) ... *29*
3.6 Simultaneous ground measurements ... 33
3.6.1 Walnut Grove Tower ... *33*
3.6.2 Tonzi Ranch Tower ... *34*
3.7 Our modeling approaches ... 34
3.7.1 Models used ... *36*
3.7.1.1 BEIGIS ... 36
3.7.1.2 MEGAN 2.0 ... 37
3.7.1.3 MEGAN 2.1 ... 37
3.7.1.4 CARB's MEGAN 2.1 adaptation ... 39
3.7.2 Driving variables ... *39*
3.7.2.1 Landcovers ... 39
3.7.2.2 Temperature and radiation ... 42
3.7.2.3 LAI ... 43
3.7.3 Model domains ... *43*
3.7.3.1 California ... 43
3.7.3.2 Ecoregions ... 43

4 EXPERIMENTAL INVESTIGATION OF SURFACE AND ENTRAINMENT FLUXES, OH DENSITIES AND DAHMKÖHLER NUMBERS *(PUBLISHED IN KARL ET AL., 2013)* ... 47

4.1 Flux profiles ... 47
4.1.1 Heat and isoprene fluxes ... *47*
4.1.1.1 Comparison between measurements and PBL scheme ... 49
4.2 Conclusion ... 52

5 AIRBORNE FLUX MEASUREMENTS OF BIOGENIC VOLATILE ORGANIC COMPOUNDS OVER CALIFORNIA *(IN REVIEW, MISZTAL ET AL., 2014)* ... 53

5.1 Observed Concentrations of BVOC from PTR-MS ... 53
5.1.1 Isoprene ... *53*
5.1.2 Monoterpenes ... *54*
5.1.3 Other VOCs ... *54*

5.1.4 Inter-comparison of concentrations from PTR-MS and GC-MS ... *58*
5.1.5 Comparison with Walnut Grove Tower ... *59*
5.2 Observed fluxes ... 60
5.2.1 Isoprene fluxes ... *61*
5.2.2 Comparison of isoprene fluxes at Tonzi Ranch Tower ... *61*
5.3 Conclusions ... 62

6 CONSTRAINING ISOPRENE EMISSION FACTORS FROM OAK WOODLANDS OVER CALIFORNIA. ... 63

6.1 CABERNET BEFs vs Landcover BEFs ... 63
6.1.1 Comparison of isoprene emission factors to MEGAN landcover 2.2 ... *63*
6.1.1.1 Spatial 2-km representations ... 63
6.1.1.2 Eco-region specific comparisons of BEFs ... 66
6.1.2 Comparison of CABERNET emissions with CARB's adaptation of MEGAN 2.1 ... *70*
6.1.3 Sensitivity runs ... *73*
6.1.3.1 Temperature ... 73
6.1.3.2 PAR ... 74
6.1.3.3 LAI ... 76
6.1.4 Regional model performance over ecoregions ... *79*
6.2 Conclusions ... 85

7 ADDITIONAL ANALYSES ... 86

7.1 Methanol emissions from Dairies ... 86
7.1.1 Methanol fluxes ... *87*
7.2 Fluxes of aromatics from oil fields ... 88
7.3 Early modeling efforts ... 92
7.3.1 Comparison of BEIGIS and MEGAN 2.0 emission factors for California ... *92*
7.4 Application of reverse G06 algorithm to the airborne fluxes ... 93

8 SUMMARY AND CONCLUSIONS ... 94

8.1 Refinement of AEC approach for BVOC flux measurements ... 94
8.2 Oak woodlands major isoprene source in California ... 94
8.3 Evaluation of input landcovers and model performance ... 95

9 RECOMMENDATION FOR FUTURE RESEARCH ... 96

10 LITERATURE CITED 97

Appendix A: Supplemental Figures..... 108

Appendix B: Abstracts of Associated Published Papers..... 111

Appendix C: PTR-MS sensitivities and settings during CABERNET 114

Appendix D: Data Set Description..... 115

LIST OF FIGURES

Figure 1. Tracks flown during CABERNET overlaid over (a) BEIGIS Isoprene Emission Factor (EF) landcover; and (b) oak-woodland ecosystems differing in spatial oak species homogeneity (according to GAP database). 5
Figure 2. A typical oak savannah ecosystem seen from the twin-otter. Note spatial differences in oak densities. The photo is showing Tonzi Ranch tower, where REA flux measurements took place (see Chapter 5.2.2). 9
Figure 3. Map showing the area covered by CABERNET research flights. Racetrack patterns flown during RF 3, 6 and 7 are highlighted in separate panels 14
Figure 4. CIRPAS flux-enabled twin otter. 16
Figure 5. Schematic representation of the three modules of the IONICON PTR-MS. 18
Figure 6. Normalized covariance between vertical wind (w') and isoprene concentrations (c') measured during RF3. 20
Figure 7. Side slip and pitch maneuver during RF6: Top panel depicts normalized roll and altitude signals, lower panel plots the motion corrected vertical wind speed *w*. 24
Figure 8. Normalized cospectra of isoprene (red) and temperature (blue) with vertical wind. Dashed lines indicate spectra calculated by wavelet transformation, solid lines are obtained by conventional FFT. The top axis indicates the spatial scale corresponding to an aircraft speed of 70 m/s. 26
Figure 9. Example of a segment integration based on roll to exclude turns and altitude to exclude large changes in altitude such as sawtooth soundings. 30
Figure 10. Flux quality control for an example flight leg (the segment from Figure 2). a) Clear peak in the covariance function; b) variances of w and isoprene; c) time-resolved wavelet cross spectra; and d) average cross-variance. 31
Figure 11. Spectral quality control of the example flight segment. Left panel: Comparison of cross spectra for isoprene flux and heat flux using the FFT and CWT methods independently; Right panel: Cumulative cross spectra for isoprene flux and heat flux using the FFT and CWT methods independently. 32

Figure 12. Isoprene flux processing. Upper panel: determination of the FFT/CWT flux ratio; lower panel: application of flux divergence coefficients (derived in racetrack profiles) to scale fluxes from aircraft altitude to surface fluxes using aircraft altitude and PBL height. 33
Figure 13. Simplified diagram showing the basic modeling process..... 36
Figure 14. Schematic of MEGAN 2.1 model components and driving variables (taken from Guenther et al., 2012)..... 38
Figure 15. Example land covers available for models. a) GAP's oak woodlands, b) BEIGIS emission factors (as dtiso+eiso) derived from the GAP/FIA database, c) MEGAN2.0 isoprene emission factors derived from landcov2.1, and d) MEGAN2.1 isoprene emission factors obtained from the most recent landcover2.2. 41
Figure 16. WRF's resolution effect on temperature bias. 43
Figure 17.USEPA Ecoregion map with overlaid CABERNET flight tracks covering most of code 6 ecoregions The shapefiles used to produce the map in ArcGIS were downloaded from ftp://ftp.epa.gov/wed/ecoregions/ca/. 46
Figure 18. Kinematic heat (<w'θ'> - red ,<w'q'> - blue) and isoprene (<w'c'> - green) fluxes for RF6. Error bars (1sigma) indicate the variability of all flux profiles flown during RF6 ... 47
Figure 19. Measured (black) and simulated (blue) $d\theta_v$ / dz profiles. The solid lines represent RF6 and the dashed lines RF7. 49
Figure 20. Local diffusion coefficient plotted vs z/zi, where zi is the PBL height. Blue solid lines represent measured diffusion coefficient for RF6 and RF7, cyan dashed lines are the corresponding modeled diffusion coefficients. 50
Figure 21. Normalized diffusion coefficient for isoprene for RF6 (blue) and RF7 (red). Bars indicate 1 σ. The solid cyan and magenta lines represent the diffusion coefficient for a non-reactive species for RF6 and RF7 respectively. The dashed blue (RF6) and red (RF7) line depict the diffusion coefficient corrected by the Damköhler number. 50
Figure 22. Spatial distributions of concentrations of a) isoprene, b) MVK+MAC, c) methanol and d) monoterpenes measured during CABERNET. 58
Figure 23. (a) Intercomparison of concentrations at Walnut Grove tower coinciding with top level of the tower. (b) Vertical profile for concentration of isoprene shows complementary value from ground-based measurements. 60

Figure 24. a) Comparison of airborne BEFs with MEGAN's landcover 2.2 for isoprene (airborne BEFs are subject to additional uncertainties introduced from T, and PAR used in normalization).b) magnified area denoted by the black rectangle in a). 65
Figure 25. Basal emission factor comparison. The box plots represent CABERNET variations within each ecoregion (blue box: 25-75th percentile; black line: 5th - 95th percentile; red line is the median and red crosses are the outliers). The green dots represent ecoregion's mean EF according to MEGAN2.1 landcover2.2..... 67
Figure 26. Robust regression for USEPA ecoregion averaged BEFs.The majority of ecoregions show good agreement between model and measurement. The outliers occur on the two sides of the fit showing no clear systematic offset for model or measurement. Note: the number of averaged points in each ecoregion may be different and not necessarily representative of the entire ecoregion. 69
Figure 27. Timeseries for emissions of modeled and measured isoprene fluxes using the approximated circular footprint areas (only the data when flux was available are shown) along the full length of the flight tracks during the CABERNET campagin. 71
Figure 28. Comparison of 2km emissions (view at higher magnification) along sections of the flight tracks..... 72
Figure 29. Comparison of isoprene emission time series for measurement and model with +/- 20% sensitivity to temperature. 74
Figure 30. Comparison of isoprene emission time series for measurement and model with +/- 20% sensitivity to PAR. 76
Figure 31. Comparison of isoprene emission time series for measurement and model with +/- 50% sensitivity to LAI. 78
Figure 32 Box plots showing distribution of emissions in each of the level IV ecoregions. The boxes correspond to midrange (25th to 75th percentiles), the whiskers indicate variability outside the lower and upper quartiles, and the circles denote outlying emission hotspots. 80
Figure 33. Scatter plots for the ecoregion averaged emissions. The vertical error bars represent the 50% model uncertainty and the horizontal error bars represent the 20% uncertainty of the measurement..... 82
Figure 34. An example of a non-homogenous landcover where half dome footprint faced upwind would be superior to full-dome footprint of the same area. 85
Figure 35. Methanol fluxes observed in CABERNET. [Preliminary data] 88

Figure 36. Toluene, benzene and C-8 aromatics concentration distributions on the RF 1 track. 90
Figure 37. Concentrations, Fluxes and Wavelet cross spectra shown for toluene, benzene, and C-8 aromatics on a 80 km segment close to oil fields (RF1). The wavelet fluxes and their cross spectra deliver more information on the source/sink profile of the encountered aromatics. 91
Figure 38. Map showing a difference between MEGAN2.0 and BEIGIS (eiso+dtiso) emission factors. The BEIGIS emission factors were roughly converted to land area units my multiplying mg g^{-1} h^{-1} by LAI 5. 92

ABSTRACT

Vegetation in California comprises a large source of isoprene, terpenes, and other biogenic volatile organic compounds (BVOC). The emitted BVOC react in the presence of NO_x and sunlight leading to production of ozone and particulate matter. Current models of BVOC emissions for California have major uncertainties, and there are very few emission measurements available to validate existing model inventories. In order to assess and improve the model inventories of BVOC emissions for use in air quality State Implementation Planning (SIP), spatially resolved data on BVOC emissions are required.

We contracted to collect a data set using an airborne PTRMS Eddy Flux measurement system over regions of California expected to have substantial isoprene emissions and to use those data to test regional BVOC emission model estimates. In the first year of the project we conducted a field measurement planning exercise to optimize the amount of information that could be gained from airborne flux observations. Oaks are the main source of isoprene in California and they grow dominantly in certain elevations (400-800 m) along the foothills encompassing the Central Valley and along the Coastal Range Mountains. These specific locations and relatively constant elevations make oaks an ideal subject for flux observations from aircraft. We examined oak distribution data used in the BEIGIS and the MEGAN BVOC emission models. We also reviewed recent advances in satellite derived landcover information, including the National Land Cover Dataset (NLCD), and plant species distribution data developed by UC-Berkeley, including oak tree distribution data, for potential use in BVOC emission modeling. Using mainly the USGS National Gap Analysis Program (GAP) landcover database, we planned our survey flights (to measure surface fluxes over long transects at constant altitude) and racetrack flights (vertical profiles to characterize flux divergence) over more or less homogeneous oak woodlands consisting of the Blue Oak Woodlands (BOW), Valley Oak Woodlands (VOW) and Coastal Oak Woodlands (COW).

In the second year of the project 40 hours of airborne measurements were conducted using an airborne VOC eddy flux system on board the CIRPAS Twin Otter aircraft to quantify regional BVOC emissions. The California Airborne BVOC Emission Research in Natural Ecosystem Transects (CABERNET) airborne campaign took place in June 2011. Measurements focused on key BVOC species that have a major role in regional air quality and are already included in

the BEIGIS model. Isoprene and total terpene emissions were measured using an airborne Proton Transfer Reaction Mass Spectrometer - Eddy Covariance (PTRMS-EC) flux system. The paths of the research survey flights and "racetrack" gradient flights covered a fairly complete sampling of the dominant Oak woodlands in California. Weather forecasting was used to ensure all the flights were conducted on cloudless days, generally between 10 am and 2 pm when isoprene emissions are expected to be at their daily maximum.

Vertically resolved isoprene flux measurements from the racetracks suggest that first order chemistry can describe the decrease of isoprene fluxes vertically throughout the PBL under typical atmospheric conditions. Concentration gradients throughout the PBL decrease as a result of chemical reactions leading to locally smaller concentration changes due to chemistry. We demonstrate that flux divergence measurements can be used to provide estimates of OH in the planetary boundary layer. Theses flux measurements can therefore provide a new way to determine average OH densities allowing investigating potential OH recycling mechanisms which have been proposed to occur during isoprene oxidation.

We successfully made airborne eddy covariance flux measurements and used them to map out source distributions of isoprene emissions for the dominant oak emitting ecosystems in California. We observed high concentrations (up to 8 ppbv) and high surface emissions of isoprene ranging from several to more than ten mg m^{-2} h^{-1} from the oak woodlands in the foothills of the Sierra Nevada and Costal Ranges. Consistent with other studies we show that in the Central Valley isoprene emissions are typically undetectably small except for the areas of Eucalyptus trees planted near the highways. The temperature ranges in California cause changes in the isoprene emissions from relatively low to extremely high due to their strong sensitivity to temperature. Calculating fluxes at high spatial resolution with 2 km averaging seemed to be a good optimum for comparing basal emission factors (BEFs) from measurements with models.

The BEFs were used to assess isoprene emission-factor landcover databases for BVOC emission models. BEFs from the landcover used by MEGAN 2.1 agreed within 10% (r^2=0.8) with measured BEFs with few discrepancies (either overestimation or underestimation).

Independently, the area emissions modeled for the same flight times and averaged for the same flux footprints were compared with measured area emissions and showed good agreement. The modeled and measured emissions were analyzed over 48 distinct USEPA ecoregions (level IV) and showed excellent agreement with half the ecoregions showing agreement to 50%, 21% of ecoregions where the model overestimated and 29% where the model underestimated emissions. We show that the landcover has the most critical influence on model-measurement agreement and to a lesser extent the meteorology and LAI. Despite a few local discrepancies, the model currently used by CARB was generally within 20% agreement with the measurements, which is well within the stated model uncertainty (50%).

1 Executive Summary

The objective of this project was to directly quantify biogenic volatile organic compound (BVOC) fluxes across spatial scales relevant for air quality models and use this information to assess and improve models for regional emission estimates in California. Vegetation in California comprises a large source of isoprene, terpenes, and oxygenated volatile organic compounds, but these BVOC emissions have not been measured extensively in a manner suitable for testing the California Air Resources Board's BVOC emission model used for air quality State Implementation Plan (SIP) development. The major objective of the project was to obtain a high quality isoprene flux data set covering the major isoprene emitting regions in California, and use it to test the validity of replacing CARB BEIGIS model with the community MEGAN model. The research included a field measurement planning exercise to optimize the amount of information to be gained from airborne flux observations, conducting field measurements, then comparing observed fluxes to modeled fluxes in order to assess and improve CARB's BVOC emission inventory.

Previous VOC measurements from oak woodlands were made almost exclusively at branch and leaf level (e.g. Winer et al., 1992) and measurements at an ecosystem scale were completely unavailable. The direct flux approach from aircraft (Karl et al., 2013; Misztal et al., 2014) enabled first time regional assessment of the emission rates from oak woodlands in California and characterized chemical losses of reactive trace gases in the vertical profile. The project resulted in the following achievements:

1) Pioneered the direct airborne BVOC flux technique for rapid and spatially explicit measurements of biogenic emissions.
2) Successful application of this technique to regional measurements of fluxes over the majority of Californian oak woodlands and other relevant regions.
3) Measured airborne basal emission factors and compared them quantitatively with model landcover emission factors.
4) Confirmed the predictions from earlier work at the branch scale that oak woodlands and to a lesser extent Eucalyptus are the major sources of isoprene in California with high emission potentials (>4 mg m^{-2} h^{-1}).

5) Evaluated model predictions at several resolutions accompanied by sensitivity analyses and determined 2 km was an optimal resolution for model – measurement comparison.
6) Demonstrated that the fundamental isoprene emission modeling framework used by ARB is effective, while pointing out where some improvements may be possible in the model inputs driving the landcover emission potentials.
7) Excellent quantitative agreement was obtained between measured and modeled emissions in the homogenous terrains of oak savannahs in the Sierra Nevada Foothills where the majority of previous measurements at the branch scale were performed. Less excellent quantitative agreement was obtained in the northern Coastal Ranges (with model landcover tending toward overestimation) and in the Central and Central-Southern Coastal Ranges (with landcover tending toward underestimation).
8) Analysis averaged by individual ecoregions showed excellent agreement of the model with measured emission factors and emissions except for a few cases where landcover is likely inaccurate and could be improved.
9) Accurate footprints were obtained based on instantaneous wavelet heat flux for explicit spatial comparison of measured fluxes with the emission inventory for corresponding area contributions.
10) Successful demonstration that airborne measurements are a viable tool for spatially and temporally explicit validation of emission models and landcover assessments.

Further research is needed to provide more airborne flux measurements to achieve better statistics in each ecoregion, measure a much broader suite of BVOCs including both biogenic and anthropogenic emissions which lead to ozone formation, and from measurements during additional seasons including hotter periods when ozone pollution is more likely to be out of compliance with air quality regulations.

2 Introduction

The overall objective of this project is to directly quantify biogenic volatile organic compound (BVOC) fluxes across spatial scales relevant for air quality models and use this information to assess and improve models for regional emission estimates in California. Vegetation in California comprises a large source of isoprene, terpenes, and oxygenated volatile organic compounds, but these BVOC emissions have not been measured extensively

in a manner suitable for testing the California Biogenic Emission Inventory GIS (BEIGIS) model used for air quality State Implementation Plan (SIP) development. The proposed research objectives are to first conduct a field measurement planning exercise to optimize the amount of information that can be gained from airborne flux observations, and then to conduct field measurements.

Volatile Organic Compounds (VOCs) play important roles in atmospheric chemistry such as fueling tropospheric ozone production, forming secondary organic aerosols, and acting as important radical sinks in regions near sources. The global annual source strength of gas-phase biogenic volatile organic compounds (BVOC) is around 1 Pg (1015 g) (Guenther et al., 2012). One half of these mass emissions (500 Tg) is constituted by a single highly reactive hemiterpene, isoprene (2-methyl-1,3-butadiene). The other half is represented by hundreds to thousands of compounds which span the atmospheric lifetime ranges from a few seconds (e.g. sesquiterpenes) to months (e.g. benzene), and are actively exchanged in both directions (emission and deposition) between the biosphere and atmosphere (Park et al., 2013). Currently, BVOC measurements (mostly of emission) have been reported at ecosystem scales primarily from fixed tower sites which offer very good temporal resolution, but lack spatial resolution across the broader landscape that is critical for understanding regional photochemistry.

Since the discovery of substantial isoprene emissions from forested regions (Rasmussen, 1970), and subsequent progress in understanding isoprene biochemistry (Loreto and Sharkey, 1990), much research has been conducted to understand the emissions of isoprene and the factors that drive them at the leaf level, including in California (Arey et al. 1991a; 1995; Baker et al. 1999; Karlik and Winer 2001; Kurpius and Goldstein 2003; Goldstein and Schade 2000; Schade et al 1999; 2000; Schade and Goldstein 2001; Winer et al. 1992). This work has led to BVOC emission models such as BEIS (Pierce et al. 1998), MEGAN (Guenther et al. 2012) and BEIGIS (Scott and Benjamin 2003) that are driven by information about weather conditions, plant distributions, leaf area, and the temperature and light response of isoprene emissions from plants. There have been isoprene flux measurements at the canopy scale in a variety of locations worldwide: Northwestern U.S. oak savanna (Lamb et al. 1986), Northeastern US mixed forest (Goldstein et al 1998), North Central US mixed forest

(Westberg et al., 2001; Apel et al, 2002), Amazonian tropical forests (Rinne et al. 2002; Kuhn et al., 2002), Central Africa rainforest (Serca et al., 2001), Borneo rainforest (Langford et al., 2010), etc. However, in California, no ecosystem scale fluxes have ever been reported for an oak dominated ecosystem that could be used to verify the modeled statewide isoprene emission inventory.

A California BVOC model called BEIGIS (Scott and Benjamin 2003) predicts significant emissions of isoprene from oak woodlands distributed throughout the foothills of the Coast Range and the Sierra Nevada mountains (Figure 1a). However, with the exception of a single site in a pine plantation (Schade et al 1999; 2000; Schade and Goldstein 2001; Goldstein and Schade 2000), and measurements in a few crops (Karl et al., 2008; Fares et al., 2011; Fares et al., 2012; Park et al., 2013), there have been no measurements of BVOC fluxes from California landscapes at a larger spatial scale than individual leaves and branches. The goal of our work was to measure the distribution of isoprene flux across the oak woodland areas of California in order to test and improve the landscape-scale emission models that are used for regional air quality assessments. California is a region where these observations are particularly needed because of its varied landscape, with BVOC emissions from biogenic areas dominated by Oaks (~7% of land area), and with anthropogenic VOC emissions from the activity of ~35 million people living in the state. Furthermore, the accuracy of isoprene

emission estimates is important for regional simulations of ozone production. x

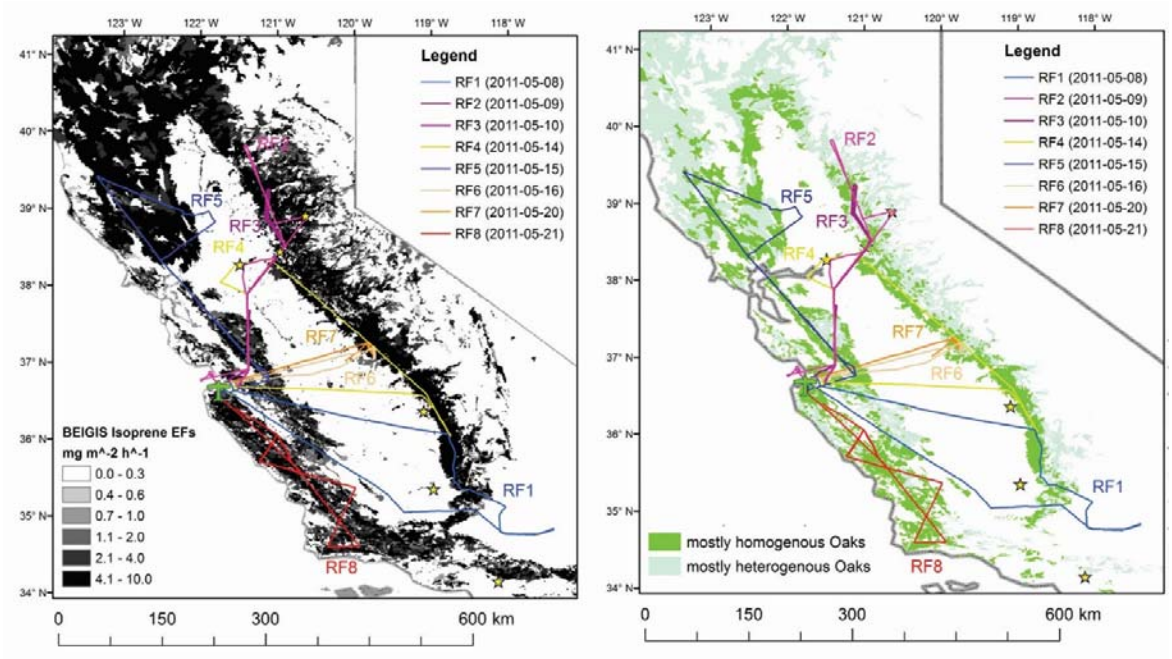

Figure 1. Tracks flown during CABERNET overlaid over (a) BEIGIS Isoprene Emission Factor (EF) landcover; and (b) oak-woodland ecosystems differing in spatial oak species homogeneity (according to GAP database).

Although the vast majority of eddy covariance measurements have been conducted on the ground, Airborne Eddy Covariance (AEC) is an established technique which has been used extensively in the last several decades to measure fluxes (e.g. of energy, ozone, carbon dioxide, etc.) directly using an aircraft (e.g. Lenschow et al., 1981; Desjardins et al., 1992; Pattey et al., 2002; Metzger et al., 2013). The first successful implementation of AEC for VOC was by Karl et al. (2009) over Mexico using a C130 aircraft.

In Chapter 5, we present the first regional BVOC flux measurements focused on transects over areas expected to dominate emissions in California (Figure 1). Vertical "racetrack" profiles were used for testing the flux methodology and derivation of flux divergence terms, which were recently described in a separate paper (Karl et al., 2013) where we demonstrated that our PTR-MS configuration in CABERNET was appropriate for measuring isoprene fluxes.

We report the observed spatial distribution of airborne fluxes and emission factors and demonstrate that they match well the emission factors from landcovers estimated using a California Air Resources Board implementation of the MEGAN model. The data have been used to improve landcover and accuracy of VOC inventories in California, which is more thoroughly explored in Chapter 6.

The motivation for conducting this regional flux study in California was driven by: 1) the need for spatially resolved data on BVOC emissions from oak woodlands which have a large impact on regional ozone concentrations, 2) our lack of information on how BVOC emissions respond to variations in landcover (plant functional type distributions, LAI, etc). and 3) verification that the state's modeled emissions for isoprene are accurate which are critical for use in air quality State Implementation Planning (SIP).

A number of direct flux measurements of conserved tracers (e.g. heat, water) have demonstrated their usefulness to investigate the horizontal and vertical structure of the atmosphere utilizing aircraft (e.g. Lenschow et al., 1980; Desjardin et al., 1997; Metzger et al., 2013). In contrast only few direct flux measurements of reactive tracers exist to date. Faloona et al. (2005) for example used a combination of ozone and dimethyl-sulfide eddy covariance measurements to estimate accurate entrainment rates in the stable marine Boundary layer. Mauder et al. (2007) investigated the influence of heterogeneous terrain on ozone deposition fluxes and the influence of meso-scale fluxes on the energy balance closure. Due to the lack of suitable flux measurements most micrometeorological studies on reactive species in the mixed layer have been conducted with large eddy simulations (LES) (e.g. Schumann et al., 1989, Peterson et al., 1999, Patton et al., 2000; Vinuesa et al., 2003). In the past, landscape scale non methane volatile organic compounds (NMVOC) emissions were often estimated using mixed layer gradient techniques based on the results of LES simulations (e.g. Greenberg et al. 1999; Guenther et al., 1996). New advances in mass spectrometric methods have recently allowed investigation of urban anthropogenic NMVOC emissions based on direct airborne eddy covariance measurements (Karl et al., 2009). Such measurement systems provide a unique opportunity to constrain emissions of NMVOC that enter the atmosphere via biogenic and anthropogenic sources over regional spatial scales that are not directly observable by any other known methods.

Here we expand airborne flux measurements of BVOC to investigate the atmospheric fate of reactive compounds above forested areas which are thought to the dominant global source of BVOC. The California Airborne BVOC Emission Research in Natural Ecosystem Transects (CABERNET) experiment took place over extended oak belts surrounding Central valley (34° 32’ to 39° 21’ N; 117° 28’ to 123° 17’ W) during June 2011. The study focused on isoprene (2-methyl - 1,3 - butadiene), a biogenic hydrocarbon, which is thought to be emitted to the atmosphere in similar amounts compared to methane (Guenther et al., 2006). Isoprene fluxes were measured on-board of the CIRPAS Twin Otter (http://www.cirpas.org/twinOtter.html) using the virtual disjunct eddy covariance method (Karl et al., 2002). Chapter 4 presents the first direct airborne isoprene flux measurements focused on vertical flux profiles while Chapter 5 reports the first regional fluxes of isoprene and other BVOC from survey transects and Chapter 6 demonstrates their comparison to modeled fluxes.

3 Methods and theory

3.1 Study region

Oaks are the main source of isoprene in California and they grow dominantly in certain elevations (400-800 m) along the foothills encompassing the Central Valley and along the Coastal Range Mountains. These specific locations, relatively constant elevations, and high emission rates make oaks an ideal subject for flux observations from aircraft. Using the USGS National Gap Analysis Program (GAP) landcover database, we planned our survey flights (to measure surface fluxes over long transects at constant altitude) and racetrack flights (vertical profiles to characterize flux divergence) over more or less homogeneous oak woodlands consisting of the Blue Oak Woodlands (BOW), Valley Oak Woodlands (VOW) and Coastal Oak Woodlands (COW). The total percentage of the sum of their primary, secondary and tertiary levels was used to map out the most homogeneous areas where oaks are the only or the dominating tree species (see Sect. 2.2 on flight track planning). Despite this biological homogeneity the oaks have highly irregular distribution patterns characterized by varying spatial densities. Figure 2 shows a typical oak ecosystem as seen from the Twin Otter flying over Tonzi Ranch tower, where ground flux measurements of isoprene were simultaneously performed for comparison with the aircraft observations (see Chapter 5.2.2).

Apart from relatively homogeneous (in terms of the species) oak woodlands mostly in the foothill bands, further away there are transition areas with coniferous regions where, according to the GAP database, the oaks grade in to Blue Oak – Ponderosa Pine (BOP) habitats and/or Montane Hardwood-Conifer (MHC), and/or Montane Hardwood (MHW). These areas are represented in Figure 1b.

Figure 2. A typical oak savannah ecosystem seen from the twin-otter. Note spatial differences in oak densities. The photo is showing Tonzi Ranch tower, where REA flux measurements took place (see Chapter 5.2.2).

3.2 Climatology during field campaign

Environmental context is important to take into account when analyzing measured BVOC fluxes because the history of temperature and photosynthetically active radiation (PAR) are the main drivers of potential vegetative emissions (Sharkey et al., 1999; Fuentes and Wang, 1999), and seasonal variability in climate is known to affect gross ecosystem production in this region (Goldstein et al., 2000). The climatological conditions in California in June 2011 were relatively colder than in June of the previous year. The preceding month and the first week of June 2011 were particularly cold followed by gradual increase in the temperature throughout the campaign with particularly hot sunny weather on the final flight of the campaign. Along with the warming, the environment was becoming dryer.

3.3 Flight track planning

The CABERNET airborne campaign took place in June 2011. The paths of the research survey flights and "racetrack" gradient flights are portrayed over the BEIGIS isoprene emission factor map (Figure 1a) and California map of oak woodland distribution (Figure 1b). Weather forecasting was used to ensure that all the flights were conducted on cloudless days, and where possible for the mean wind direction to be perpendicular to the flight paths. A test flight on June 1st was performed over the ocean to calibrate the sensors using pitch and yaw maneuvers, according to Lenschow, 1986. These were used to test the accuracy of coefficients for wind vector transformations to ensure the vertical wind speed is not affected by aircraft motion. More detailed information on these maneuvers made during CABERNET can be found in Karl et al. (2013).

The true air speed (TAS) was kept as constant as possible on all the flights. For the entire campaign the TAS ranged from around 52 to 67 m/s with an average of 58 m/s, and a standard deviation of 2.3 m/s. The measured air temperature at aircraft altitude ranged from 19.4 to 25.9 ºC (mean: 22.5 ºC, s.d.: 1.28 ºC) while the temperature at 2 m above the surface (WRF model) was wider in range (from 10.9 to 34.8 ºC) and higher by 3.6 ºC average temperature.

The available forty hours of flight time was divided into eight research flights (RF) which were carried out for approximately 4-5 hours each during the mid-day. The individual flown tracks are described in chapters 3.3.1 to 3.3.8.

Summary information specific to planning of each research flight (RF) is provided in Table 1.

Table 1. Selected flight parameter data specific to each research flight.

	RF1 June 8	RF2 June 9	RF3 June 10	RF4 June 14	RF5 June 15	RF6 June 16	RF7 June 20	RF8 June 21
Temperature close to the surface (2 m WRF) (ºC)								
mean (median)	20.6 (21.5)	23.1 (23.8)	24.4 (25.3)	27.8 (28.6)	28.5 (29.4)	24.8 (25.4)	29.7 (30.3)	32.5 (33.4)
s.d.	3.21	3.21	3.46	2.88	3.24	3.96	2.64	3.54
min	11.3	10.9	11.4	11.7	12.2	11.8	12.1	11.7
max	25.9	28.0	29.6	32.1	33.8	31.4	34.9	37.2
5th percentile	14.4	17.1	17.7	23.4	22.6	16.8	26.0	27.0
95th percentile	24.6	27.1	28.5	31.1	32.3	29.6	32.4	36.0
Altitude (m a.g.l.)								
mean (median)	603 (437)	551 (449)	831 (685)	529 (470)	511 (489)	836 (721)	852 (730)	462 (396)
s.d.	436	309	575	233	193	461	565	210
min	127	119	126	209	127	55.3	50.0	160
max	2410	1830	2790	1720	1460	2610	1870	1540
5th percentile	251	266	285	301	278	291	289	268
95th percentile	1670	1300	2090	949	712	1640	1830	887
Relative humidity at aircraft altitude (%)								
mean (median)	49.9 (42.7)	51.1 (51.1)	45.5 (46.9)	46.5 (46.7)	35.1 (36.5)	31.1 (29.9)	33.7 (34.2)	28.9 (26.6)
s.d.	17.6	16.2	15.7	7.62	9.11	13.3	11.0	8.87
min	21.2	18.4	12.0	18.4	11.1	9.78	8.8	13.2
max	100	100	95.6	83.4	68.6	99.2	85.8	68.6
5th percentile	31.2	27.1	18.0	33.3	17.3	13.0	11.7	18.5
95th percentile	86.1	95.6	70.2	58.0	48.2	45.9	47.7	48.1
Other flight characteristics								
Take off time UTC (local/PDT)	17:30 (11:30)	18:15 (12:15)	18:10 (12:10)	18:05 (12:05)	18:00 (12:00)	19:05 (13:05)	19:05 (13:05)	18:55 (12:55)
Touchdown time UTC (local/PDT)	22:20 (16:20)	22.45 (16:45)	22:10 (16:10)	22:35 (16:35)	22:30 (16:30)	0:05 (18:05)	00:30 (18:30)	23:30 (17:30)
Flight focus	Survey	Survey	Survey, Racetrack	Survey	Survey	Racetrack	Racetrack	Survey
Total length (km)	983	908	802	896	875	1020	835	935
PBL height range (km)	0.9 - 2.8	1.4 - 1.7	0.8-1.1	0.4-1.9	1.1-1.1	1.6-1.7	1.2-1.2	0.7-1.4
VOC-related *m/z* measured (10 Hz)*	69, 33, 79, 93, 107	69, 71, 33, 81, 137, 87	69, 71, 75, 33	69, 71, 33, 81, 137, 87	69, 71, 33, 81, 137, 45	69, 71, 87	69, 71, 75	69, 71, 33, 137, 87

**m/z* 21, 32, and 37 were also measured on every flight at 10, 20 and 20 Hz respectively.

3.3.1 RF 1 – June 8

Research flight 1 occurred on the coolest (but still clear) day of the field study and passed to the WSW across the Central Valley, then above the most southern segment of the oak band of the Sierra Nevada foothills and further towards the shrublands of the Mojave Desert. The returning leg diagonally cut through some of the more polluted regions of the Central Valley,

passing over oil fields, dairies and other anthropogenic VOC sources. It may be relevant that the preceding period prior to June 8 was particularly cold so the biogenic emission capacity was expected to be increasing on this flight and the flight the next day. The VOCs measured included some anthropogenic VOC masses not measured in other flights, comprised of isoprene (*m/z* 69), methanol (*m/z* 33), benzene (*m/z* 79), toluene (*m/z* 93) and C-8 aromatics (C2-benzenes, benzaldehyde) (*m/z* 107).

3.3.2 RF 2 – June 9

Research flight 2 occurred during cool-weather and measured fluxes to the north east passing near the Walnut Grove tower (WGC), Tonzi Ranch Tower (TRT) and the Blodgett Forest site (BF). This flight continued up to 40 ºN latitude of the northern Sierra Nevada foothill oak band and returned on the same path providing data near the WGC, TRT and BF sites located approximately half way and seen by the aircraft twice over a 2 hour period. The region covered by this RF overlapped about 50% with RF 3 and 4. The compounds measured included: isoprene (*m/z* 69), methyl vinyl ketone and methacrolein (MVK + MACR) (*m/*z 71), methanol (*m/z* 33), monoterpenes (*m/z* 81, 137), and methyl butenol (MBO) (*m/z* 87).

3.3.3 RF 3 – June 10

Research flight 3 was half spent doing the first vertical "racetrack" profile flight, and the rest was devoted to segments overlapping spatially with the ground WGC and TRT based towers and with RF 2 and 4. The racetrack legs were relatively long in order to oversample and then determine the optimal track lengths for wavelet flux determination with this particular aircraft. Targeted compounds were isoprene (*m/z* 69), MVK+MACR (*m/z* 71), hydroxyacetone (*m/z* 75), and methanol (*m/z* 33).

3.3.4 RF 4 – June 14

Research flight 4 was a survey that shared the same initial route to the San Joaquin as the two previous flights and after reaching the Sierra foothills it continued South right over the oak woodlands until intersection with the route used in RF1. This provided extensive coverage of a portion of the oaks on the eastern edge of the central valley. The return flight followed the same path until reaching Bakersfield to the left and then proceeded straight across the Central Valley above some of the many dairies in the region. Isoprene (m/z 69), MVK+MACR (m/z

71), methanol (m/z 33), monoterpenes (m/z 81, 137), and MBO (m/z 87) were the measured compounds.

3.3.5 RF 5 – June 15

Research flight 5 went to the North through the San Francisco Bay Area and near Santa Rosa to measure emissions from oak woodlands in the coastal regions. After reaching the most northern point the plane flew towards the San Joaquin Delta region near rice paddies. A biomass burning episode from one rice field was explored with the aircraft to observe methanol, acetaldehyde, and possibly furan (see supplementary video). Measured compounds were isoprene (m/z 69), MVK+MACR (m/z 71), methanol (m/z 33), monoterpenes (m/z 81, 137), and acetaldehyde (m/z 45).

3.3.6 RF 6 – June 16

Research flight 6 was focused on performing a vertical gradient racetrack profile over relatively homogeneous oak terrain in the Sierra foothills near Madera. The racetrack consisted of 5 sequential segment lengths of 15 km at evenly distributed altitudes within the PBL. The racetrack started at the top level directly following a saw-tooth sounding. The plane performed one lap at each height on the decent down and again on the ascent back up. When the top level was reached another saw-tooth sounding was performed and the whole racetrack sequence was repeated. Since this paper is focused on the results from survey transects, the reader is referred for details of vertical profile racetrack results to Karl et al. (2013). Just three masses were measured: isoprene (*m/*z 69), MVK+MACR (*m/*z 71), and MBO (*m/*z 87).

3.3.7 RF 7 – June 20

Research flight 7 was also focused on racetrack profiles and was situated in a similar location to the racetrack in RF 6, but was rotated for the predicted wind direction to be perpendicular to the straight side of the track. One main difference was that this racetrack saw higher temperatures than RF6 four days earlier which was reflected in observed higher concentrations. However, the flux divergence terms obtained from both racetracks 6 and 7 were very similar. The measured masses corresponded to the following targeted compounds: isoprene (*m/z* 69), MVK+MACR (*m/z* 71), and hydroxyacetone (*m/z* 75).

3.3.8 RF 8 – June 21

Research flight 8 was a survey towards the south of Monterey covering the coastal oak savannahs during the hottest day of all RFs. While in previous flights concentrations of a few ppb of isoprene were observed, the instantaneous maximal concentrations in this RF reached 8 ppb. The following compounds were targeted on this flight: isoprene (*m/z* 69), MVK+MACR (*m/z* 71), methanol (*m/z* 33), monoterpenes (*m/z* 137), and MBO (*m/z* 87).

3.3.9 Racetrack flight planning

The vertical profiling strategy was developed to optimize aircraft speed and maneuverability with sufficient horizontal averaging statistics. Figure 3 depicts a map showing the racetracks in the separate panels next to the CABERNET study area.

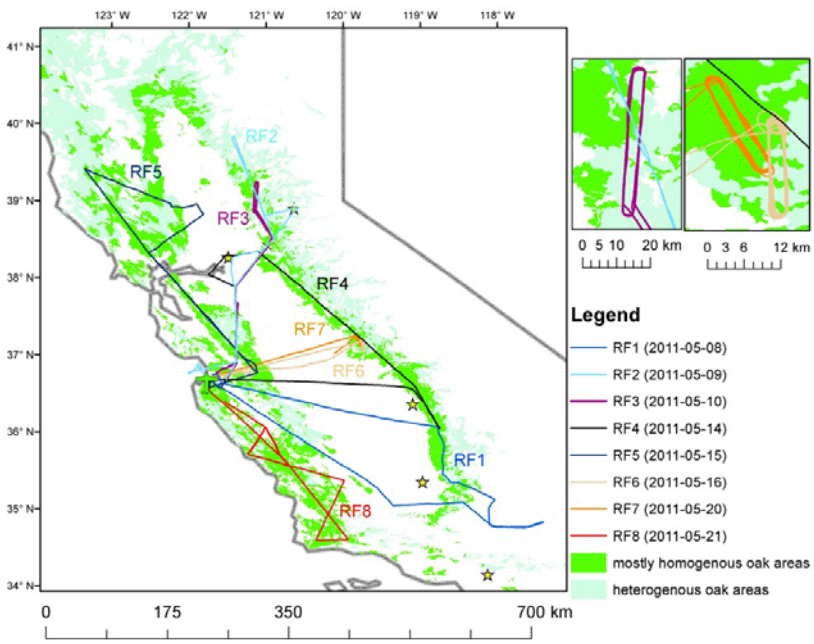

Figure 3. Map showing the area covered by CABERNET research flights. Racetrack patterns flown during RF 3, 6 and 7 are highlighted in separate panels

Research flights (RF) RF3, RF6 and RF7 were planned so that profiles could be flown between 12-16h local time. RF3 targeted an area NW of Sacramento between waypoints 39° 04’ 53” N, 121° 09’ 32” W and 39° 13’ 50” N, 121° 07’ 12” W. RF6 and RF7 were conducted east of Madera between waypoints 37° 02’ 31” N, 119° 44’ 95” W and 37° 14’ 10” N, 119° 50’ 05” W. The profiles were flown at 10:10-12:40, 10:35 – 15:00 and 12:40 – 15:00

PST during RF3, RF6 and RF7 respectively. On the incoming leg, a saw tooth sounding was performed in order to determine the height of the planetary boundary layer (PBL) at the start of the profiling maneuver. A stacked profile consisting of 3 (RF3) or 5 (RF6 and RF7) levels was then spaced equally between 300 m a.g.l and the height of the PBL. A racetrack of 40 km (RF3) or 16 km length (RF6 and RF7) and 2 km width was flown at each level descending from the top. After two profiles (down and up) another sounding in the form of a spiral was conducted. Thus, one profile was completed in about 45 min during RF6 and RF7 and in 70 min during RF3. Following the last profile another saw tooth sounding was flown on the outbound leg. The shorter length during RF6 and RF7 was a final compromise between constraints imposed by footprint, stationarity and available operational time on the aircraft. The PBL height typically varied by less than 15 % during RF3, RF6 and RF7 profiling maneuvers.

3.4 Aircraft

A two-engine UV-18A Twin Otter (the military version of model Series 300) research aircraft (Figure 4) was operated by the Center for Interdisciplinary Remote Piloted Aircraft Study (CIRPAS) of the Naval Postgraduate School out of the airport located in Marina, CA near Monterey, CA. The aircraft is equipped with micrometeorological sensors and is capable of flux measurements (Karl et al., 2013). The CIRPAS payload during CABERNET included total temperature measured by a rosemount probe, dew point temperature (chilled mirror, EdgeTech Inc., USA), barometric, dynamic, and radome-angle pressures based on barometric and differential transducers (Setra Inc., USA), TAS, mean wind, slip- and attack angles measured by a radome flow angle probe, GPS pitch, roll and heading (TANS Vector platform attitude, Trimble Inc., USA), GPS latitude, longitude, altitude, ground speed and track (NovAtel, Inc., USA), and latitude, longitude, altitude, ground speed and track, pitch, roll and heading measured by C-MIGITS-III (GPS/INS, Systron, Inc., Canada).

Figure 4. CIRPAS flux-enabled twin otter.

Air was drawn from a 3-inch isokinetic pipe inlet extending above the nose of the plane. Ambient air gets diffused from a 2.047 inch ID orifice at the tip (area ratio of about 2) to another diffuser with an area ratio of 5, resulting in a flow speed inside the tube of about 10% of the aircraft speed (~ 60 m s^{-1}). Vertical wind speed was measured by a five-hole radome probe with 33º half-angles at the nose of the aircraft. The measured vertical wind speed is unaffected by the aircraft movement and flow distortion at the nose, as long as corrections based on "Lenschow maneuvers" are applied (Lenschow, 1986). More detailed descriptions of this particular aircraft can be found elsewhere (Hegg et al., 2005; Reid et al., 2001). The aircraft payload is relatively large allowing for extensive set of instrumentation and between 1 and 3 research crew on board. The list of instrumentation included: 1) NCAR's airborne PTR–MS for VOC fluxes; 2) an adsorbent-cartridge automatic sampler for GC-MS VOC speciation and validation of contributions to m/z measured by PTR-MS; 3) Picarro 2 Hz methane/CO2 analyzer; 4) Slow ozone analyzer (2B Tech) and dry chemo-luminescent fast-ozone sensor (NOAA); and 5) Water-based Condensation Particle Counter (CPC, TSI Inc.). The cartridges were installed in banks of four with double-ended shut-off style quick connect fittings to attach them to the instruments chassis. Each bank was rapidly swappable, when the aircraft was on the ground.

The VOC cartridge sampler containing 8 adsorbent tubes was manually activated during the flight and was recorded by a datalogger analog input to mark the timing of each sample, which was drawn automatically through the cartridge for 8 min at a 335 sccm constant flow. In addition, one tube served as a blank for each flight and one tube was kept open inside the cabin for passive absorption of VOCs present in the cabin air to help in the identification of potential tube leaks.

3.5 Our Measurement Approach: airborne eddy covariance flux measurements

Mass spectrometric techniques have proven to be extremely valuable for the measurement of atmospheric chemical fluxes due to their high data acquisition rates. In particular, chemical ionization mass spectrometers used to detect atmospheric trace gases have found a wide application to the study of many processes important in the atmosphere. In the last 10 years, Proton Transfer Reaction Mass Spectrometry (PTR-MS) has been used extensively for quantifying the VOC composition during various ground and airborne field campaigns including INDOEX, TEXAQS2000, TEXAQS2006, ITCT2001, MINOS, NEAQS, MILAGRO, ITCT2004, BLODGETT (e.g., Holzinger et al. 2006, Holzinger et al. 2007, de Gouw et al. 2003). The PTR-MS measurements are typically combined with GC measurements, canister samples or cartridge sampling system to collect air samples for an offline analysis by a GC-MS to aid in VOC speciation and validation of the PTR-MS masses.

3.5.1 Proton Transfer Reaction Mass Spectrometry (PTR-MS)

The Proton Transfer Reaction Mass Spectrometer (PTR-MS) is a fast sensor which can measure concentrations of VOC in a high frequency (10 Hz) virtual disjunct mode (Karl et al., 2002). Unlike a disjunct sampler which rapidly grabs a sample periodically, a PTR-MS instrument can be regarded as a virtual disjunct sampler where the ambient air is sampled continuously but *m/z* are analyzed sequentially by the quadrupole detector, creating a disjunct dataset with high frequency data (e.g. 10 Hz) separated by a relatively longer gap (e.g. 2 Hz).

The PTR-MS instrument (Figure 5) consists of three parts: The ion source where ions are produced by a hollow cathode discharge using water vapor as the molecular source of ions;

the drift tube where proton transfer reactions to the trace constituents in the air occur; and finally the ion detector which provides sensitive detection of mass specified ion scans of the molecules of interest.

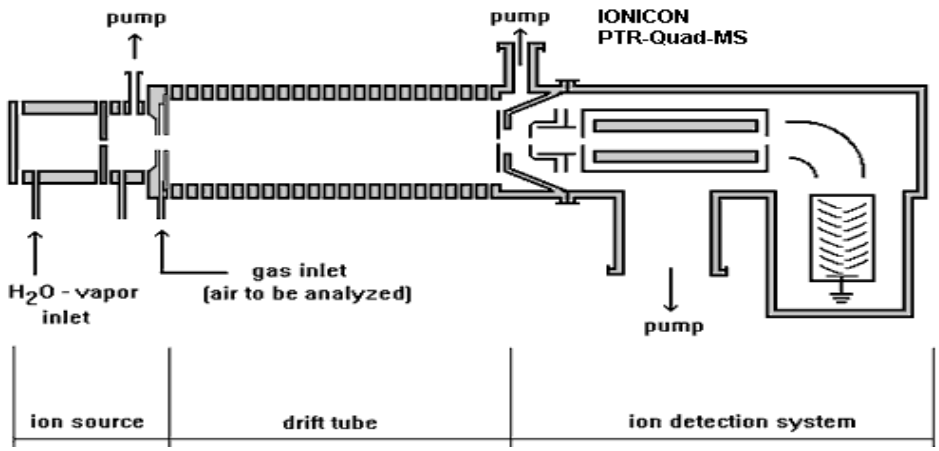

Figure 5. Schematic representation of the three modules of the IONICON PTR-MS.

The hollow cathode ion source converts water vapor in the plasma discharge into H_3O^+ ions via well-known ion-molecule reactions. Ions extracted from the source enter a short "source drift region," also filled with water vapor, in which the ions are collisionally equilibrated with water vapor. The drift velocity of the ions is maintained at a sufficiently high value, by the applied electric field, that clustering of the hydronium ions with water molecules to form higher hydrates is efficiently suppressed. Reactant ion purity is thus easily controlled and a drift field of 120 Td is sufficient to ensure that more than 90% of all reactant ions are present as the unsolvated hydronium ion, H_3O^+ and to a small fraction as its monohydrate. H_3O^+ ions transfer protons to nearly all VOCs with rates equal to the respective gas kinetic collision frequencies. Reactant ions are injected into the drift tube. The drift tube is maintained at a buffer gas pressure of typically 2 mbar. The air to be analyzed operates as buffer gas. After entering the drift region proton transfer reactions occur between H_3O^+ and any molecules R_i whose proton affinity exceeds that of water and the product ions $[R_iH^+]$ are monitored in the downstream quadrupole mass spectrometer. A detailed description about operating conditions and instrument validation was previously documented (de Gouw et al., 2003).

The instrument deployed in CABERNET was NCAR's high sensitivity PTR-MS (Karl et al., 2009). Its internal vacuum inlet system was specifically redesigned to enable stable operation across a wide range of altitudes and to ensure internal lag-time of less than 100 ms. The instrument outputs an analog signal, which contained synchronization and error flagging information which were decoded at the time of post processing. This allowed the PTR-MS data to be merged with the data produced by the other sensors on the aircraft. This was particularly important for calculating the fluxes, which are covariances between the PTR-MS output and the turbulence data measured by the aircraft.

The instrument was typically operated at 2.3 mbar drift pressure and 560V drift voltage. Isoprene was calibrated using a multicomponent NMVOC standard, which contained a mixture of methanol, acetonitrile, acetaldehyde, acetone, isoprene, methyl vinyl ketone, methyl ethyl ketone, benzene, toluene, m,o,p-xylenes and camphene. Typical instrument sensitivities for isoprene were 15 ncps/ppbv (normalized counts per second per ppbv), which for a primary ion signal of about 2 x 10^7 cps (counts per second) led to a sensitivity of 300 cps / ppbv. The disjunct sampling interval was 0.5 s at 5 Hz sampling time. Lenschow et al. (1984) reviewed instrumental requirements to accurately measure fluxes in the mixed layer. The required instrument sensitivity for uncorrelated noise to be negligible is $S = Q / (\langle c \rangle \Gamma)$, where $\langle c \rangle$ is the concentration, Γ the integral time scale and Q the total counts required. Q must be greater than $\langle c \rangle^2/(4\sigma_c^2)$, thus one can derive a critical threshold for the mixed layer, where

$$Q > 0.15 \frac{w_*^2 \cdot \langle c \rangle^2}{F^2} \qquad (1).$$

During CABERNET $F/\langle c \rangle$ ratios for isoprene were in the range of 0.09 and 0.4 m/s. Typical length scales in the mixed layer are 100 m, leading to Γ of 100 (m) / 60 (m/s) = 1.6 s for this study. For w*=2 m/s and typical isoprene concentrations of 1 ppbv we calculate required count rates of 2.3 - 46 counts within one integral timescale. The integrated count rate over Γ during this study was 300*0.2/0.5*1.6 = 192 counts, thus sufficient for measuring isoprene fluxes. Figure 6 shows a typical example of the covariance between isoprene and vertical wind velocity measured at 1000 ft above ground.

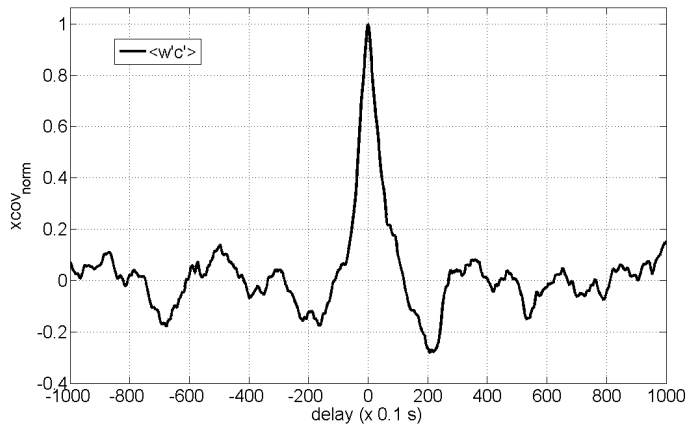

Figure 6. Normalized covariance between vertical wind (w') and isoprene concentrations (c') measured during RF3.

The delay time through the isokinetic pipe was estimated to be <0.2s. The PTR-MS was connected to this flow via a 3m long ¼" Teflon (PFA) line (I.D.: 0.5 cm) pumped by a sampling pump at a flow rate of about 1.5 l/min. This led to an overall delay time of about 2.4 s.

The instrument operation and routine were kept consistent for each flight. Current FAA regulations do not allow for the instrumentation to be running overnight, requiring specific steps to achieve stable instrument operation quickly after an instrument start-up. A flight-optimized vacuum system and internal capillary components result in fast transfer time from the inlet to the drift tube and independence of ambient pressure variations on the drift-tube pressure at high altitudes. The valves between the water reservoir and the ion source reduce the time to achieve ion source stability and low oxygen ion levels in the drift tube. Approximately three hours before the take-off the instrument was powered up, and approximately 1 hour before the take-off, if the O_2^+ signal went below 6% of the primary ions, an SEM and ion source check with optimization was followed by a dynamic calibration using two VOC standards (Apel-Riemer), one high concentration (available during pre-flight) containing low-fragmenting compounds for daily sensitivity curves (i.e. benzene (1.11 ppm), toluene (1.07 ppm), xylenes (4.22 ppm), trimethylbenzene (1.94 ppm), dichlorobenzene (2.61 ppm), and trichlorobenzene (1.14 ppm)) diluted with VOC-free air and another low-concentration standard containing isoprene (10.0 ppb) (also available in-flight) which was

also used as a back-flushing gas during the take-offs and touch-downs to prevent the exhaust plumes from contaminating the inlet. Zeros were measured using three different sources: Pt-catalyzed ambient air; ultra-pure compressed air (Air Liquide); ambient air at the top of the tooth sounding well above the PBL height. The calibrated normalized sensitivities for calibrated VOCs experienced day-to-day variabilities of less than 30%. The average sensitivity for isoprene was 15.1 ncps ppbv^{-1} as a sum of *m/z* 69 (13.4 ncps ppbv^{-1}) and *m/z* 41 (2.2 ncps ppbv^{-1}). The *m/z* 41 ion was used to assess the stability of isoprene fragmentation but only *m/z* 69 was used in the calculation of concentrations. These sensitivities resulted in detection limits of less than 10 pptv for isoprene corresponding to one km of flight. The primary ion count rates monitored at *m/z* 21 were around 20,000,000 cps (±20%) so the absolute sensitivities were approximately 20 times higher than the normalized sensitivities (i.e. ~300 cps ppbv^{-1} for isoprene). The sensitivities for compounds not present in the standard were approximated for each day from combining sensitivity curves of the daily calibrations with sensitivity curves from post-campaign calibrations using several different standards at a range of humidities. The accuracy of sensitivities was estimated at ±10% for direct calibration (5% standard certification + 5% from dilution) and ±30% for the approach combining post-campaign calibrations. The settings, sensitivities and further methodological remarks are included in Appendix E.

3.5.2 Airborne eddy covariance (AEC)

The preferred micrometeorological method for measuring trace gas fluxes in the turbulent boundary layer is eddy covariance (EC). This approach is a direct measurement of the fluctuating vertical wind velocity and trace gas concentration. The flux is determined from the mean covariance between vertical wind velocity (*w*) and concentration (*c*) fluctuations and can be expressed as

$$F = \overline{w'c'} \qquad (2)$$

where *w*' is the difference between the instantaneous and mean vertical wind speed and *c*' is the difference between the instantaneous and mean trace gas concentration. Here we use *w*'*c*' to represent the time average of the product of these two variables. The major components of an EC flux system are: 1) an instrument that measures vertical wind speed with a fast (typically <100 ms) response time; 2) an instrument that measures the targeted atmospheric

constituent with a fast response time; and 3) a system to receive and store the data (e.g, datalogger or computer). Instruments with slower (> 100 ms) response times can be used to measure the flux associated with lower frequencies but will underestimate the total flux. In some cases this may result in an acceptable error while in other cases an attempt can be made to account for the loss of flux due to inadequate sensor response (Moore, 1986; Rowe et al., 2011). The correction involves using another scalar that is measured with a fast response sensor and then estimating the reduction in flux that results if a digital filter is used to simulate response time of the slower instrument.

EC is used extensively to measure sensible and latent heat fluxes, and has recently been used for networks dedicated to quantifying carbon dioxide fluxes from various landscapes (Baldocchi, 2003). Commercial fast response instruments are available for some compounds (e.g. CO_2, ozone, isoprene) and others can be built for other chemical species. EC is generally preferred as the most direct method which does not require parameterizations. Fluxes of VOC with short lifetimes can be estimated from flux divergence measurements (Lenschow et al., 1980).

Wyngaard and Brost (1984) proposed that the surface fluxes could also be estimated from measurements of vertical concentration profiles in the daytime mixed boundary layer (MBL) that lies above the surface layer and can extend up to several km. This method assumes that the mean vertical gradient of a VOC in the MBL is determined by the depth of the MBL (z_i), the convective velocity scale (w^*), and the fluxes at the bottom and the top of the MBL. We used vertical profiles of temperature and humidity measured during "saw-tooth soundings" (steep climbs through PBL and part of the free troposphere [e.g. up to 3 km] at a constant angle followed by the similarly steep decent) to directly characterize z_i and measured sensible heat fluxes to quantify w^*. The MBL gradient-flux technique assumes that boundary layer mixing is dominated by convective turbulence and that boundary layer conditions evolve slowly compared to the convective turnover time of about 10 minutes. The results are not affected by vertically homogeneous horizontal advection or time dependence in the mean concentration and the method can account for entrainment.

A time scale at a fixed point in the PBL can be related to a length scale by multiplying the time scale by the average wind speed, as long as the "frozen turbulence" hypothesis known as Taylor's hypothesis (e.g. Panofsky and Dutton, 1984) is fulfilled. This hypothesis enables approximate conversion from turbulence's temporal to spatial statistics. Since aircraft can fly an order of magnitude faster than the mean wind, Taylor's hypothesis is more easily fulfilled, so the length scales can be calculated by multiplying the measured time scale by the true airspeed.

3.5.2.1 Area source emission measurements

Area source emission was measured using the airborne eddy covariance technique. Eddy covariance was used to directly measure fluxes of predetermined compounds. Because quadrupole systems analyze mass to charge ratios sequentially, only several compounds can be selected for inclusion into the flux mode to keep the disjunct gap relatively small. As the project was focused on California vegetation and in particular oak woodlands, the number of masses ranged from three to six during eight research flights. Isoprene (*m/z* 69) was measured on all the eight research flights, MVK+MACR (*m/z* 71) and methanol (*m/z* 33) on seven flights. Other VOCs measured on a smaller number of flights included monoterpenes (m/z 81, 137), MBO (m/z 87), acetaldehyde (m/z 45), benzene (*m/z* 79), toluene (*m/z* 93), and C8-aromatics (*m/z* 107). Spatially resolved eddy covariance fluxes were calculated using Wavelet Analysis (Mauder et al., 2007) along flight tracks through the mixed layer. The horizontal spatial resolution depends on the blending height (e.g. Claussen M, 1990), which can be calculated according to $(u^*/U)^2 \times L$. (u^* - friction velocity, U – horizontal wind speed at blending height, L – horizontal scale of the surface heterogeneity).

According to Lenshow et al. (1994) the altitudes and speeds must be low to keep the random and systematic errors minimal. For example, our CIRPAS twin otter aircraft flew on average at about 400 m altitude and lower at approx. 60 m/s speed which boosted the overall sensitivity for VOC fluxes by several factors compared to faster and higher-flying aircraft. The low altitudes at CABERNET resulted in footprints of the order of the resolution required for validating model landcover inputs (e.g. 1-2 km).

3.5.2.2 Corrections related to aircraft motion

After each research flight, in-flight calibrations of the radome pressure system were performed by conducting a side slip and pitch maneuver (e.g. Lenschow et al., 1978). Reverse heading and speed maneuvers were conducted during the test flight. Figure 7 shows corrected vertical wind velocity during a side slip and pitch maneuver.

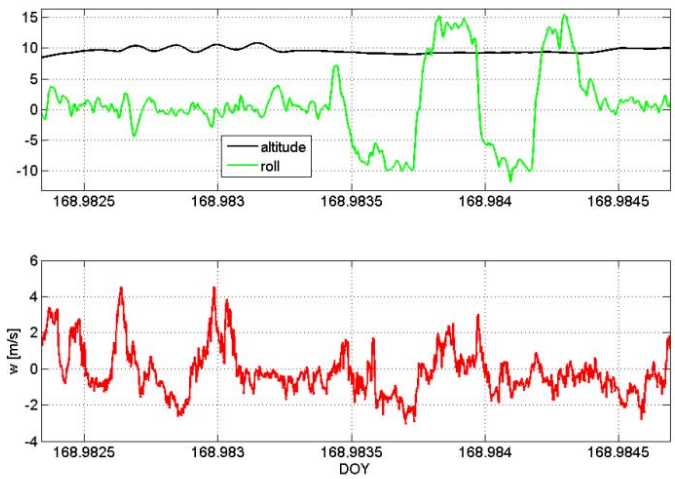

Figure 7. Side slip and pitch maneuver during RF6: Top panel depicts normalized roll and altitude signals, lower panel plots the motion corrected vertical wind speed *w*.

3.5.3 Airborne virtual Disjunct Eddy Covariance (AvDEC)

The difference between virtual and conventional disjunct eddy covariance is that sampling flow is continuous but the dataset becomes disjunct because the quadrupole detector cycles through the *m/z* sequentially, producing regular gaps between high-frequency data points. For the small number of *m/z* scanned by the PTR-MS detector, AvDEC measurements are nearly equivalent to continuous AEC. In order to minimize the disjunct error the relative gap vs. sampling frequency should be kept minimal by limiting the number of *m/z* in the duty cycle and keeping the integration time long. We kept the number of VOC-related *m/z* between 3 and 6 at 0.1 s dwell time. In addition, on each flight, we monitored three control masses: hydronium ions (*m/z* 21), oxygen ions (*m/z* 32), and water vapor (*m/z* 37) at 0.1, 0.05, and 0.05 s, respectively, so the total cycle length varied from 0.5 to 0.8 s between different flights.

Generally slow aircraft speeds can reduce the bias due to disjunct sampling strategies. Following Lenschow et al. (1994), we calculate the relative error of fluxes measured by the disjunct eddy covariance method. The integral timescale (Γ) obtained from figure 1 is 1.66 s, which at an airspeed of 60 m/s, comes close to a length scale of 100 m. The disjunct sampling interval (Δ) divided by Γ was therefore 0.3. The error ($\delta F_{disjunct}$) due to disjunct sampling, where the averaging interval (T) is much larger than Γ, can therefore be calculated in its asymptotic form, where Δ < Γ:

$$\delta F_{disjunct} = 2 \cdot \frac{\Gamma}{T} \qquad (3)$$

Equation 4 leads to $\delta F_{disjunct}$ of 6 $^{0}/_{00}$ for RF6 and RF7 and 2.5 $^{0}/_{00}$ for RF3. We conclude that a disjunct sampling interval of 0.5 s was sufficiently small to have a negligible effect on the calculated fluxes.

We deploy conventional fast fourier transform (FFT) and wavelet analysis to investigate turbulent fluxes. Briefly, following general considerations outlined by Torrence and Compo (1998) and considering bias rectification proposed by Liu et al. (2007), we implemented a wavelet transformation routine using the Morlet wavelet (Thomas and Foken, 2005). Two advantages of wavelet transforms include that (1) it does not rely on the ergodic hypothesis and therefore does not require stationarity, and (2) it allows investigating time resolved spectral contributions to the measured flux. Figure 8 shows a typical example of a normalized power spectrum for sensible heat and isoprene flux using conventional FFT and wavelet transformation. It should be noted that the spectral analysis of VOC data is limited to the Nyquist frequency imposed by the disjunct sampling interval of 0.5 s. Integrated co-spectra (i.e. fluxes) typically agreed to within ± 10% between FFT and wavelet transforms for the profiling flights. The rationale for using wavelet analysis is that a substantial part of the CABERNET mission was dedicated to the investigation of horizontally segregated patterns of isoprene surface fluxes (Chapter 5).

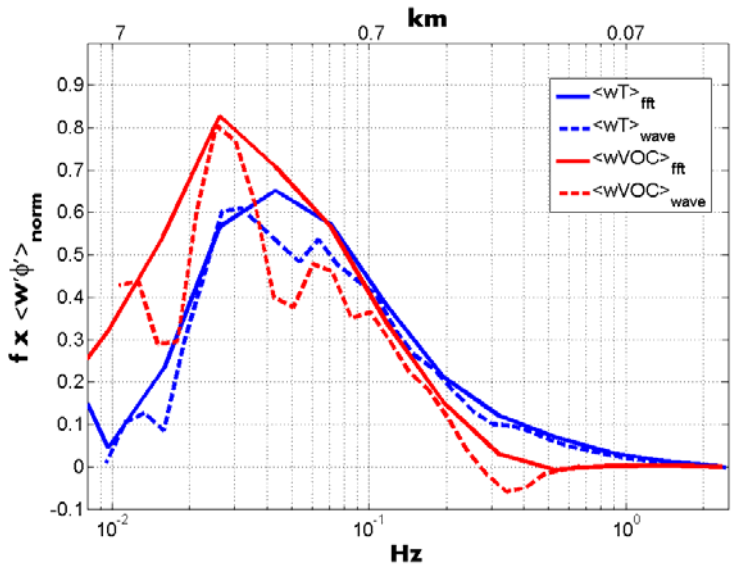

Figure 8. Normalized cospectra of isoprene (red) and temperature (blue) with vertical wind. Dashed lines indicate spectra calculated by wavelet transformation, solid lines are obtained by conventional FFT. The top axis indicates the spatial scale corresponding to an aircraft speed of 70 m/s.

The advection flux was calculated parallel and perpendicular to each racetrack. For RF03, RF06 and RF07 the advection fluxes were on the order of 28%, 4.9% and 3.8% relative to the average turbulent flux of isoprene. Due to a limited vertical resolution of 3 levels in total and only two obtained in the PBL at z/zi = 0.7 and z/zi=0.95 , further analysis of concentration gradients will therefore mainly focus on RF6 and RF7.

Sufficiently strong north-westerly winds during RF6 and RF7 prohibited the establishment of the Fresno eddy (e.g. Lin et al., 1995) leading to consistent upslope winds during these research flights. Profiles were flown during cloud-less conditions.

3.5.4 Fast Fourier Transform (FFT)

Fast Fourier Transform (FFT) is the conventional method to compute airborne flux. This method provides a single value for a given segment of flight, which limits the spatial resolution. The optimal integration stretch would be a sufficiently long pass to capture the optimal range of frequency distribution, but not so long that the turbulent structures are affected by diurnal effects. Therefore, resolution finer than 10 km would be challenging and uncertain using the FFT approach. Another challenge in this method is that it is prone to non-

stationarities. However, as an independent method it can be very useful for comparison with fluxes obtained from wavelet analysis (see Sect.3.5.5).

3.5.5 Continuous Wavelet Transform (CWT)

Wavelet analysis, originally demonstrated to work with seismological data, has recently become increasingly popular in environmental and biological applications. Examples can be found in the analysis of the turbulent structures (Thomas and Foken, 2005; Mauder et al., 2007; Steiner et al., 2011; Metzger et al., 2013), and analysis of environmental processes at multiple scales (Stoy et al., 2009; Vargas et al., 2010).

The mathematic principle for the one-dimensional wavelet transform of a given signal $f(t)$ can be presented as:

$$T_p(a,b) = \int_{-\infty}^{+\infty} f(t)\overline{\Psi_{p,a,b}(t)}dt\,, \qquad (4)$$

where T_p(a,b) are wavelet coefficients and $\Psi_{p,a,b}(t)$ is the wavelet function given by:

$$\Psi_{p,a,b} = \frac{1}{a^p}\Psi\left(\frac{t-b}{a}\right), \qquad (5)$$

where Ψ $((t-b)/$a) is termed "the mother wavelet", of which shape and locations are determined by the scale parameter of the wavelet a and by the translation parameter b. The normalization factor $1/a^p$ keeps the energy of the original mother wavelet (for p=1). A general description of wavelet methodology can be found in Torrence and Compo (1998). For example, the Mexican-Hat mother wavelet works well with detection of single events, for example in the analysis of coherent structures of ejections and sweeps from a closed-canopy forest (Steiner et al., 2011). On the other hand, the complex Morlet function wavelet is suited to analysis of variance spectrum (Thomas and Foken, 2007). Nordbo and Katul (2013) looked at periodicities of long-term CO_2 fluxes from soil. They showed that the intrinsic smoothing property of the wavelet produces results that are more easily interpretable, without the need of excessive manipulation of the original signal (e.g. averaging, smoothing, and tapering) or without restrictive assumptions (e.g. periodicity, stationarity).

The CWT method has an advantage over FFT in that it does not require homogeneity or stationarity, and can reconstruct the time domain to provide specific information on where in space/time and on which frequency the flux occurs. The wavelet flux method allows for the reconstruction of both the frequency and time domains of the flux within an integrated straight stretch of the desired length, and therefore can produce "instantaneous" or "discrete" fluxes which can be directly compared with model estimates. From the pragmatic point of view, integration of a stretch or a flight segment (e.g. of 100 km) results in not just a single flux value but delivers spatially resolved fluxes at discrete intervals sometimes informally referred to as instantaneous fluxes. Considering the footprint and wavelet scaling parameters, it is possible for an aircraft flying low at approximately 60 m s^{-1} to provide meaningful spatial flux representation at the 1-2 km resolution needed for investigating landscape heterogeneity in high resolution biogenic emission models, although in principle even shorter intervals could also be resolved. An average of the wavelet fluxes can be compared to the Fourier flux from the same stretch. Given the independent approaches, the agreement between the methods adds to the confidence of the flux estimates and the ratio can be used as an additional measure of data quality.

Finally the cross-spectra from the two methods can be compared. If no high-frequency attenuation losses exist, the cross-spectra should be similar. The wavelet approach can also be used for the correction of the FFT high-frequency spectral attenuation if it is related to tubing effects or factors other than the instrument response (Nordbo and Katul, 2013). Here, as the mother wavelet we used the Morlet wavelet. More detailed methodology of wavelet analysis used in this work has been presented by Karl et al. (2013) which was a further development from Karl et al. (2009). Vertical flux divergence of isoprene is expected to be primarily controlled due to its relatively short lifetime and was measured directly using "racetrack" profiles at multiple altitudes. It was found to be linear and in the range 5% to 30% depending on the ratio of aircraft altitude to PBL height (z/z_i). We estimated the contribution of the storage term to the isoprene flux divergence to be of the order of 2-5%, negligibly small compared to sensible heat fluxes. Fluxes were generally measured by flying consistently at 400 m ±50 m (a.g.l.) altitude, and extrapolated to the surface according to the determined flux divergence. The wavelet coefficients were optimized for the CWT analysis to perform well on

stretches between 15 and 200 km with a typical ratio of FFT single flux value to CWT instantaneous flux average of between 1.0 and 1.3.

3.5.6 Flux footprints

The footprint for each flux point was derived using the Horst and Weil (1992) approach and depends on the wind speed, relative altitude to the PBL height, and the convective velocity scale. Here we use scaling developed for the mixed layer according to:

$$dx_{0.5} = 0.9\frac{u \cdot z_m^{2/3} \cdot h^{1/3}}{w^*}, \qquad (6)$$

where $dx_{0.5}$ is the half width of the horizontal footprint, u the horizontal windspeed, z_m the height above ground, h the PBL height and w^* the convective velocity scale which is derived from the wavelet heat flux in each transect.

The source contribution area can be approximated by projecting an upwind-pointed half dome with the $dx_{0.5}$ parameter representing a radius of that half dome.

As an example this leads to a footprint of 3.1 km for h=2000 m, z_m=1500 m, u = 3.5 m/s and w^* = 1.7 m/s encountered during RF6. The upwind fetch was on the order of 12 km for RF6 and RF7.

The footprint is represented by the half-widths which can be regarded as a distance between the points of the Gaussian curve where the flux falls to the half of its maximum. Therefore, the flux contribution is not the same within the halfwidth. The area of such a footprint is approximately 90% of the flux contribution relative to the entire footprint (the full Gaussian). This approximation assumes a symmetrical footprint, but in reality the footprint area is larger along the direction that the wind is blowing.

3.5.7 Error analysis (quality of fluxes)

As with eddy covariance on the ground, AEC fluxes must undergo a rigorous quality assessment, if not more so. The total uncertainty in reported airborne flux is the superposition of errors from calculation of concentrations (10% for calibrated compounds [5% standard accuracy+5% dilution system], 30% from relative lab-based sensitivity-relative transmission

approach), survey-flight-specific random (5%) and systematic (1%) errors related to relative altitude within the PBL and to the aircraft leg, random error related to disjunct measurement (less than 1%). For reactive tracers which require divergence corrections to yield the surface flux, uncertainty in PBL estimation (interpolated from saw-tooth soundings) is +/-100 m which translates to 10% of up to 30% of the divergence correction, thus ~3%. We estimate the total accuracy for the reported surface fluxes to be 20% for calibrated compounds and 40% for other compounds.

The calibrated concentration data filtered for interferences (e.g. a biomass burning episode; see supplementary video) were used with corrected vertical wind speed data to derive covariance functions for each eligible stretch. The segments to be integrated (see example in Figure 9) were selected based on constant roll angle of the aircraft between turns, and on consistency of altitude, excluding maneuvers with significant altitude changes such as soundings.

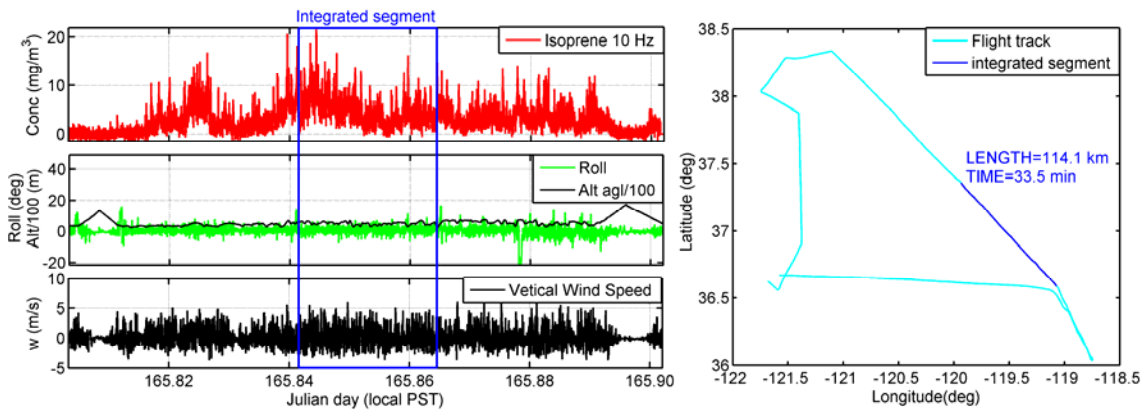

Figure 9. Example of a segment integration based on roll to exclude turns and altitude to exclude large changes in altitude such as sawtooth soundings.

Of segments prescreened for validity, only those with a clear peak in the covariance function (Figure 10a) within the lag-time window of 5 s were accepted. The segment data were subsequently examined for similarities in the variances of concentration and vertical wind speed (Figure 10b) together with the time series of wavelet frequency cross-spectra (Figure 10c) within the cone of influence (COI) which is the region where the end of the power spectrum may be impacted by edge effects. Rather than excluding the part falling outside the COI, each of the ends of the time series are padded with zeros and excluded afterward, so the

results are not affected by the COI. By comparing the wavelet cross-spectra with average cross-variance (Figure 10d) it is possible to determine where in the wavelet period (inverse of frequency) the flux contribution occurs, enabling for example the visualization of the updrafts associated with high emissions.

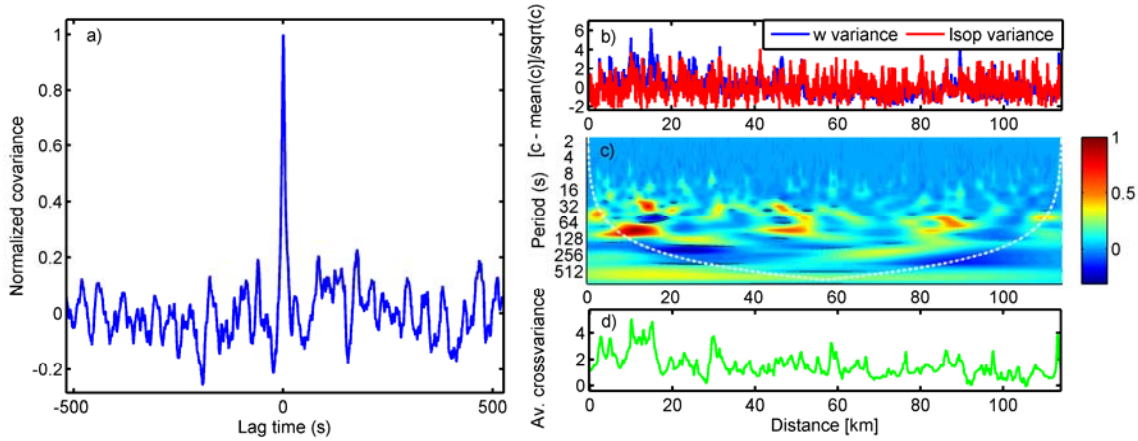

Figure 10. Flux quality control for an example flight leg (the segment from Figure 2). a) Clear peak in the covariance function; b) variances of w and isoprene; c) time-resolved wavelet cross spectra; and d) average cross-variance.

Each stretch was finally analyzed for spectral characteristics, independently for the FFT and CWT methods (see Figure 11). Identical procedures were applied to the fast temperature sensor for comparison. As the cross-spectra and ogives demonstrate, the VOC sampling system was not limited by high frequency attenuation owing to the short 0.1 s dwell time and small number of preselected VOCs in the quadrupole mass spectrometer cycle. It was found that the majority of the flux contribution (~90%) was occurring between between 0.1 and 0.01 Hz which translates to the spatial scales of 0.6 to 6 km.

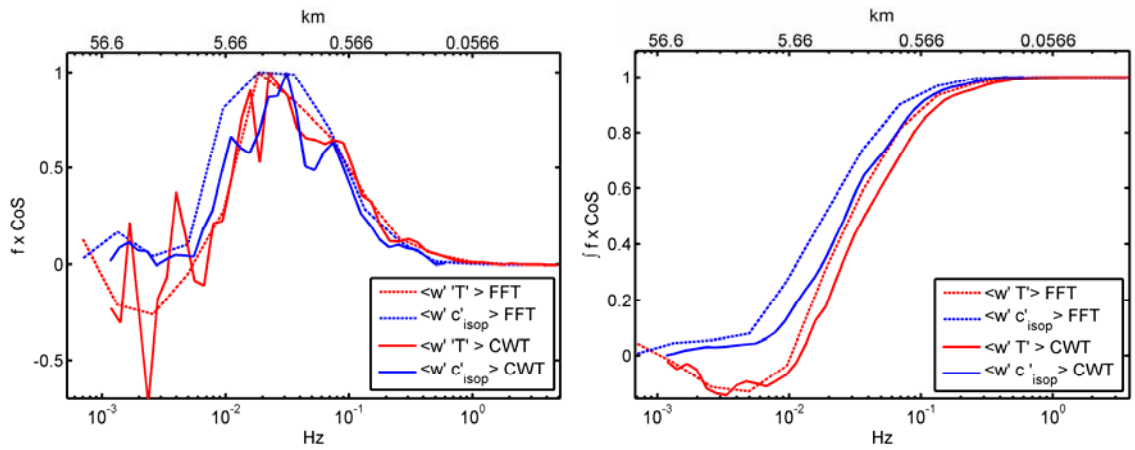

Figure 11. Spectral quality control of the example flight segment. Left panel: Comparison of cross spectra for isoprene flux and heat flux using the FFT and CWT methods independently; Right panel: Cumulative cross spectra for isoprene flux and heat flux using the FFT and CWT methods independently.

Additional quality measures were the ratio of the FFT and CWT fluxes (Figure 12, upper panel), which for isoprene were usually 1 ± 15% for survey transect flights. Identical values from the two methods were not expected as the FFT flux is affected by nonstationarities and inhomogeneities in contrast to the CWT flux, but the generally good agreement adds confidence to the results. Occasionally, a ratio higher than 1.15 was seen on short segments, or over a nonhomogeneous transect, or when the fluxes were close to zero. In sporadic cases when the fluxes were strongly non-stationary (characterized by the ratio higher than 1.3), the FFT flux was tagged as rejected and the CWT flux was only accepted if all the other quality criteria were fulfilled.

The generally good quality of fluxes in CABERNET was due to a combination of factors such as instrument sensitivities, response times, slow aircraft speeds and proximity to the source by flying at relatively low altitudes and finally lack of spectral interferences (e.g. from propellers). Figure 12 (lower panel) shows the application of flux divergence (only reactive compounds such as isoprene) coefficients from racetrack profiling to derive the surface fluxes from the aircraft fluxes. In the remainder of the manuscript when discussing fluxes, we focus exclusively on the CWT fluxes due to the much higher spatial resolution of the flux and also because of their higher accuracy in cases with inhomogeneity and non-stationarity.

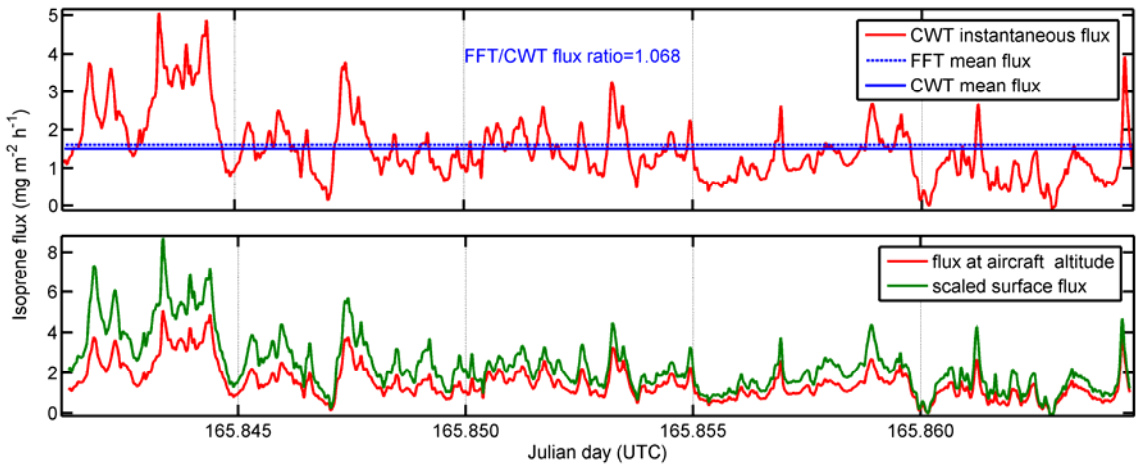

Figure 12. Isoprene flux processing. Upper panel: determination of the FFT/CWT flux ratio; lower panel: application of flux divergence coefficients (derived in racetrack profiles) to scale fluxes from aircraft altitude to surface fluxes using aircraft altitude and PBL height.

3.6 Simultaneous ground measurements

Ground based measurements coinciding with aircraft passes in time and space were performed at two sites: The 525-m tall Hearst-Argyle Tower in Walnut Grove, California (WGC) located in the San Joaquin Delta region (38.2636, -121.4899, elevation 1 m) and the 23-m tall Tonzi Ranch Tower (TRT) (38.4308, -120.9656, elevation 177 m) located in the relatively homogenous oak forest savannah between the Sierra Nevada foothills and the San Joaquin Delta.

3.6.1 Walnut Grove Tower

A PTR-MS was measuring vertical profiles of VOC concentrations at WGC as part of a separate study and we flew by the tower on RF 2 and RF 4 to take advantage of the opportunity to intercompare measurements. The vertical profile data from WGC also provides a broader perspective on the diurnal cycle and vertical distribution of BVOCs over California's Central Valley than can be obtained from the aircraft data which focused almost exclusively on midday and a specific altitude.

Briefly, the setup at WGC featured a PTR-MS analyzing air from 5 different heights (10, 131, 262, 394 and 525 m) for 2 min at each level per 10 min measurement cycle. There were 24 *m/z* monitored at 0.1 s dwell time each. The measurement footprint of the Tower increases with height and the top levels can pick up VOCs from the Central Valley's extensive agricultural, industrial, wetland, dairy, biomass burning and other activities from as far as the San Francisco Bay area hundreds of km away. The immediate vicinity of several km are mostly farmlands and wetlands with patchy biogenic sources constituted by mixed deciduous trees and broadleaf trees such as California Laurel (*Umbellularia californica*) therefore being only a small relative portion of the footprint at lower levels. The twin otter flew close to the tower on RF2 and more closely on RF4 (13:18) at 513 m (during an initial climb before the tooth sounding) coinciding with the sampling of the tower at the top level (525 m) for which the intercomparison is shown in Chapter 5.1.5.

3.6.2 Tonzi Ranch Tower

Tonzi Ranch tower is part of the FLUXNET long-term flux measurement network (Baldocchi and Ma, 2013; Baldocchi et al., 2006). During CABERNET, BVOC fluxes were measured for the first time at this site using a compact relaxed eddy accumulation (REA) system custom built by NCAR and deployed at 23 m height to measure half-hourly flux data. The aircraft flew near the tower during RF2 and RF3. The closest flights which were compared passed right above the tower on June 9 at 11:41:15 at 280 m a.g.l., and on the returning leg on the same day at 13:33:19 at 410 m a.g.l. The intercomparison is discussed in Chapter 5.2.2.

3.7 Our modeling approaches

Modeling of BVOC emissions involves a framework including emission factors, short-term and long-term emission algorithms and a canopy environment model, along with data bases of landcover and meteorological driving variables (Figure 13). We explored use of the following models and input databases to simulate isoprene emissions for California:

1) BEIGIS (California ARB Model) using the GAP landcover database for oaks, with Forest Inventory Analysis (FIA, USGS product) species composition

2) MEGAN 2.0, landcover 2.1 (Guenther et al. 2006) based on WestGAP landcover database and FIA

and

3) MEGAN 2.1, landcover 2.2 (Guenther et al. 2012) – based on the NLCD/FIA/plant functional type (PFT) datasets. As this model provided the most currently advanced landcover, this model was thoroughly explored, and it was then adapted and used by CARB and UC Berkeley to evaluate statewide emissions estimates of isoprene in comparison to our CABERNET measured fluxes.

These three model architectures are extremely similar because they all evolved from the same roots. Differences between the model outputs occur mainly due to differences in the landcover driving variables (plant species composition, leaf area index) and meteorological driving variables (light, temperature). When comparing different models with observations, it is important to first determine the effects of different input variables that are used and perform extensive sensitivity studies. The resolution and evaluation of these driving variable databases is particularly critical in the areas close to the mountains that typically have high gradients of temperature and where meteorological stations may not be as densely spaced compared to near the urban areas or where gradients in temperature are smaller. Since the major isoprene source regions in California are predominantly oak savannas in the foothills where temperature estimates are uncertain, this can lead to a major contribution to uncertainties in isoprene emission estimates.

To evaluate the accuracy of the landcover used as the basis for the models' emission factor, we used the 2km resolution measured flux data normalized for temperature and PAR according to the Guenther et al. (2006) algorithm to create "observed" CABERNET airborne basal emission factors (BEFs). To evaluate the meteorlogical driving variables, we compared hourly temperature data simulated by the WRF 4x4 km model with available weather station data along some of the CABERNET flight tracks.

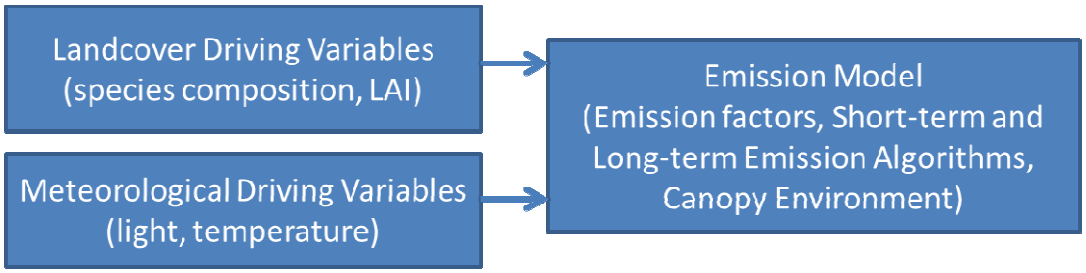

Figure 13. Simplified diagram showing the basic modeling process

.

3.7.1 Models used

3.7.1.1 BEIGIS

The Biogenic Emission Inventory processing model (BEIGIS) (Scott and Benjamin, 2003) was developed by CARB. BEIGIS uses California land use/land cover, leaf mass, and emission rate databases with a geographic information system (GIS), is a regional model specific to California, and is spatially resolved at 1 km^2 and temporally at 1 hour. The initial set of BEIGIS inputs includes GIS-based maps of land use and land cover types. They are based on a USGS Gap Analysis Project (GAP) biodiversity database which covers natural areas of California (Scott et al., 1993; Davis et al., 1995; Chung and Winer, 1999). The database was generated from summer 1990 Landsat Thematic Mapper satellite images, 1990 high altitude color infrared imagery, vegetation maps based on historical field surveys, and other miscellaneous vegetation maps and ground surveys. The urban and crop areas are not represented by the GAP database and use independent maps. These maps are subsequently used to assign mostly branch-scale emission factors which in the case of GAP covered areas come from a compilation by Benjamin et al. (1996) and a specific leaf weight (to convert LAI to biomass density) database (Nowak et al., 2000) . The landscape emission factor layers are subsequently formed and are used with environmental correction algorithms (Guenther et al., 1993; Harley et al., 1998) using hourly temperature and solar radiation datasets gridded at 4 km^2. A canopy environment model is not used in BEIGIS, and it is assumed that the branch-scale emission factors account for shading and canopy environment effects.

The model has many similarities to the predecessor of the MEGAN model (Guenther et al., 1993, 1995) since it is using similarly derived emission factor maps (GAP/FIA, branch-scale emission factors) and a similar framework for application of light and temperature algorithms, except that the BEIGIS model was specifically optimized for California. This includes using an 8-day LAI and phenology database, where specific phenology masks are applied to deciduous trees and shrubs, grasses and herbaceous plants to turn on and off their emissions at different times of year, while evergreen trees and some shrubs are assumed to have emissions all year.

3.7.1.2 MEGAN 2.0

The Model of Emissions of Gases and Aerosols from Nature (MEGAN) v. 2.0 (Guenther et al., 2006) was used in the initial stages of our study to plan CABERNET flight tracks and was also tested in the early stages of measurement model comparisons using the observed airborne BEFs. MEGAN is designed for both global and regional emission modeling and has global coverage with 1 km^2 spatial resolution. This version of MEGAN defined emission factors as the net flux of a compound into the atmosphere which was intended to account for losses of primary emissions on their way into the above canopy atmosphere. The model uses an approach that divides the surface of each grid cell into different PFTs and non-vegetated surface. The PFT approach enables the MEGAN canopy environment model to simulate different light and temperature distributions for different canopy types (e.g., broadleaf trees and needle trees). In addition, PFTs can have different LAI and leaf age seasonal patterns (e.g., evergreen and deciduous). MEGAN2.0 accounts for regional variations using geographically gridded databases of emission factors for each PFT. The standard MEGAN global classification included 7 PFTs, but for regional modeling a classification scheme can have any number of PFTs.

3.7.1.3 MEGAN 2.1

The MEGAN version 2.1 model (Guenther et al., 2012) includes enhancements to MEGAN. The main architecture of the model is very similar (see Figure 14) but there are several significant differences in how emission factors are represented, deposition is accounted for (relevant for species such as methanol but not isoprene), more generic PFTs are used for global modeling, and most importantly a new land cover database (v.2.2) is included that was

derived by combining high resolution imagery (60 m, and 30 m) with species composition data. The base MEGAN version 2.1 land cover v.2.2.includes more than 2000 ecoregions which allows the emission factor for a PFT (e.g. temperate needleleaf trees) to differ in each region. The MEGAN landcover product is further described in Sect. 3.7.2.1.

While the previous version of MEGAN (v2.0) defined emission factors as the net flux of a compound into the atmosphere, the MEGAN2.1 emission factor represents the net primary emission that escapes into the atmosphere but is not the net flux because it does not include the flux of chemicals from the above canopy atmosphere down into the canopy. Emission factors based on scaled up leaf level emissions inherently exclude the deposition component. In order to use above canopy flux measurements to establish emission factors, an estimate of the deposition flux is added to the above canopy flux measurements to determine the MEGAN2.1 emission factors. For isoprene this deposition flux estimate is equal to zero.

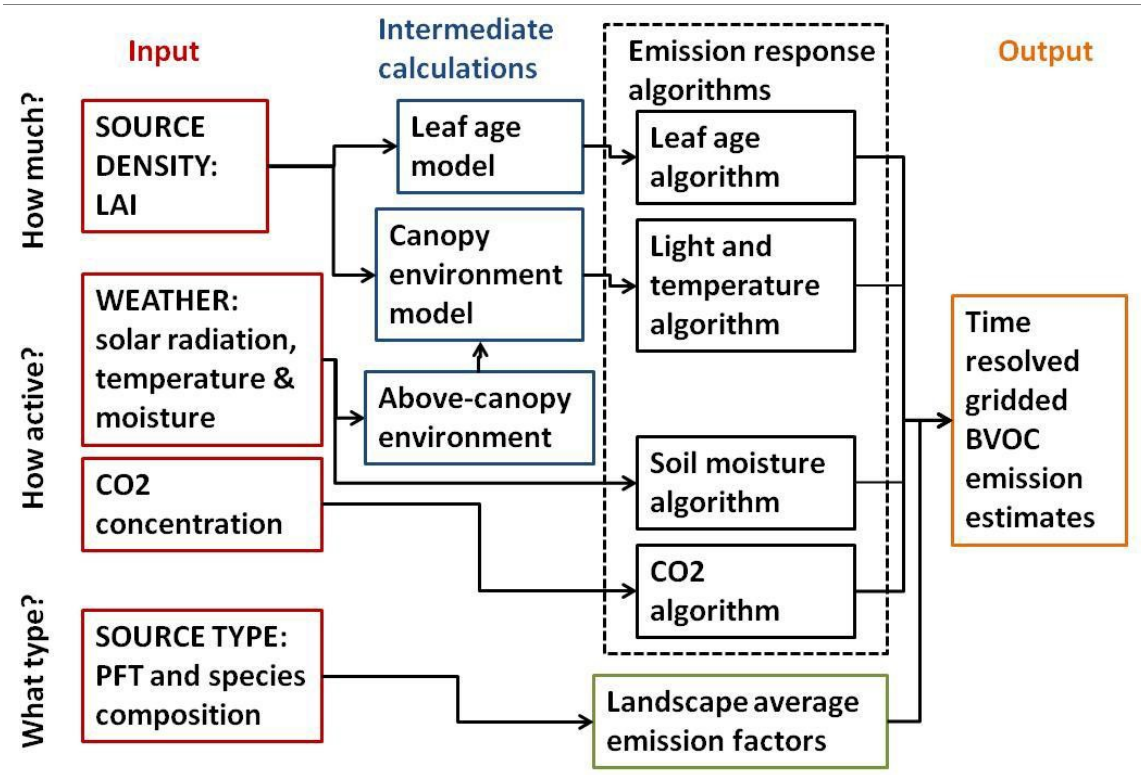

Figure 14. Schematic of MEGAN 2.1 model components and driving variables (taken from Guenther et al., 2012)

3.7.1.4 CARB's MEGAN 2.1 adaptation

The MEGAN2.1 model as described in Section 3.7.1.3 is run at 2 km^2 resolution using meteorology at 4 km^2. This adapted version incorporates the advances in MEGAN2.1 into the CARB's modeling infrastructure. This model most closely agreed with the measured fluxes and was thus used for the final model – measurement comparison. This model is also currently used for all BVOC emission modeling by CARB. The model fluxes for exact times and footprints to simulate observed fluxes are calculated in the GIS environment as follows:

1) convert the grid cell emissions to grid cell fluxes

2) calculate the area weighted average flux (based on intersecting the grid with the flux footprint)

3) convert the flux to an emission rate by multiplying by the ArcGIS area for each flux footprint.

The flux footprint corresponding to each aircraft measurement is calculated as the half-width of the Gaussian (see earlier Sect. 3.5.6), and the halfwidth area acounts for 90% of the flux contribution. In order to account for the footprint's remaining emission contribution, 10% is added on top of each simulated grid emission.

3.7.2 Driving variables

When comparing BEIGIS with MEGAN2.0 it became obvious that the driving variables used with the models are much more important for prediction accuracy than the different model architectures. This is consistent with reports comparing different process-based models (e.g. MEGAN vs other global emission models) which differ in the modeling framework but give similar estimates when exactly the same input variables are used (Arneth et al., 2011).

3.7.2.1 Landcovers

The land cover used to drive the model has a critical influence on model performance because it defines the type of vegetation or PFT, land fraction, and finally determines the emission factor. Up-to-date land cover products should give more accurate results because the land cover can change due to growing and senescing vegetation, fires, and land-use change or plant species composition change. The airborne flux measurement-model comparison provides an opportunity to identify any inaccuracies in landcover databases which can then be used to improve them.

Land covers used by the models in this study are presented in Figure 15. The GAP database (see Sect. 3.7.1.1) can be used to construct the spatial distribution of oak woodland areas (Figure 15a), and these are extremely similar to the BEIGIS emission factors (Figure 15b) which were based on GAP. While the global MEGAN2.0 landcover 2.1 (Figure 15c) was also based on FIA and WestGAP datasets and interestingly showed almost identical EF means for isoprene as BEIGIS isoprene EFs, the standard deviations were much different with EF distribution that were more smoothed out across many areas of California. The latest MEGAN2.1 landcover 2.2 (Figure 15d) is a state-of-the-art product which showed the most accurate match with airborne fluxes (see Sect. 6). This land cover is based on a high resolution (60 m) PFT database using the CLM4 PFT scheme generated for the US for the year 2008 and is available with the MEGAN2.1 input data (http://bai.acd.ucar.edu/MEGAN/) (Guenther et al., 2012). The database was created by combining the National Land Cover Dataset (NLCD, Homer et al., 2004) and the Cropland Data Layer (see http://nassgeodata.gmu.edu/CropScape/), which are based on 30-m LANDSAT-TM satellite data, with vegetation species composition data from the Forest Inventory and Analysis (www.fia.fs.fed.us) and the soil database of the Natural Resources Conservation Services (http://sdmdataaccess.nrcs.usda.gov/). The processing included adjusting the NLCD tree cover estimates in urban areas to account for the substantial underestimation of the LANDSAT-TM data (Duhl et al., 2012). This was accomplished using the regionally specific adjustment factors for urban NLCD developed by Greenfield et al. (2009) using high resolution imagery.

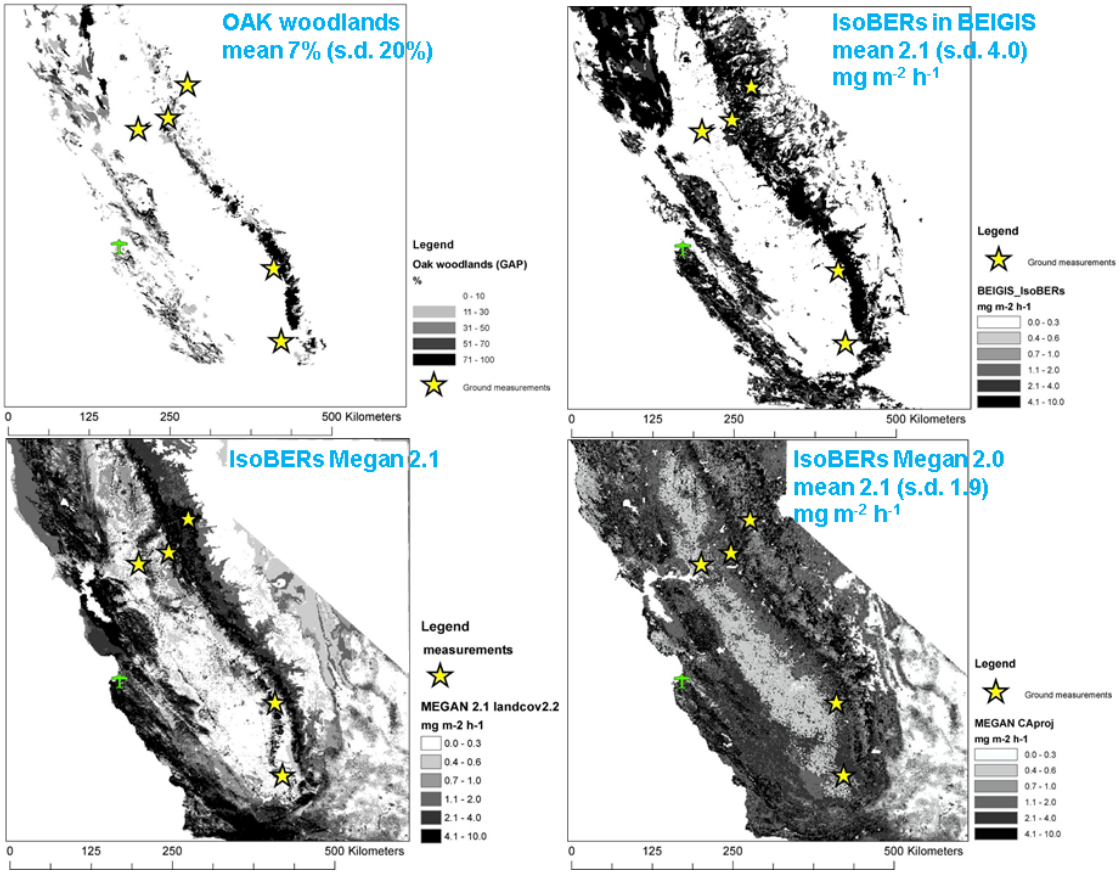

Figure 15. Example land covers available for models. a) GAP's oak woodlands, b) BEIGIS emission factors (as dtiso+eiso) derived from the GAP/FIA database, c) MEGAN2.0 isoprene emission factors derived from landcov2.1, and d) MEGAN2.1 isoprene emission factors obtained from the most recent landcover2.2.

A CAIN database from the UC Davis repository (http://cain.ice.ucdavis.edu/caml) contains exactly the same habitats as the GAP database but was independently derived. The CAIN database augmented several datasets linked to the National Biological Information Infrastructure (NBII) which was linked to the Fire Resource and Assessment Program (FRAP). This database was also based on the FIA, and complements the GAP database, in particular in southern CA. The northwest region of CA is more extensively represented by GAP. Combination of the GAP and CAIN dataset therefore is useful in the context of BVOC emission modeling in California.

Another data base that may be useful for representing vegetative areas of California but has not been used as extensively is the "Existing Vegetation Data" product called CALVEG

developed by USGS (http://www.fs.usda.gov/main/r5/landmanagement/gis). In addition there are multiple independent databases compiled as "vegetation collections data sets"(available at: http://daac.ornl.gov/cgi-bin/dataset_lister.pl?p=21) and vegetation data sets belonging to NASA's CASA model (http://geo.arc.nasa.gov/sge/casa/) that could be further explored for use in BVOC modeling.

3.7.2.2 Temperature and radiation

Hourly temperature data were simulated by WRF at 4x4 km resolution. Based on comparison (Figure 16) with weather station close to race-track profile in RF6 and RF7, we found that WRF spatial resolutions lower than 8 km^2 can lead to temperature inaccuracies of more than 3 ºC during peak periods. Similar conclusions were made by Yver et al. (2013). Another dataset that has been explored for the use in modeling was the remote infrared sensor on the airplane during the CABERNET flights (IRT Nad). However, this sensor was calibrated for the ocean skin temperature and significantly overestimated ground temperature with variable offsets, and therefore was not used in the analysis. For validation of WRF temperature data a California meteorological model (CALMET) was used by CARB (J. Avise). Despite mostly good agreement, areas were identified with large discrepancies. Since CALMET interpolates in 2D the temperature surface from the available met stations, inaccuracies may be expected in areas were stations are not densely represented. The approach which was found to be optimal was use of the 4 x 4 km WRF model nudged by CALMET. This approach was used to derive the temperature dataset applied here for comparison of emission factors and emission rates.

Photosynthetically Active Radiation satellite datasets used for modeling were those recently validated by Wang et al. (2012) and Guenther et al. (2012).

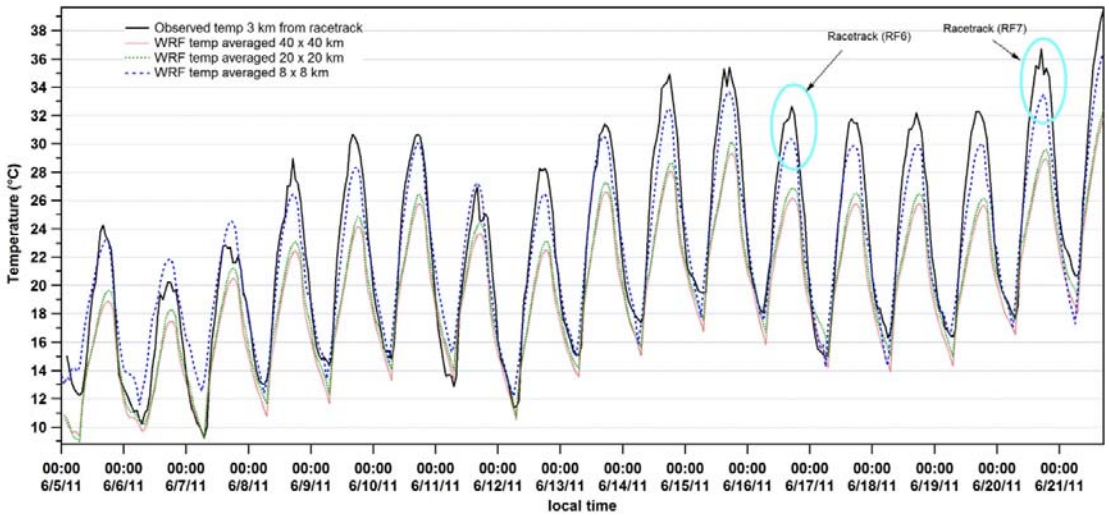

Figure 16. WRF's resolution effect on temperature bias.

3.7.2.3 LAI

The LAI dataset used was the current LAI from MODIS for the flight days.

3.7.3 Model domains

3.7.3.1 California

The CABERNET flights covered a large portion of the California including most of the areas with high densities of oak trees which are expected to dominate the statewide isoprene emissions. For comparison of emissions between different ecoregions, the entire flight tracks were used and assumed to be representative of the whole ecoregion for California.

3.7.3.2 Ecoregions

Ecoregions denote areas of general similarity in ecosystems and in the type, quality, and quantity of environmental resources (Griffith et al., 2011).

A map of California ecoregions is shown in Figure 17 overlaid with the CABERNET flight tracks. Most of the subecoregions (level IV) belonging to the 6th ecoregion (level III:Central California Foothils and Coastal Mountains) denoted in yellow were covered, as well as some

subecoregions of the 7th ecoregion (Central California Valley) in brown, 5th ecoregion (Sierra Nevada) in green, and the 14th ecoregion (Mojave Basin and Range) in pink. Of the 48 subecoregions flown over during the CABERNET campaign, 29 subecoregions were of the 6th ecoregion which comprises most of the oak woodlands in California.

The primary distinguishing characteristic of the 6th ecoregion is its Mediterranean climate of hot dry summers and cool moist winters, and associated vegetative cover comprising mainly of isoprene emitting oak woodlands. The 6th ecoregion also includes non/low- isoprene emitting chaparral and grasslands which occur in some lower elevations and patches of pine are found at the higher elevations. Surrounding the lower and flatter Central California Valley (7th ecoregion), most of the region consists of open low mountains or foothills, but there are some areas of irregular plains and some narrow valleys. Large areas in the 7th ecoregion are used as ranch lands and grazed by domestic livestock. Relatively little land in this ecoregion has been cultivated, although some valleys are major agricultural centers such as the Salinas area or the wine vineyard centers of Napa and Sonoma. Natural vegetation includes coast live oak woodlands, Coulter pine, unique native stands of Monterey pine in the west, and blue oak, black oak, and grey pine woodlands to the east (EPA, 2014).

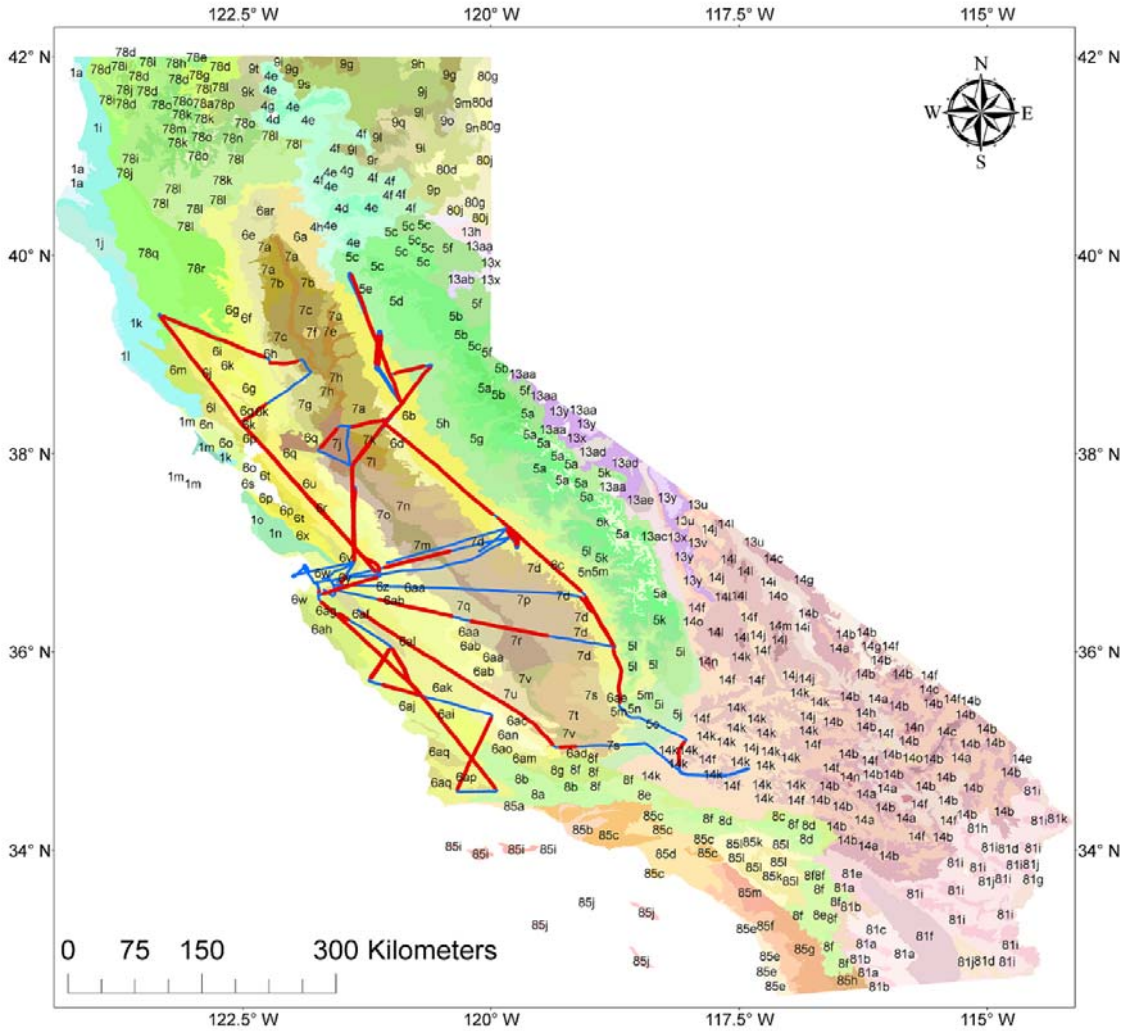
122.5° W
120° W
117.5° W
115° W
42° N
40° N
38° N
36° N
34° N
N
S
W
E
0 75 150 300 Kilometers

Figure 17.USEPA Ecoregion map with overlaid CABERNET flight tracks covering most of code 6 ecoregions The shapefiles used to produce the map in ArcGIS were downloaded from ftp://ftp.epa.gov/wed/ecoregions/ca/.

4 Experimental investigation of surface and entrainment fluxes, OH densities and Dahmköhler numbers *(published in Karl et al., 2013)*

4.1 Flux profiles

4.1.1 Heat and isoprene fluxes

Figure 18 depicts the average of all measured kinematic heat fluxes (<w'θ'> and <q'w'>) as well as isoprene fluxes for RF6. We generally define the height of the PBL as minimum of the <w' θ '> flux at the inversion. The <'w'q'> flux generally decreased at the inversion layer. The <w'q'> flux profile suggests a relatively wet PBL, when compared to the free troposphere (FT), and follows a very similar flux profile compared to idealized LES runs (e.g. Patton et al., 2004).

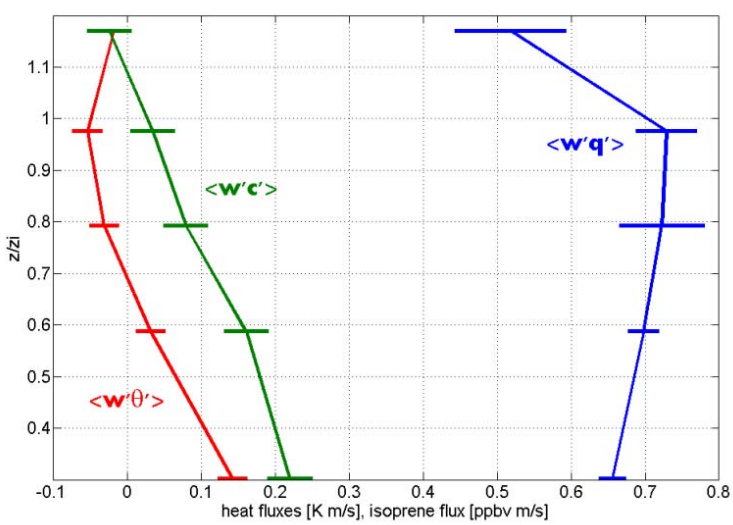

Figure 18. Kinematic heat (<w'θ'> - red ,<w'q'> - blue) and isoprene (<w'c'> - green) fluxes for RF6. Error bars (1sigma) indicate the variability of all flux profiles flown during RF6

Reducing the buoyancy flux equation to,

$$\frac{\partial <\Theta>}{\partial t} = -\frac{\partial <w'\Theta'>}{\partial z} \quad (7)$$

we can test whether the flux divergence of the buoyancy flux is comparable to the heating rate of the planetary boundary layer (PBL) by assuming a linear flux profile (<w'θ'> = a – b z). This leads to a simple expression where the heating rate is equal to the linearized PBL slope of <w'θ'> in Figure 18. From Figure 18 we obtain b=0.6±0.1 K. The observed temperature change $\frac{\partial <\Theta>}{\partial t}$ was 0.4±0.2 K. Isoprene fluxes linearly decrease throughout the PBL owing to its short atmospheric lifetime. From the slope we can calculate the lifetime, OH density and Damkoehler number, which is defined as the ratio of the mixing timescale to the chemical timescale. Table 2 summarizes these quantities for RF3, RF6 and RF7. Calculated entrainment velocities were 5.5, 9.6 and 1.4 cm/s for RF3, RF6 and RF7 respectively.

Table 2. Summary of PBL height, w^*, τ, OH densitiy, Damkoehler number, isoprene fluxes and entrainment velocity for RF3, R6 and RF7.

	PBL height [m]	w^* [m/s]	T [s]	OH [molecules/cm^3]	Da	F (z/z_i) [ppbv m/s]	v_e [cm/s]
RF3	1000±100	2.0±0.3	2300±50	(4.4±0.3)E+06	0.2	-(0.32±0.08) * z/z_i + (0.33±0.08)	5.5±1.0
RF6	2000±100	1.7±0.3	1520±50	(6.6±0.3)E+06	0.9	-(0.31±0.05) * z/z_i+(0.28±0.05)	9.6±1.5
RF7	1200±100	2.0±0.3	1400±50	(7.2±0.3)E+06	0.5	-(0.21±0.03) * z/z_i +(0.22±0.03)	1.4±0.3

In-situ OH observations still remain challenging (Mauldin et al., 2012, Williams et al., 2011) and recent debate about the magnitude of the oxidizing capacity of the atmosphere in isoprene dominated environments has fueled speculation about unknown OH recycling mechanisms (Lelieveld et al., 2008, Hofzumahaus et al., 2009). Vilà-Guerau de Arellano et al. (2011) performed a sensitivity analysis illustrating the interrelationship between physical and chemical constraints on OH loss and production rates in the PBL; they suggest that vertical transport terms need to be considered when interpreting field datasets of isoprene concentrations. Our measurements demonstrate that the isoprene flux divergence follows a linear dependency as has been suggested previously by LES modeling studies (e.g. Vinuesa,

2003). In addition, we show that isoprene flux divergence measurements can be successfully used to assess the average oxidizing power of the PBL without any assumptions. We estimate OH densities in the range of 4 – 7 x 10^6 molecules / cm^3. Damköhler numbers up to 0.9 suggest that the chemical reactivity of isoprene is comparable to its turnaround time in the PBL. We further investigate the influence on the modified diffusion coefficient for a 1st order PBL parameterization scheme.

4.1.1.1 Comparison between measurements and PBL scheme

Figure 19 compares measured $d\theta_v$ / dz profiles with a calculated profile based on one commonly used PBL scheme (Yonsei University YSU: Hong et al., 2006). The YSU scheme is based on earlier 1st order non-local diffusion schemes (e.g. Troen and Mahrt et al. 1986), which have been extensively used in mesoscale models. Overall the model is in reasonably good agreement with CABERNET measurements.

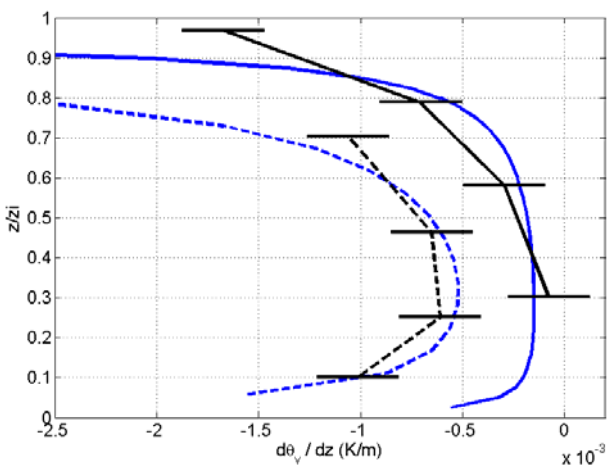

Figure 19. Measured (black) and simulated (blue) $d\theta_v$ / dz profiles. The solid lines represent RF6 and the dashed lines RF7.

We normalize data shown in Figure 19 by defining a local diffusion coefficient according to:

$$K := -\frac{<w'\theta_v'>}{\partial\theta_v/\partial z} \qquad (8)$$

Figure 20 depicts K plotted as a function of PBL height for RF6 and RF7.

For a reactive species, such as isoprene, the diffusion coefficient has to be modified.

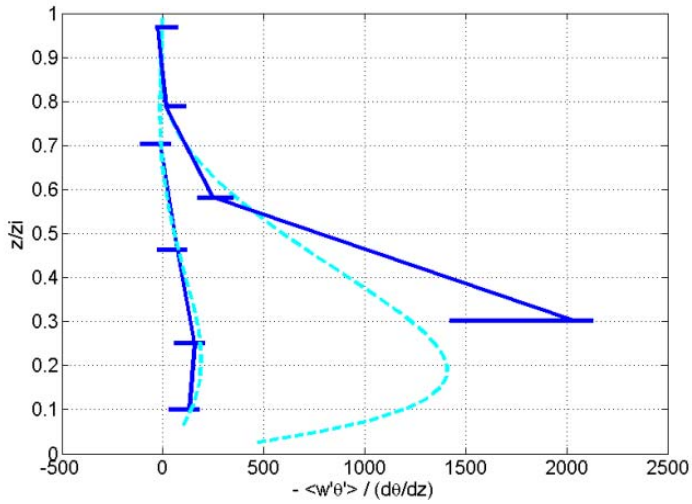

Figure 20. Local diffusion coefficient plotted vs z/zi, where zi is the PBL height. Blue solid lines represent measured diffusion coefficient for RF6 and RF7, cyan dashed lines are the corresponding modeled diffusion coefficients.

Following Kristensen et al. (1997) and Hamba (1993) we adopt the following expression for a first order loss:

$$K_{reactive} = \frac{K}{1+Da} \qquad (9)$$

Figure 21 illustrates the effect of chemically reactive species, which leads to a decrease of the local diffusion coefficient.

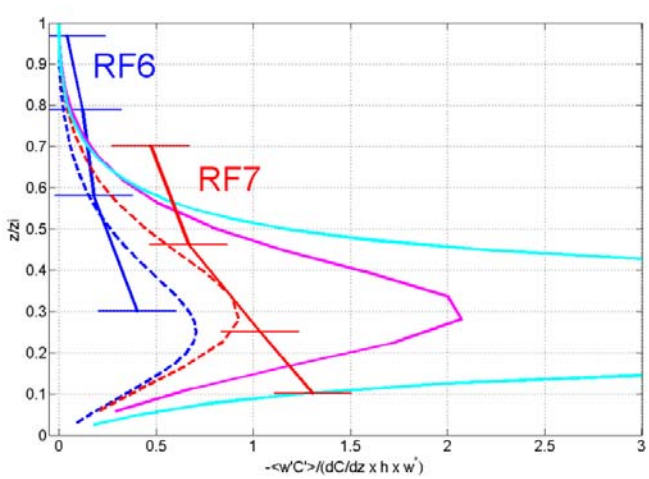

Figure 21. Normalized diffusion coefficient for isoprene for RF6 (blue) and RF7 (red). Bars indicate 1 σ. The solid cyan and magenta lines represent the diffusion coefficient for a non-reactive species for

RF6 and RF7 respectively. The dashed blue (RF6) and red (RF7) line depict the diffusion coefficient corrected by the Damköhler number.

The local diffusion coefficient based on flux observations is smaller for isoprene than for a conserved tracer. Correction according to eq. 9 improves the discrepancy. As a consequence the rate of the local concentration decrease for a reactive species is smaller than for a conserved species. Kristensen et al. (1997) postulated that, in the surface layer, the error of an estimated flux based on a non-corrected diffusion coefficient should be equal to the Damköhler ratio. Based on these results we discuss the impact on bottom-up, top-down diffusion functions (e.g. Moeng et al., 1994; Patton et al., 2003) that have been used for mixed layer gradient and mixed layer variance methods to estimate fluxes (Greenberg et al., 1999; Spirig et al., 2004; Karl et al., 2007). Fluxes estimated based on the mixed layer gradient method rely on inverting mixed layer concentration measurements by splitting the contribution into a bottom up (BU) and top down (TD) diffusion process. Parameterization of BU-TU diffusion functions are typically based on idealized LES model results (e.g. Moeng et al., 1994; Patton et al., 2004; Vinuesa et al., 2003). Here the correction for the mean tracer inversion is assumed to be proportional to the Da number (eq. 6). The isoprene concentration gradient (dc/dt) in the mixed layer was $2.4 \cdot 10^{-4}$ ppbv/m and $2.8 \cdot 10^{-4}$ ppbv/m for RF 6 and RF 7 respectively. Based on the measured flux divergence we calculate a theoretical concentration gradient of $1.4 \cdot 10^{-4}$ ppbv/m and $1.75 \cdot 10^{-4}$ ppbv/m, thus 37% and 41% lower than measured. After correction for the effect of chemical reactivity the difference between modeled to measured dc/dt improves to 18% higher and 8% lower for RF6 and RF7 respectively. As a conservative limit, isoprene fluxes in the Amazon basin obtained by the MLG method (Karl et al. 2007) have previously been corrected by about 14%. Taking estimated OH densities of $1.2 \cdot 10^{6}$ - $5 \cdot 10^{6}$ molecules/cm^3 and w* of 2 m/s the Da number was on the order of 0.08-0.19 during the TROFFEE Amazon experiment (Karl et al., 2007). Based on measurements presented here we conclude that a simple first order correction based on the Da number (eq. 7) can be used to correct isoprene fluxes obtained by the MLG method reasonably well.

The mixed layer variance method is generally less susceptible to reactive losses. For example corrections for the variance budget suggested by Vinuesa et al. (2003) would imply a bias of 20% and 9% for RF6 and RF7 respectively. A larger influence on the variance of a species

can originate from surface heterogeneity. For example, Patton et al. 2005 have investigated the impact of heterogeneous surface characteristics on the variance. They found changes of up to a factor of 2 for the streamwise velocity variance. Here the variance of isoprene could have to some extent been impacted by surface heterogeneity during RF7. For conditions described in Table 1 the measured standard deviation for isoprene in the ML was about 41 % higher for RF7 than what would have been calculated based on MLV functions, which were developed for homogeneous conditions. During RF6 the measured standard deviation was on average within 10% of the calculated standard deviation based on MLV functions.

This dataset suggests that the MLV method is more susceptible to experimental uncertainties over complex and heterogenous terrain compared to the MLG method. This has also been tentatively suggested by Patton et al. (2005). More modeling and experimental evidence however is needed to fully constrain uncertainties associated with BU-TD parameterizations under these conditions.

4.2 Conclusion

We present novel eddy covariance measurements of isoprene during the CABERNET experiment. Vertically resolved measurements suggest that first order chemistry can describe the decrease of isoprene fluxes throughout the PBL under typical atmospheric conditions. Experimentally determined Dahmköhler numbers were in the range of 0.3 to 0.9. Concentration gradients throughout the PBL decrease as a result of chemical reactions leading to locally smaller concentration changes due to chemistry. Modification of turbulent diffusion coefficients have been proposed according to theoretical considerations developed for the surface layer (Kristensen et al. 1997). This improves the measurement to model comparison for a 1st order non-local diffusion scheme. It is demonstrated that measurements of isoprene flux divergence can be used to study entrainment processes over land. Typical entrainment velocities observed during 3 research missions were 5.5, 9.6 and 1.4 cm/s respectively. We propose that future airborne eddy covariance measurements of biogenic volatile organic compounds can be used to characterize heterogeneous surface emissions using wavelet decomposition and help develop a more robust landcover representation of reactive trace gas fluxes. In addition we demonstrate that flux divergence measurements can be used to provide estimates of OH in the planetary boundary layer. Theses flux measurements can therefore

provide a new way to determine average OH densities allowing to investigate potential OH recycling mechanisms which have been proposed to occur during isoprene oxidation.

5 Airborne flux measurements of Biogenic Volatile Organic Compounds over California *(In review, Misztal et al., 2014)*

5.1 Observed Concentrations of BVOC from PTR-MS

The spatial distributions of concentrations for VOC measured on most research flights are shown in Figure 22. We show and discuss in this section the individual compounds measured in CABERNET in terms of their concentrations.

5.1.1 Isoprene

Isoprene concentrations were low, typically less than 50 ppt (0.05 mg m^{-2} h^{-1} in fluxes) in the Central Valley over agricultural terrains and over urban areas but were very high over the oak woodlands which cover approximately 7% of California, and were the focus of the CABERNET campaign flight plans. In general, observed isoprene concentrations over oak woodlands ranged from less than 1 ppb on cool days up to several ppb on warmer flights. A maximum of 8 ppb was observed on the hottest day. The aircraft also saw marked increases of isoprene near some highways with eucalyptus trees planted alongside. Although no study of regional scale emissions of VOC in California was previously conducted, the pattern of concentrations observed during CABERNET is consistent with an expected pattern based on extrapolation of earlier studies from enclosures of dominant plant species of California which suggested oaks (mostly blue oaks), and to some degree eucalyptus trees, to be likely the most important isoprene emitters in California (e.g. Karlik and M Winer, 2001). The broad range of temperatures encountered in different flights (mean range 21 – 33 ºC) was responsible for quantitative differences in concentrations over the overlapping segments. The actual concentration at the surface is expected to be significantly higher than observed at aircraft height, as is shown to be the case when flying near the tall tower at Walnut Grove where the top levels (394 and 525 m) saw very tiny concentration of isoprene consistent with the

concentrations seen by aircraft although the lowest tower levels (10 and 131 m) saw much higher concentrations (Figure 23b). However, the areas with significant biogenic emissions of isoprene covered a relatively small fetch within the footprint of the Walnut Grove tower.

5.1.2 Monoterpenes

Measurements of monoterpenes from aircraft are subject to several challenges which include 1) relatively small source strength, for example, ~10% relative to isoprene measured over coniferous regions; 2) relatively lower PTR-MS sensitivity compared to lighter compounds when using a quadrupole MS; 3) relatively shorter atmospheric lifetimes for some monoterpenes. The majority of the CABERNET aircraft tracks focused on isoprene emitters (e.g. oak woodlands) and not monoterpene emitters (e.g. coniferous forests), so the monoterpene signals were small and therefore we have not attempted to derive fluxes. However, averaging concentration signals to a 0.5 km resolution along the flight path was sufficient to decrease detection limits for monoterpenes to a few ppt and to demonstrate the presence of emissions from the densely forested areas, for instance, on a track towards Blodgett forest and on parts of the mixed conifer habitats along Coastal Ranges. Very high concentrations of monoterpenes exceeding 300 ppt were found in the GC cartridges on the flight legs passing near the Mojave Desert scrublands but *m/z* 81 and 137 were not included in ions measured by the PTR-MS on that flight.

5.1.3 Other VOCs

Although we focus on isoprenoids, the aircraft PTR-MS also measured concentrations (and fluxes) of other compounds with non-biogenic or partially biogenic sources such as dairies (methanol), isoprene photochemistry (MVK+MACR, hydroxyacetone), MBO to exclude interferences with isoprene, and sporadically other compounds such as acetaldehyde or aromatics. The data for these compounds are available and are expected to be reported in future publications.

a)

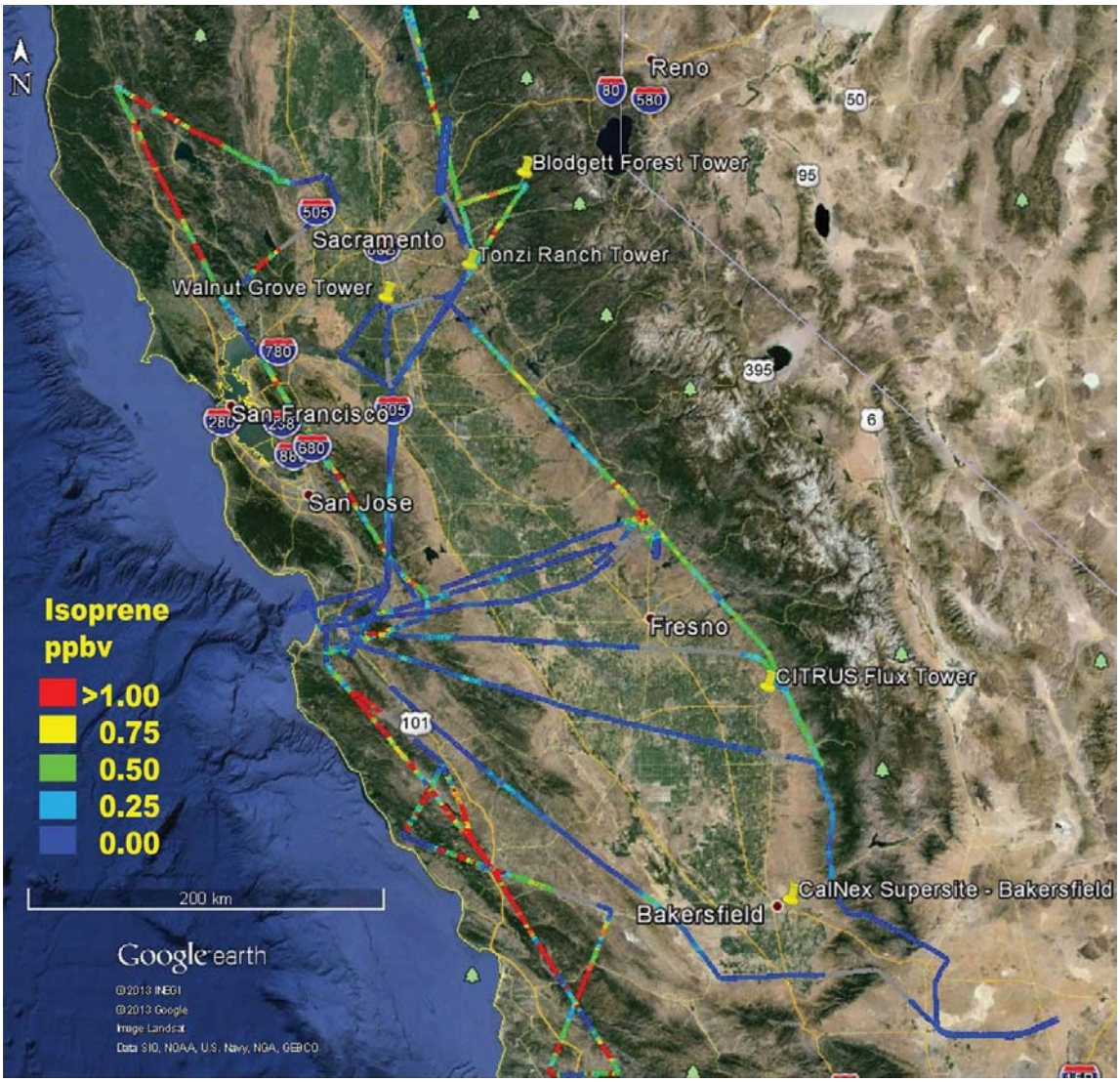
N
Reno
Blodgett Forest Tower
Sacramento
Tonzi Ranch Tower
Walnut Grove Tower
San Francisco
San Jose
Fresno
CITRUS Flux Tower
CalNex Supersite - Bakersfield
Bakersfield
Isoprene
ppbv
>1.00
0.75
0.50
0.25
0.00
200 km
Google earth

b)

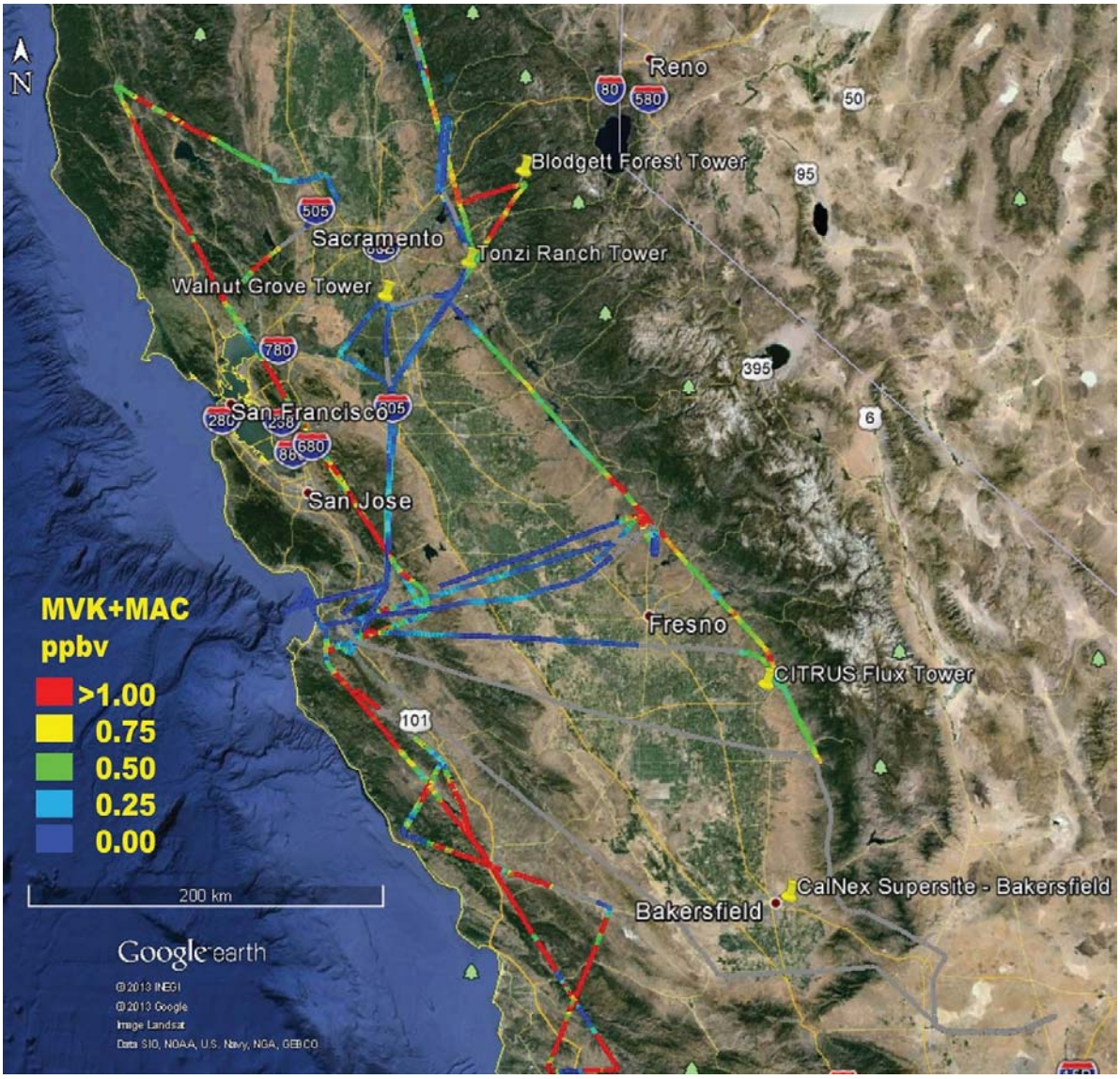
N
Reno
Blodgett Forest Tower
Sacramento
Tonzi Ranch Tower
Walnut Grove Tower
San Francisco
San Jose
Fresno
CITRUS Flux Tower
CalNex Supersite - Bakersfield
Bakersfield
MVK+MAC
ppbv
>1.00
0.75
0.50
0.25
0.00
200 km
Google earth
© 2013 INEGI
© 2013 Google
Image Landsat
Data SIO, NOAA, U.S. Navy, NGA, GEBCO

c)

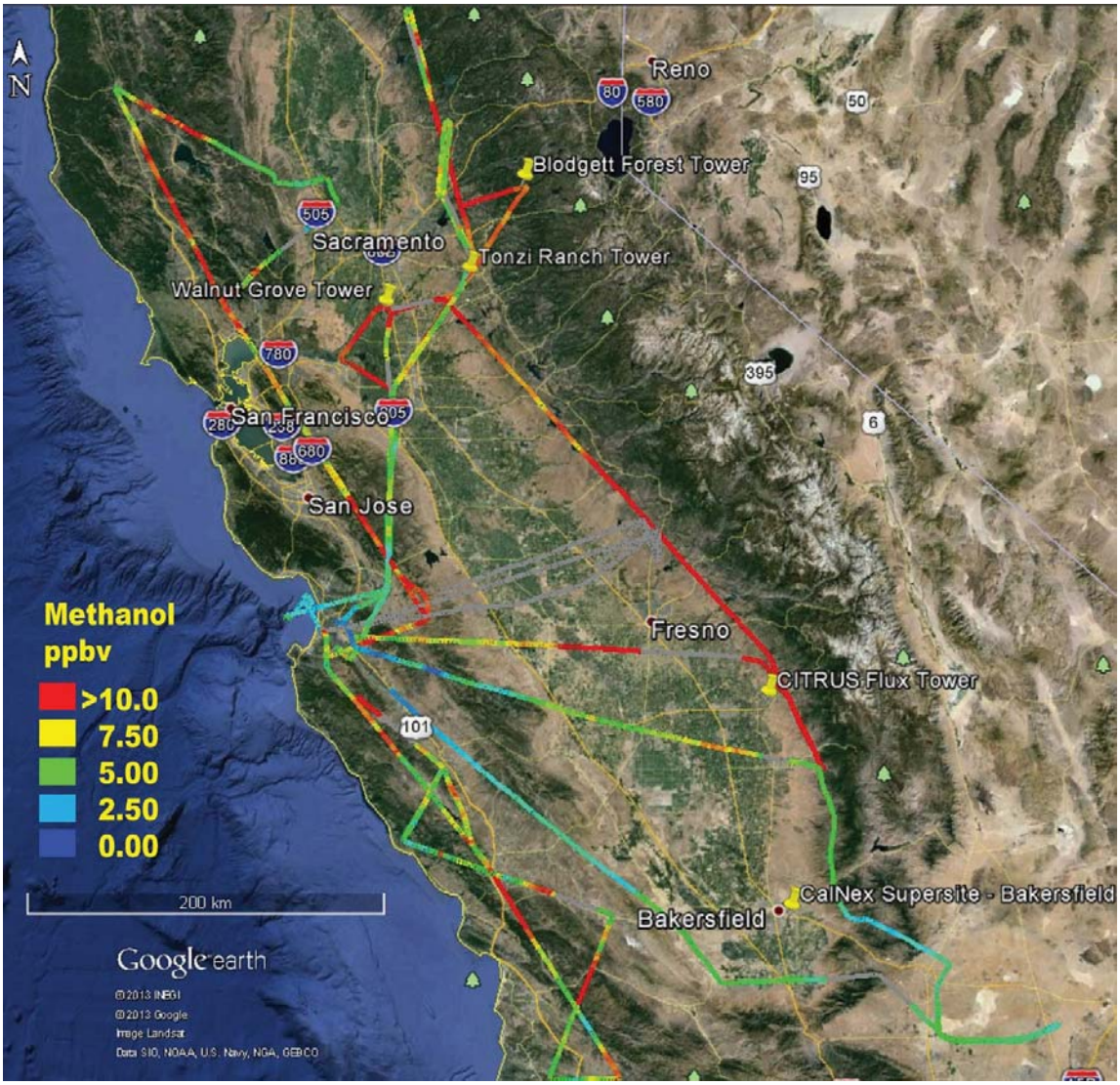
N
Reno
Blodgett Forest Tower
Sacramento
Tonzi Ranch Tower
Walnut Grove Tower
San Francisco
San Jose
Fresno
CITRUS Flux Tower
CalNex Supersite - Bakersfield
Bakersfield
Methanol
ppbv
>10.0
7.50
5.00
2.50
0.00
200 km
Google earth

d)

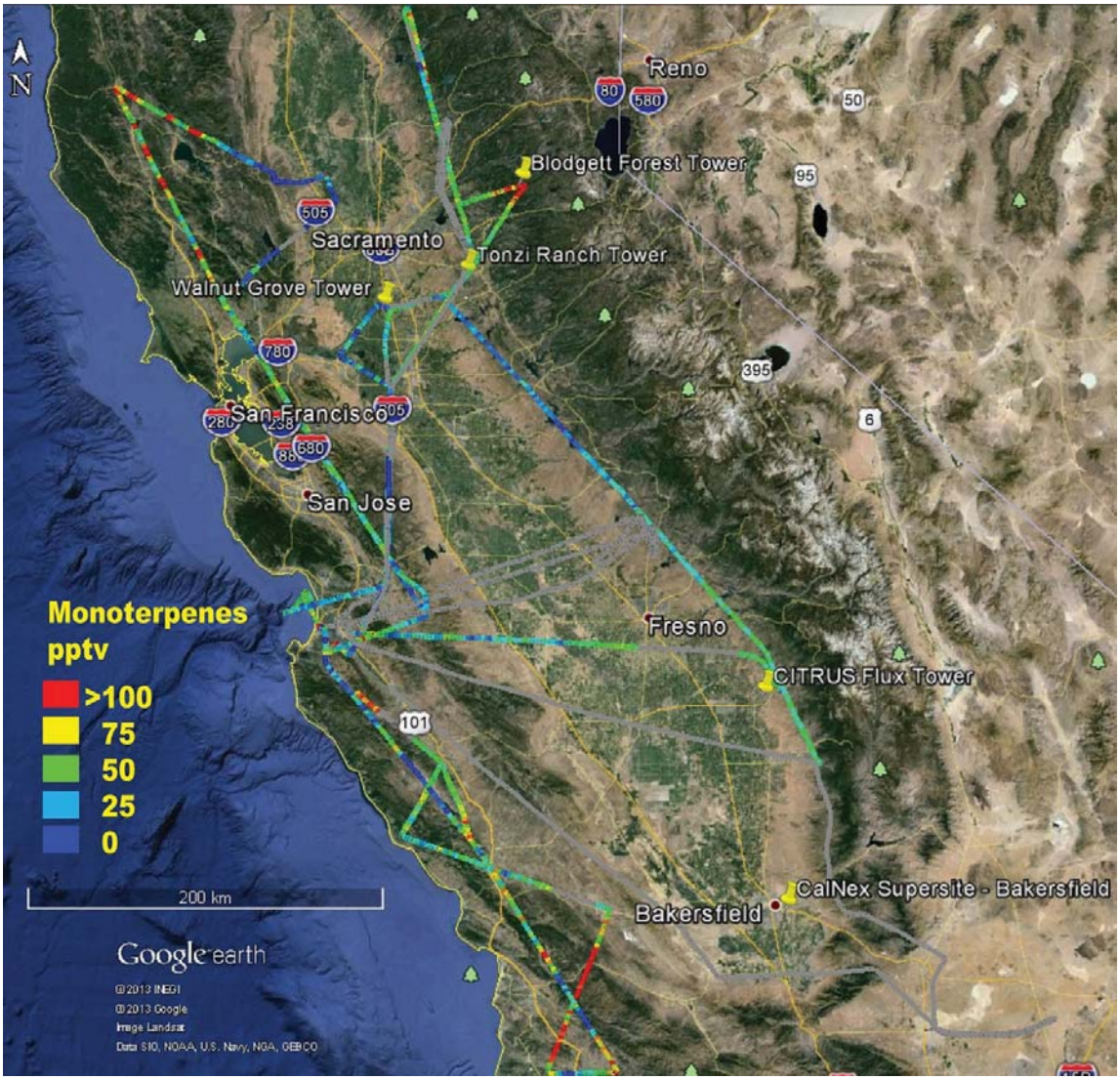

Figure 22. Spatial distributions of concentrations of a) isoprene, b) MVK+MAC, c) methanol and d) monoterpenes measured during CABERNET.

5.1.4 Inter-comparison of concentrations from PTR-MS and GC-MS

Measured concentrations of isoprene by GC-MS from cartridge samples collected at constant flow rate for 8 minutes during the flights generally agreed well with PTR-MS measurements averaged for the same periods, but there were occasional outliers most probably caused by cartridge sampling or analysis issues. The comparisons for each flight are presented in Appendix B. Linear fits (excluding tubes which were found leaking or not sampled) ranged from R^2 0.79 for RF 1 (which was the flight with coldest weather and consequently lowest

isoprene concentrations) to 0.98 for RF4, and was typically around R^2 0.9. The slope of the comparison ranged from 0.9 to 1.15 so within the combined measurement uncertainties (10+10%). The analysis of the cartridges helped also in the exclusion of potential interferences at measured *m/z*.

5.1.5 Comparison with Walnut Grove Tower

WGC monitored VOC concentrations by a PTR-MS at 5 different heights (10, 131, 262, 394 and 525 m). The twin otter flew close to the tower on RF2 and RF4 (13:18). The ground-airborne comparison was focused on methanol, isoprene, and MVK+MAC. Overall, the comparison for methanol suggested agreement within 30%. However, looking at simultaneous fine resolution data from the two PTR-MS instruments (Figure 23a), a dip in methanol concentration was seen consistently by both the aircraft and the tower when the plane was closest to the tower's top level, with excellent measurement agreement (11.6±1.16 ppbv seen by the tower at 525 m vs 11.9±1.19 ppbv measured by the aircraft at 513 m). The variability of the methanol concentration over a five minute segment adjacent to the tower was within several ppbv, giving insight into spatial variability of methanol at that time and altitude. The WGC region is mostly agricultural with a variety of sparsely distributed trees. The measurement during the aircraft pass at 13:18 showed very little isoprene (below 50 ppt) at the top level of the tower (as mentioned in 3.1.1, and Supplementary Figure 23b) even though concentrations close to 1 ppb were observed at the 10 m level. The agreement for MVK+MAC (0.18 ±0.02 ppbv aircraft vs 0.20±0.02 ppbv 525 m tower) was also good.

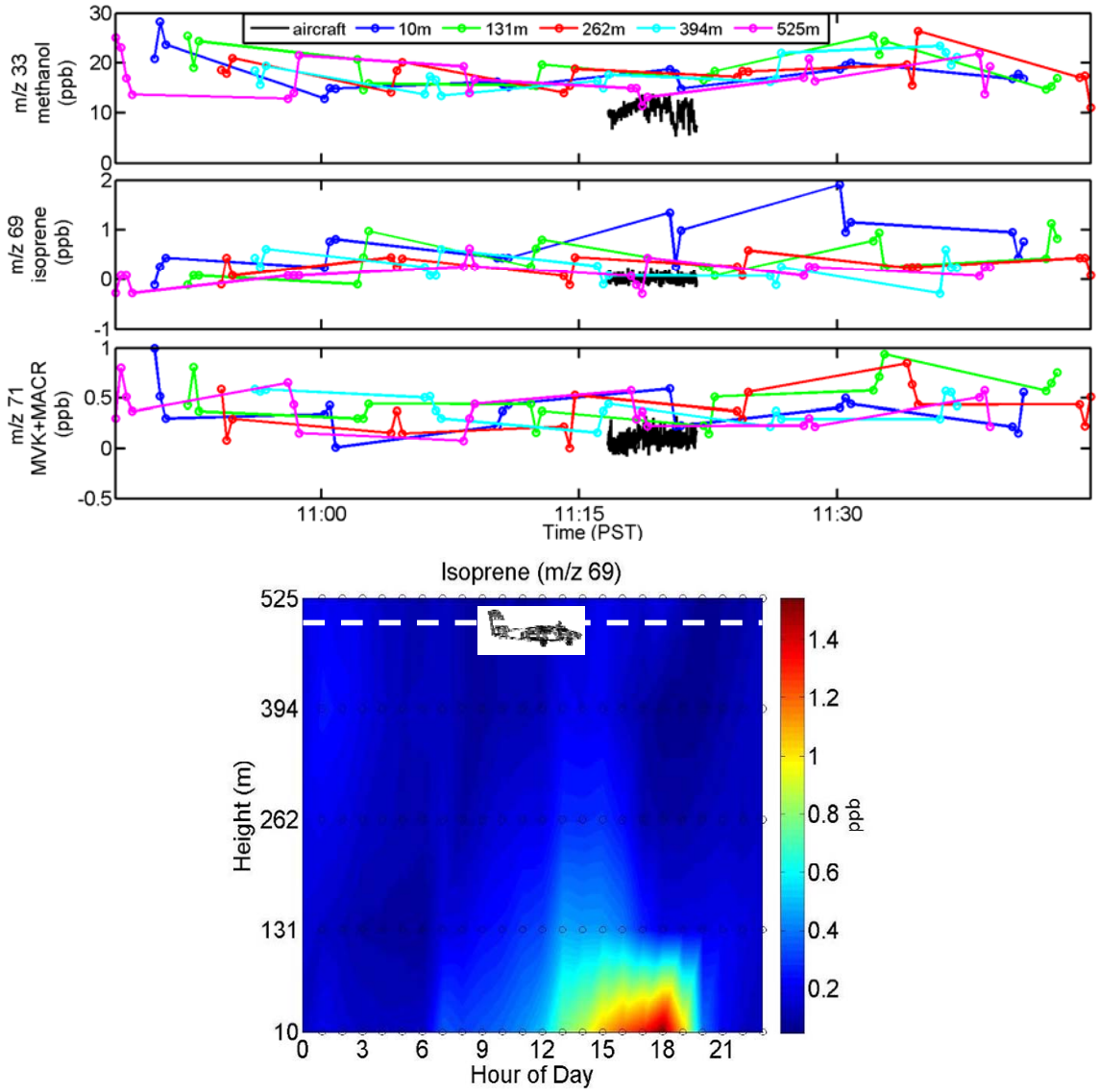

Figure 23. (a) Intercomparison of concentrations at Walnut Grove tower coinciding with top level of the tower. (b) Vertical profile for concentration of isoprene shows complementary value from ground-based measurements.

5.2 Observed fluxes

Isoprene and methanol showed the strongest fluxes of all measured compounds. In this paper we focus on reporting isoprene surface fluxes.

5.2.1 Isoprene fluxes

The observed surface emission rates of isoprene over oak woodlands ranged from around 1 to 15 mg m^{-2} h^{-1}. The measured isoprene flux distribution shown in Figure 7 (CWT fluxes, 2 km resolution) visually confirms earlier predictions that isoprene emissions are almost exclusively produced by oak with a limited contribution from eucalyptus trees. For example, when entering the Sierra Nevada foothill oak band isoprene emissions rose remarkably above the low background in the Central Valley. Karlik and McKay (2002) used an isoprene emission factor from branch enclosure for blue oak of 27 μg g^{-1} h^{-1}, and leaf areas and weights from 14 blue oak trees from Sierra Nevada to estimate a leaf-level emission factor of ~8 mg m^{-2}(leaf) h^{-1}, corresponding to a landscape emission factor of ~4 mg m^{-2}(land) h^{-1} for a setting were oaks occupied half of the land surface area. In CABERNET the airborne emission factors for isoprene over oak woodlands varied from less than 1 to ~10 mg m^{-2} h^{-1} with the average EF comprising all the flights over areas with oak presence (>=20% coverage of oak species according to GAP database) of 1.8 mg m^{-2} h^{-1}. However, the woodlands varied in species homogeneity, and more significantly, in the fraction (i.e., sparseness and patchiness) of tree coverage. It is necessary to emphasize that while the LAI of oak covered land surfaces has a relatively small range, about 3 to 6 m^2 m^{-2}, the fraction of the land surface covered by oaks can range from < 0.1 to 1. For example, Karlik and McKay (2002) using a precise method of calculating the areas of leaves from 14 trees divided by the areas of their crowns, measured an LAI of 4.3 m^2 m^{-2} for oak crown areas but the oaks only covered 42% of the land surface resulting in an area average LAI of 1.8 m^2 m^{-2}. For the more sparse terrains the LAI can often be lower than 1 m^2 m^{-2}. Compared with the forests with closed canopies, modeling emissions from oak woodlands in California can be regarded as a specific case to which assessment by airborne flux measurements are particularly applicable. Measured airborne emissions reflect the true emissions from these California ecosystems of variable LAI ranging from less than 1 to about 5 m^2 m^{-2}.

5.2.2 Comparison of isoprene fluxes at Tonzi Ranch Tower

The aircraft flew over the Tonzi Ranch Tower twice, allowing two snapshot comparisons between the airborne CWT and ground based REA flux measurements. It is important to note that the airborne CWT averages over ~0.5 minute (2 km), while the ground based REA averages over 30 minutes, and that the footprints related to each measurement are necessarily

quite different, likely do not have the same oak biomass density, and thus the comparison is not expected to be perfect. In the first instance, the half-hourly REA flux was in excellent agreement with the 2-km average wavelet surface flux over the tower (i.e. 0.12 mg m^{-2} h^{-1} REA vs 0.12 mg m^{-2} h^{-1} aircraft) while on the returning flight the ground based flux was 1/3 of the aircraft flux (i.e. 0.26 mg m^{-2} h^{-1} REA vs 0.87 mg m^{-2} h^{-1}). Interestingly, the next half-hour REA flux was 0.96 mg m^{-2} h^{-1}, much closer to the aircraft value. This may be due to a shift in wind direction and variability in oak biomass density around the tower but it should also be noted that the uncertainty in a single REA flux measurement is high and individual values are typically averaged to improve accuracy. These comparisons obviously suffer from significant uncertainties due to different footprints at different altitudes, different temporal coverage, and even temperature/PAR homogeneities. Nevertheless, the comparison provides insight about the variability's in measurements at different scales, confirms observations at these scales are in a similar range, and indicates the complementing power of having both airborne and tower measurements. A larger period of overlap in a future campaign is needed for gaining better statistics on such comparisons.

5.3 Conclusions

We successfully made airborne eddy covariance flux measurements and mapped out horizontally varying source distributions of isoprene emissions for the dominant oak emitting ecosystems in California. The extensive oak woodlands in California are the most important regional source of isoprene which may be particularly relevant for air quality near heavily polluted regions of Central Valley. We observed high concentrations (up to 8 ppbv) and high surface emissions of isoprene ranging from several to more than ten mg m^{-2} h^{-1} from the oak woodlands in the foothills of the Sierra Nevada and Coastal Ranges. Consistent with other studies we show that in the Central Valley isoprene emissions are typically undetectably small at aircraft level except for the areas of Eucalyptus trees planted near the highways. The temperature ranges in California cause changes in the isoprene emissions from relatively low to extremely high due to their strong temperature sensitivity. The ability of CWT for calculating fluxes at high spatial resolution (e.g. 2 km averaging) provides an optimal data set to compare BEFs from measurements with models. The data from this study have been used

to assess isoprene emission-factor databases and isoprene emission response to landcover characteristics predicted for BVOC emission models.

6 Constraining isoprene emission factors from oak woodlands over California.

6.1 CABERNET BEFs vs Landcover BEFs

6.1.1 Comparison of isoprene emission factors to MEGAN landcover 2.2

6.1.1.1 Spatial 2-km representations

Isoprene emission model estimates are based on basal emission factors, landcover characteristics, and the changes in emission associated with the environmental parameters temperature and photosynthetically active radiation (PAR). The measured airborne surface fluxes from the CABERNET campaign can be compared directly to the modeled fluxes as we shown in section 6.1.4. However, it is also instructive to normalize the measured fluxes for temperature and radiation using the Guenther et al. (2006) activity factor to derive airborne basal emission factors (BEFs) which can then be directly compared to emission factors used by various models (e.g. the MEGAN emission factors version 2.2). A spatial comparison of measured versus modeled BEF's is shown in Figure 24. This comparison approach has some uncertainty due to the temperature and PAR datasets and the algorithm used for calculating the activity coefficient, which are much higher than the uncertainty of the measured surface fluxes because of high sensitivity to errors in temperature and PAR, but it is useful because we can then compare the measured BEF (essentially the measured emission potential for that ecosystem) to the BEF used to drive the model. The qualitative comparison clearly shows a remarkable correspondence between airborne BEFs derived at 2 km spatial resolution with landcover BEFs at a similar resolution. The transition from the low emitting environment in the Central Valley to highly emitting areas occupied by oak woodlands is clear (as shown

earlier in Figure 1). The most accurate matches can be seen, for example, in the central part of the Sierra foothills and on the southern Coastal Range, to the south east of Monterey Bay and in the oak savannas near San Francisco Bay (East Bay hills, and Diablo Valley). The BEFs decline to zero over water bodies (e.g. San Francisco Bay, or lakes on the central-northern Sierras). There are some areas which do not agree well, for example, in the north-east over the Sierras which are dominated by conifers where airborne BEFs were somewhat lower than predicted. On the other hand, there are areas where the aircraft observed higher BEFs (e.g. beginning of the Central Coastal Range track going the south of the Monterey Bay in the 6ag ecoregion) that are most likely related to inaccuracies in the oak landcover database.

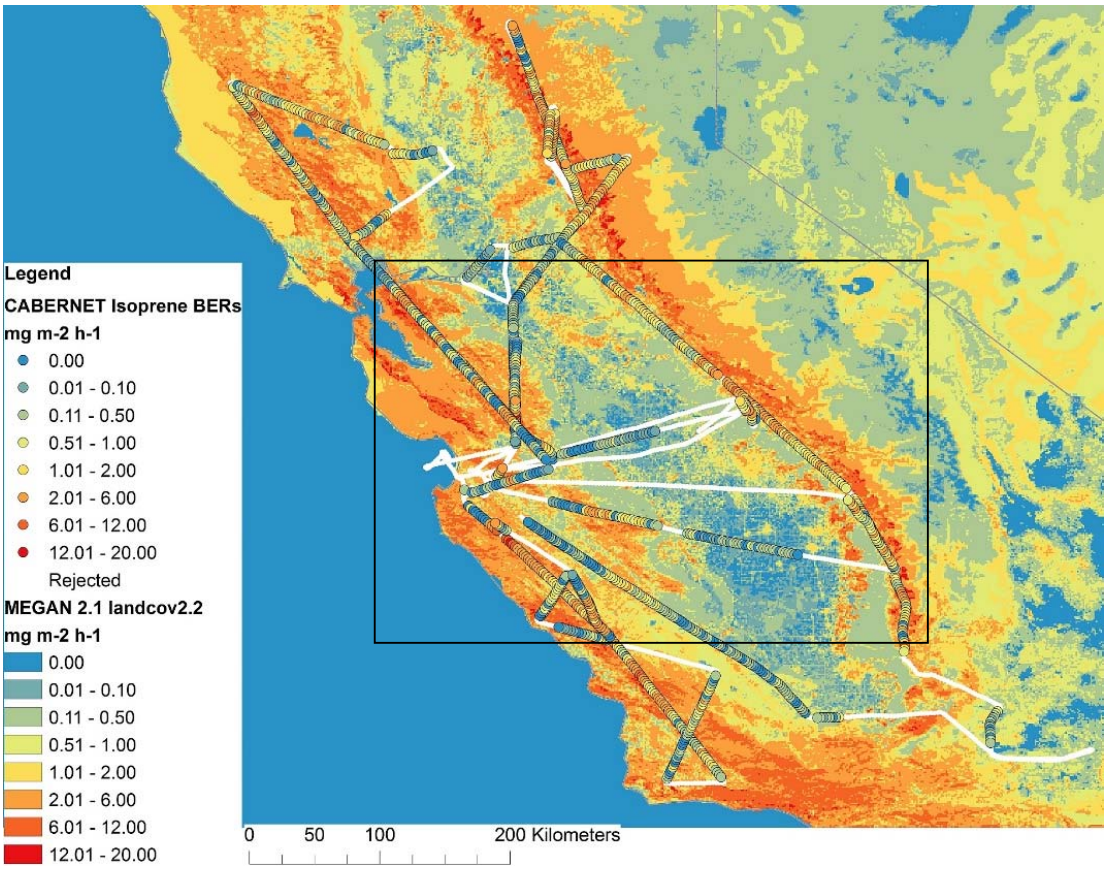

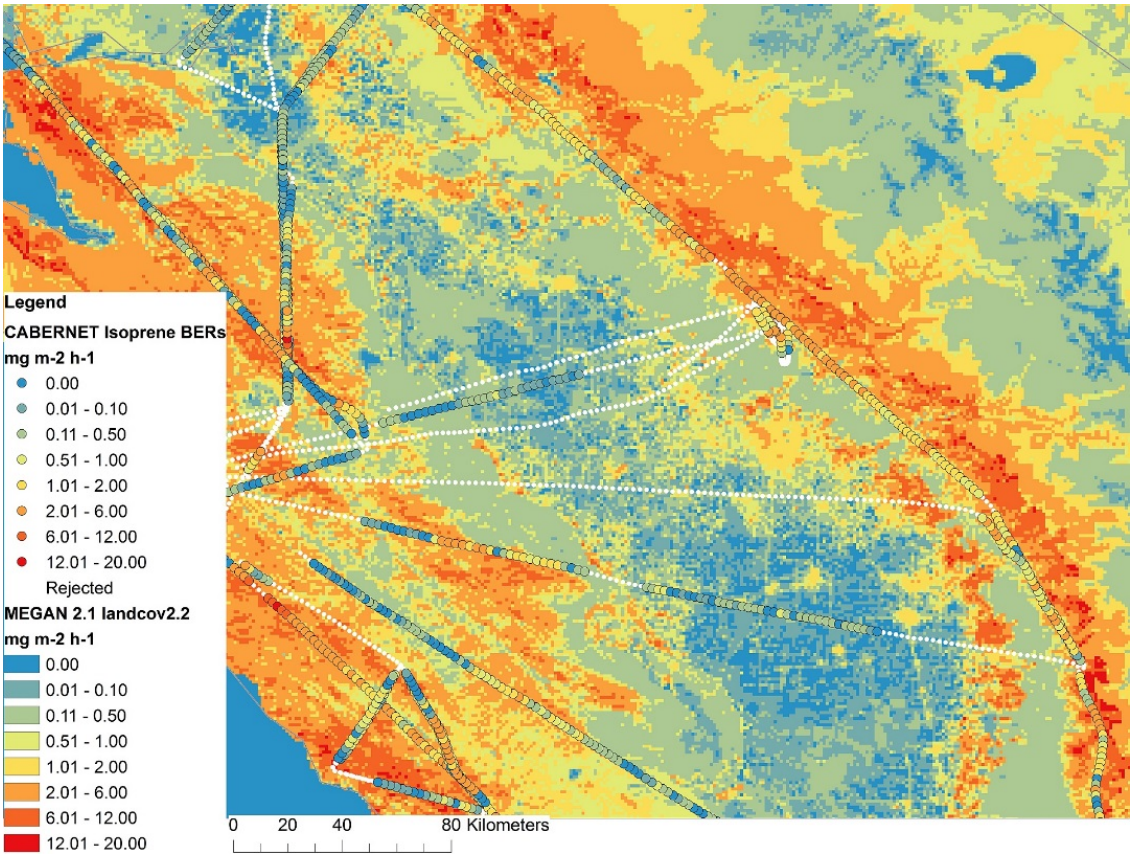

Figure 24. a) Comparison of airborne BEFs with MEGAN's landcover 2.2 for isoprene (airborne BEFs are subject to additional uncertainties introduced from T, and PAR used in normalization).b) magnified area denoted by the black rectangle in a).

6.1.1.2 Eco-region specific comparisons of BEFs

California landscapes differ in plant distributions, plant functional types, and fractional coverage of vegetation. It therefore makes sense to look at model-observation comparisons separately for distinct ecological zones. We flew over 48 distinct subecoregions (level IV) nested within 4 distinct larger ecoregions (level III). Ecoregion 6 comprises most of the oak woodlands in the Central California Foothills and Coastal Mountains, and we flew over 29 of its 44 subecoregions (6a-6ar). Ecoregion 7 is characterized by very low isoprene emission potential and includes most of the Central California Valley, and we flew over 14 of its subecoregions. We also transected 2 subecoregions of the Sierra Nevada (code 5) and 3 of the Mojave Basin and Range (code 14).

As shown in Figure 25, the measured isoprene BEF's were much higher over the 6th and 5th ecoregions than over the 7th and 14th. Within the 6th ecoregion's subecoregions there was significant variability of BEFs ranging from near zero to above 10 mg m^{-2} h^{-1}. The BEFs from landcover 2.2 in most cases fell in the same range as measured BEFs, but in some cases they were higher. However, the landcover BEF means are the averages of the entire area of each ecoregion while measured BEFs represent only the part of those areas where CABERNET flights were done. This could be particularly important for the Sierra foothills where the footprint was often overlapping with the less dense portions of the oaks in the lower part of the foothills, and therefore may not be representative of the subecoregion average.

Comparison of the measured versus modeled emissions integrated over the same flux footprint areas are shown in Sect. 6.1.4. Nevertheless, this BEF comparison is independent of the footprint calculation and is indicative of the relatively good agreement we observed between measured and modeled isoprene emissions for most ecoregions.

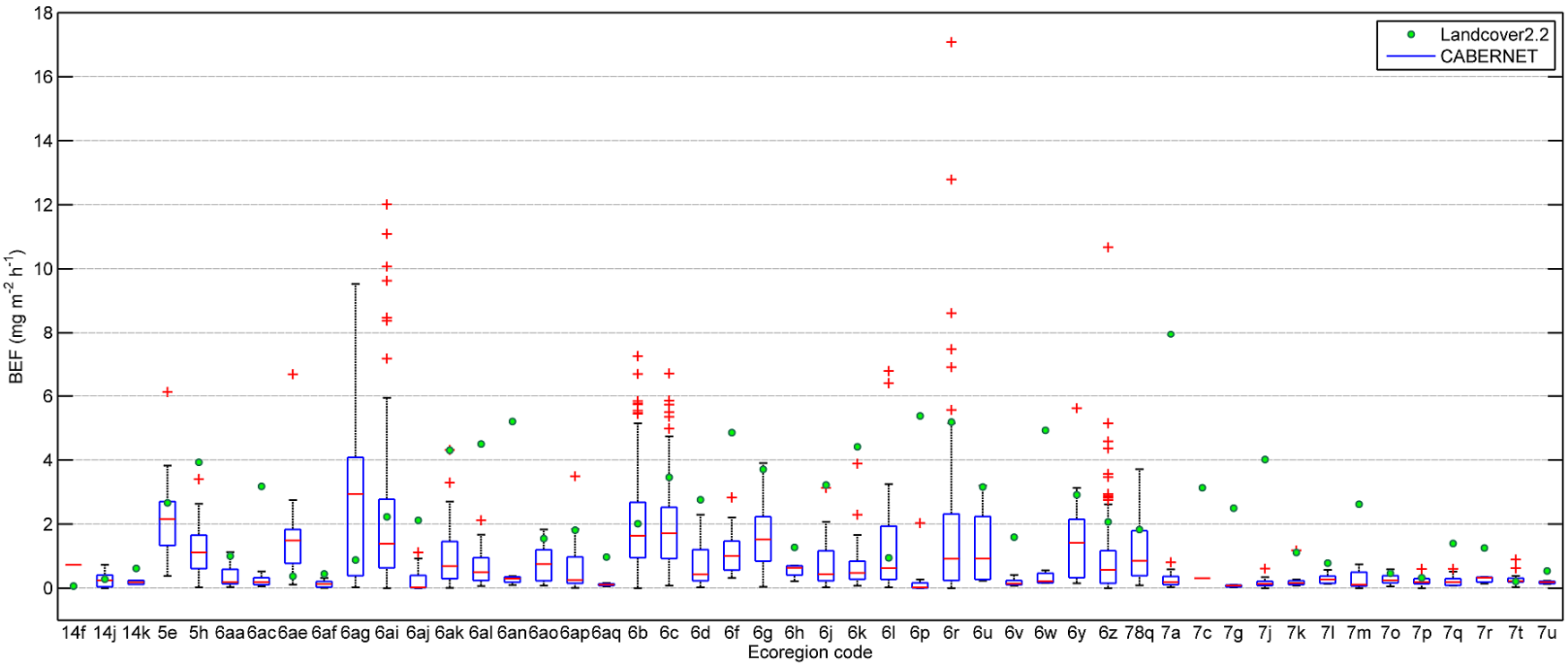

Figure 25. Basal emission factor comparison. The box plots represent CABERNET variations within each ecoregion (blue box: 25-75th percentile; black line: 5th - 95th percentile; red line is the median and red crosses are the outliers). The green dots represent ecoregion's mean EF according to MEGAN2.1 landcover2.2.

By looking at scatter plot of average modeled and measured BEFs (Figure 26), it is possible to assess if the model does a reasonable job over each of these different ecoregions. Robust statistics which give a smaller weight to outliers and a higher weight to the points falling within the bounds of the regression model suggests that the measurement-model agreement is very good (R^2=0.8, slope 1.1). The majority (70%) of ecoregions fall within 95% confidence intervals of the fit, while the remaining ecoregions occur more or less equally in the region of model overestimation or underestimation. Overall the model agrees with observations within 10% which is well within the stated 50% model uncertainty and the 20% measurement uncertainty that we estimated (section 3.5.7).

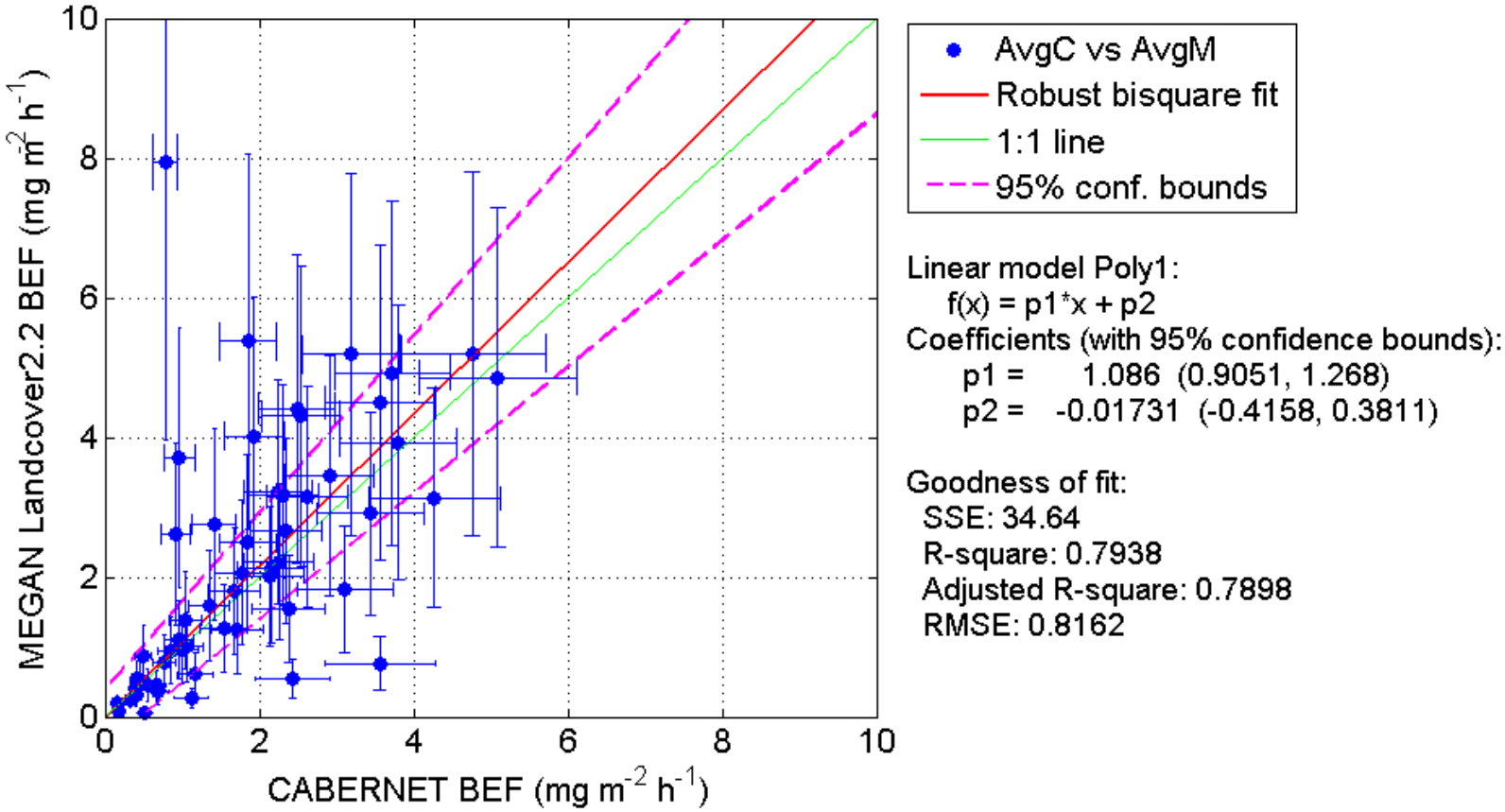

Figure 26. Robust regression for USEPA ecoregion averaged BEFs.The majority of ecoregions show good agreement between model and measurement. The outliers occur on the two sides of the fit showing no clear systematic offset for model or measurement. Note: the number of averaged points in each ecoregion may be different and not necessarily representative of the entire ecoregion.

6.1.2 Comparison of CABERNET emissions with CARB's adaptation of MEGAN 2.1

One of the project goals was to verify the accuracy of isoprene emission inventories used by CARB. For this reason, the emissions were simulated by MEGAN2.1 for exactly the same times and areas matching the CABERNET flux footprints to be compared with analogous 2-km measured emissions. Out of numerous simulations which were conducted at 4 km and 1 km resolutions and different footprint approaches, the best model-observation agreement was achieved for 2km resolution and the most accurate footprints based on wavelet heat flux, wind speed and z/z_i. In this report we use non-directional symmetrical footprints. Upwind half-dome oriented footprints are currently under development and may be utilized in future peer reviewed publication of this research. Although the half-dome approach should be the most accurate it is less practical in terms of the application to the existing modeling infrastructure. We determined that the full-dome approach we use here should be similarly accurate except for a few areas at the boundaries of the oak woodland fetch or if there is drastic inhomogeneity in land cover as indicated later in the analysis.

In Figure 27 and Figure 28 the time series of simulated and measured emissions are shown to be generally in extremely good agreement (plotted along the complete flight tracks). Some local discrepancies are observed in specific areas along the flight track and are discussed further in Sect.6.1.4.

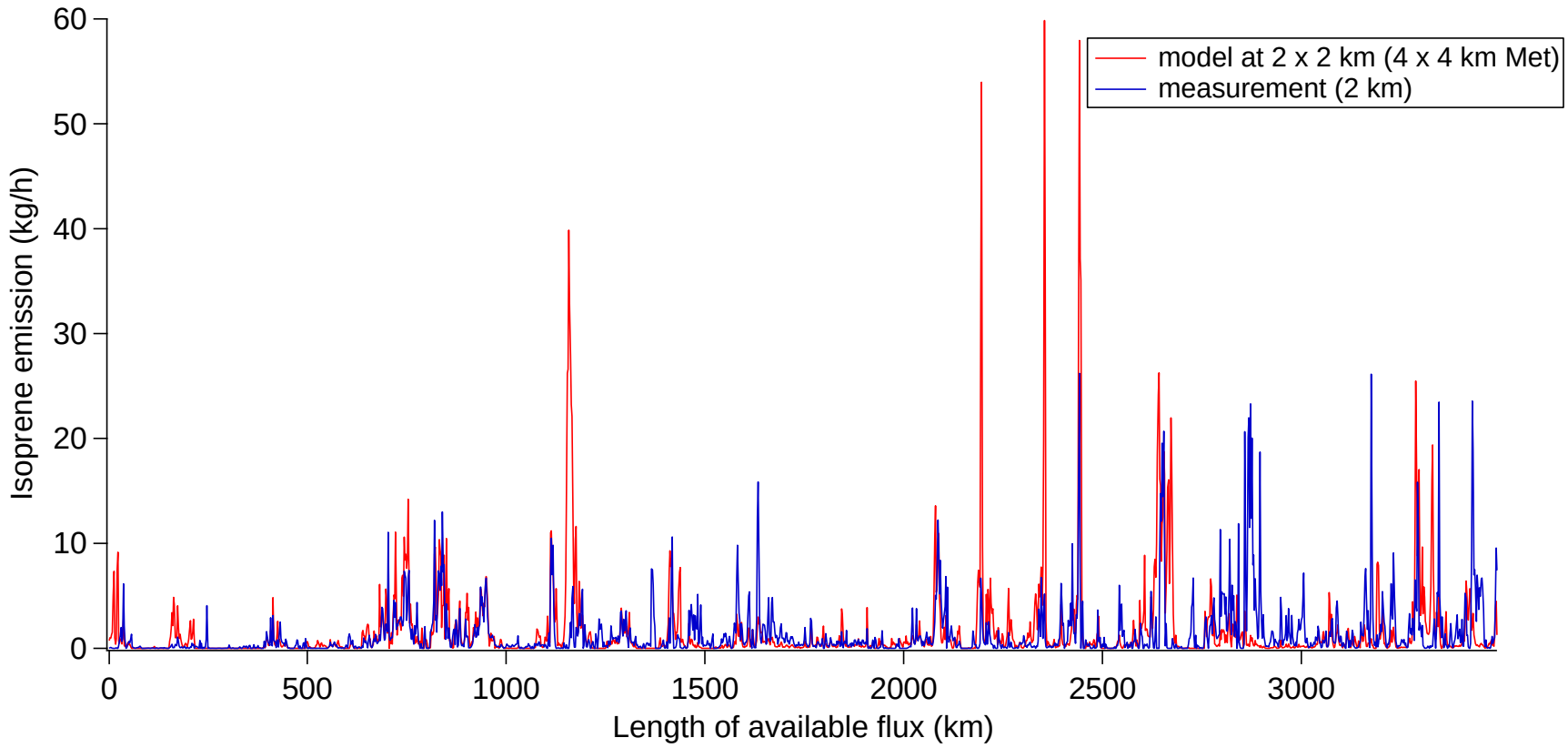

Figure 27. Timeseries for emissions of modeled and measured isoprene fluxes using the approximated circular footprint areas (only the data when flux was available are shown) along the full length of the flight tracks during the CABERNET campagin.

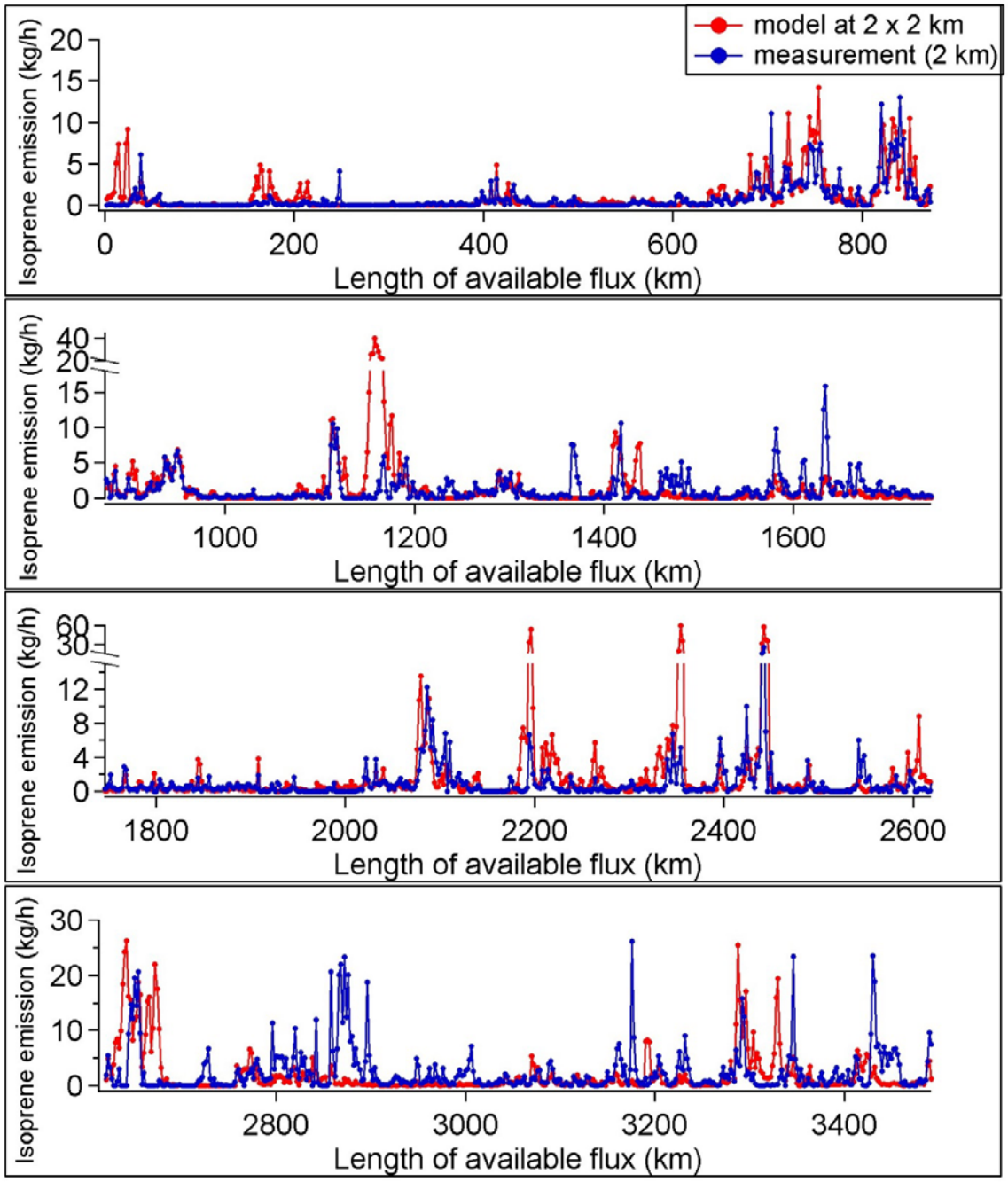

Figure 28. Comparison of 2km emissions (view at higher magnification) along sections of the flight tracks.

6.1.3 Sensitivity runs

The modeled emissions are prone to uncertainties in the driving variables (temperature, PAR, LAI), so we performed sensitivity analyses to estimate their effect on the simulations.

6.1.3.1 Temperature

A ±20% sensitivity analysis was done for the temperature input (Figure 29) and showed that the measured emissions were within the range of modeled emissions for most of the dataset. The several occasional model overestimation or underestimation episodes were likely unrelated to the temperature (or LAI or PAR) but rather due to the landcover inhomogeneity or the footprint mismatch. The temperature dependence of isoprene emissions is exponential so the highest sensitivity is expected to be in the higher temperature region. For example at 20 ºC 20% would correspond to a 4 ºC difference while at 30 ºC to a 6 ºC difference. Because of the exponential character a 20% change in temperature could lead to changes in emissions as large as 100% above 30 ºC. The highest errors in temperature used for simulations would be likely to occur in the areas close to the mountains where large gradients of temperatures occur on the order of a few km and shift spatially during a day.

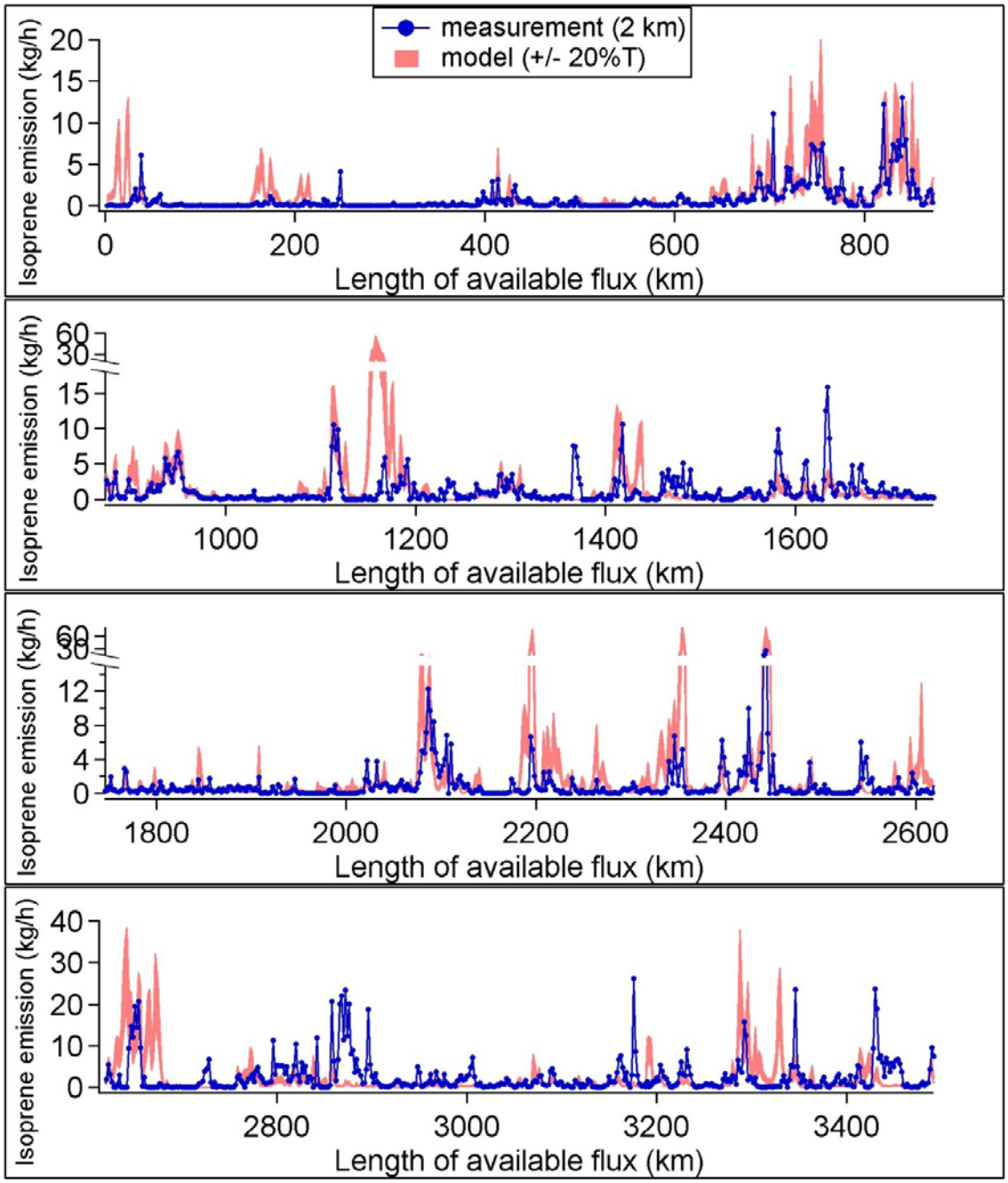

Figure 29. Comparison of isoprene emission time series for measurement and model with +/-20% sensitivity to temperature.

6.1.3.2 PAR

Similarly a ±20% sensitivity analysis for the PAR input was tested in the model simulations and the comparison of time series is shown in Figure 30. The resulting range of emissions was narrower than in the case of temperature sensitivity but the general picture was similar. It seems that a systematic offset in PAR (or temperature) would not improve significantly the generally excellent agreement, but it could improve or worsen the local agreement. For the cloudless skies in CABERNET it is unlikely that inhomogeneities in the spatial distribution of PAR could be significant although there could be impact of aerosol haze layer and high clouds in some areas.

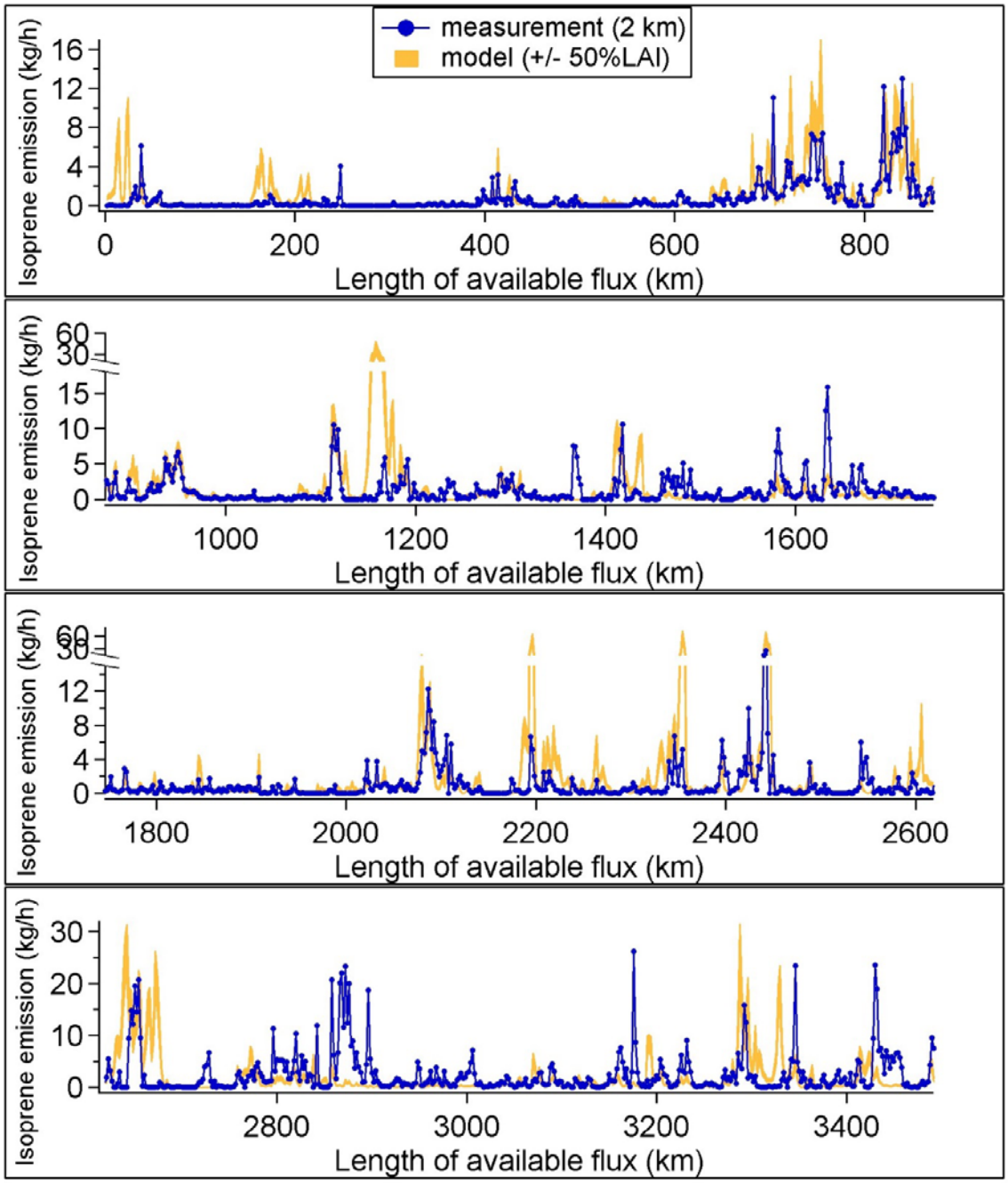

Figure 30. Comparison of isoprene emission time series for measurement and model with +/-20% sensitivity to PAR.

6.1.3.3 LAI

The LAI and the cover fraction of oak woodlands can vary greatly in the Sierra foothills (As discussed earlier in Sect. 5.2.1), and it is expected that the LAI products from MODIS may not work ideally for oak terrains and may not discriminate from grasses. A ±50% uncertainty in LAI is therefore expected, thus we apply this uncertainty to the model and compare with the measurements. As indicated by Figure 31 this range in LAI did not result in changes in modeled emissions larger than a factor of 2 and no constant systematic offset was observed. It is therefore assumed that the LAI used in the simulation was sufficiently accurate.

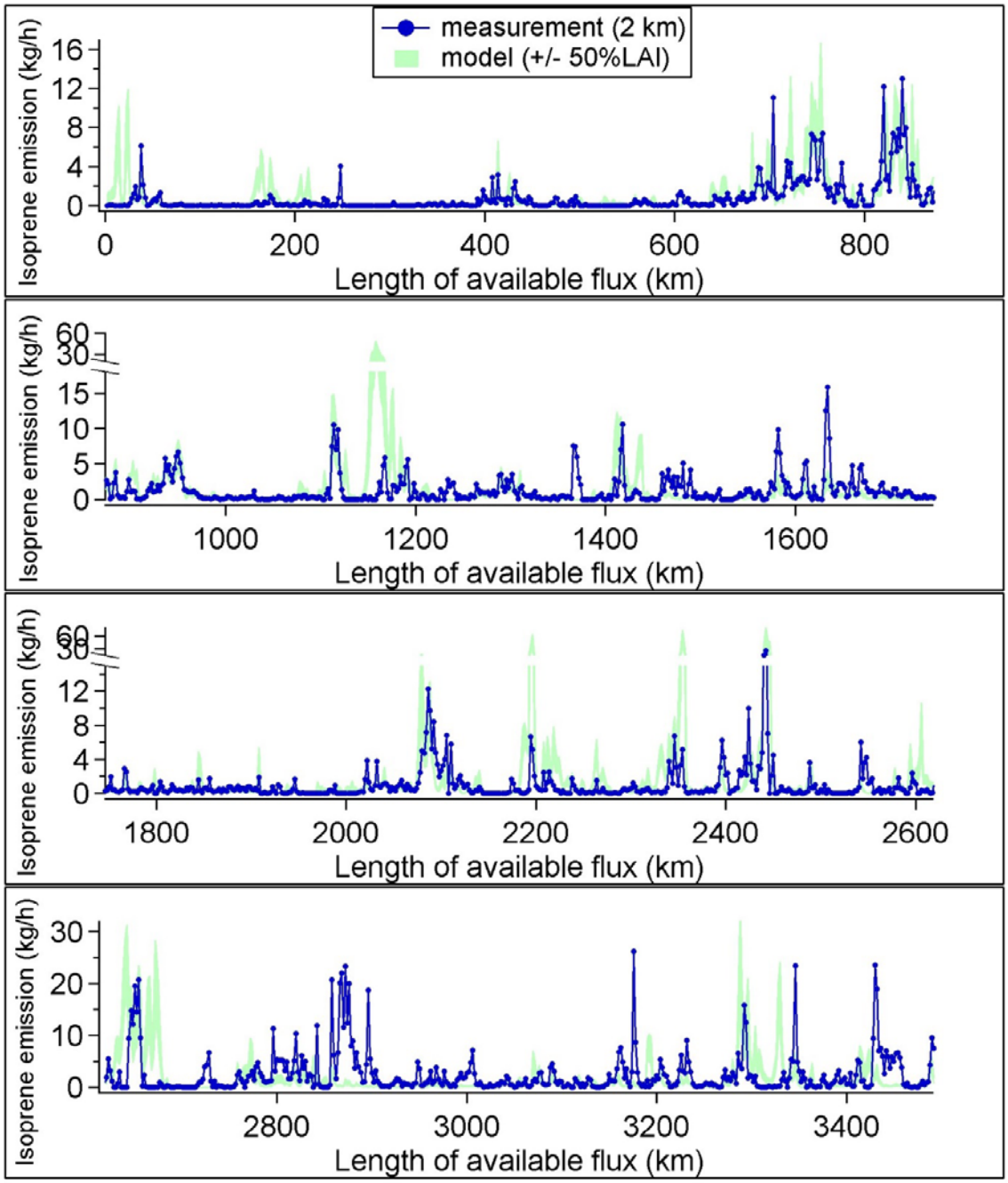

Figure 31. Comparison of isoprene emission time series for measurement and model with +/-50% sensitivity to LAI.

6.1.4 Regional model performance over ecoregions

To test the regional performance of the model the data have been grouped over ecoregions and the resulting variabilities are shown independently for each of these ecoregions in Figure 32a (full scale) and Figure 32b (lower emission scale). The direct comparison of measured-modeled fluxes suggests agreement is remarkably good in most cases not only for the midrange from the statistical distribution but also in the case of episodic spatial events (e.g. see 6ai, 6b, 6r, and 6z). The direct flux comparison agrees generally quite well with the BEF comparison approach earlier presented in Figure 25, but a few exceptions are apparent such as for 6ao and 6h. These two subecoregions showed the highest discrepancy between the model and measurement in terms of the emissions but not in terms of BEFs. Since the major difference was in footprint integration, it is assumed that in these two regions the inhomogeneity of footprint could be the cause of the discrepancy, in particular in 6h (Western Valley Foothills/Dunnigan Hills) which is very close to the boundary with Central Valley, where changes in elevation and PBL homogeneity could cause variable footprints on scales less than 2 km. Further analysis of the directional footprint may help decrease this local discrepancy where simulated emissions significantly overestimated the measured emissions. In the second instance, 6ao (Caliente Range) modeled emissions underestimate measured emissions, but this was not apparent earlier with BEF comparisons. In this case it is possible that the proximity to the Sierra Madre Mountains resulted in a non-homogenous footprint (but in the opposite direction). Nevertheless, these two most differing ecoregions were represented by only 4 and 5 points, for 6h and 6ao, respectively, so represent only 10 km of the track and perhaps could even have been omitted from this comparison. The high similarities between BEFs and fluxes in the remaining vast majority of subecoregions suggests that the footprint approach works well and shows that the inventory which CARB is using agrees extremely well with observations.

Although isoprene emissions were generally very low in the Central Valley, ecoregions 7m and 7o had considerable measured emissions which were not predicted by the model. These ecoregions correspond to the San Joaquin basin and Westside Alluvial Fans and Terraces, respectively and the landcover database is likely missing isoprene sources which were within the aircraft flux footprint, although may still be accurate when averaged over entire ecoregion 7m or 7a (Figure 25). Another interesting observation is that the emissions simulated by

CARB for flux footprint areas follow more closely the measured emissions, than the measured BEFs from the flights compared with BEFs averaged over entire ecoregions. To compare the BEFs in the same way would require using the similar footprint approaches as with the emissions but in any case both independent methods are consistent in the overall very good agreement between measured and modeled emissions.

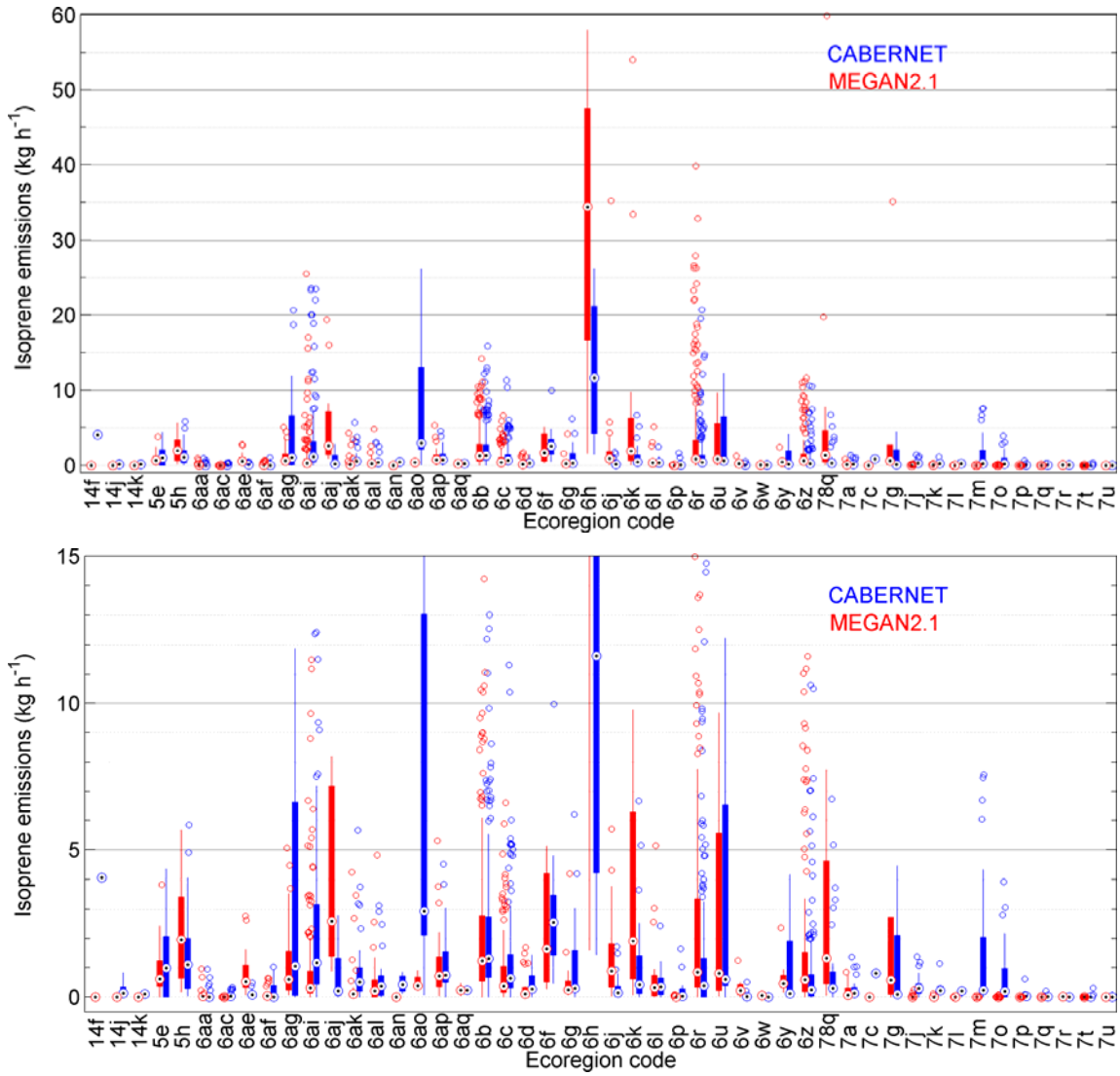

Figure 32 Box plots showing distribution of emissions in each of the level IV ecoregions. The boxes correspond to midrange (25th to 75th percentiles), the whiskers indicate variability outside the lower and upper quartiles, and the circles denote outlying emission hotspots.

We quantitatively compare measured and modeled fluxes in Figure 26a-c, and the X-Y plot in Figure 33 shows a robust regression. Because the comparison is more like the BEF case which looked at BEFs averaged over entire level IV ecoregions rather than for the corresponding areas of the flux footprint the R^2 is 0.96 with more than 70% of the points within the 95% confidence intervals. The 6h and 6ao ecoregion outliers are the most outstanding and have been discussed above. In the lower emission graph regions 5h , 6r, 6j, 6k, 6z simulated emissions seem to be overestimated. Region 5h is the Sierra Lower Mountain Forest ecoregion, and the other four are located in the northwestern coastal part of CA which is characterized by less homogenous coastal oak terrains, and could therefore be more sensitive to accuracies in spatial footprint positioning since some but not all of these overestimates were the case in the BEF comparison. This relatively small number of overestimates is balanced by underestimates (e.g. regions 7m, 7c, 14f, 6ag) where in some cases the modeled emissions were close to zero, suggesting inaccuracies of the landcover. Approximately 30 ecoregions showing extremely good agreement demonstrate the emissions are accurately simulated based on the approaches we chose in these comparisons.

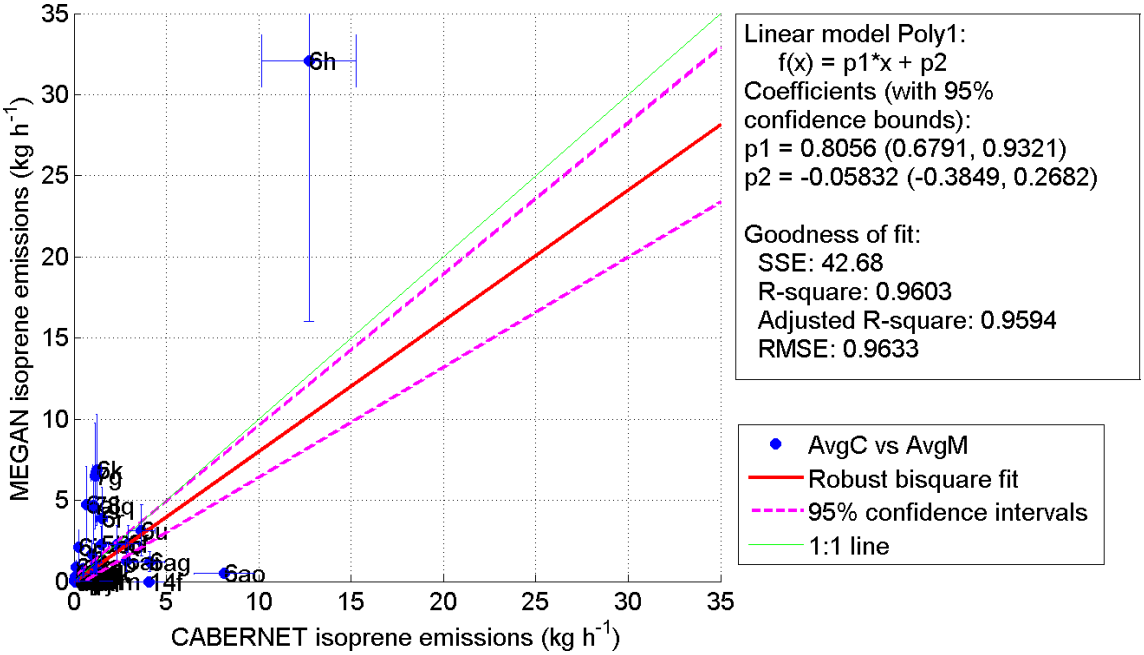

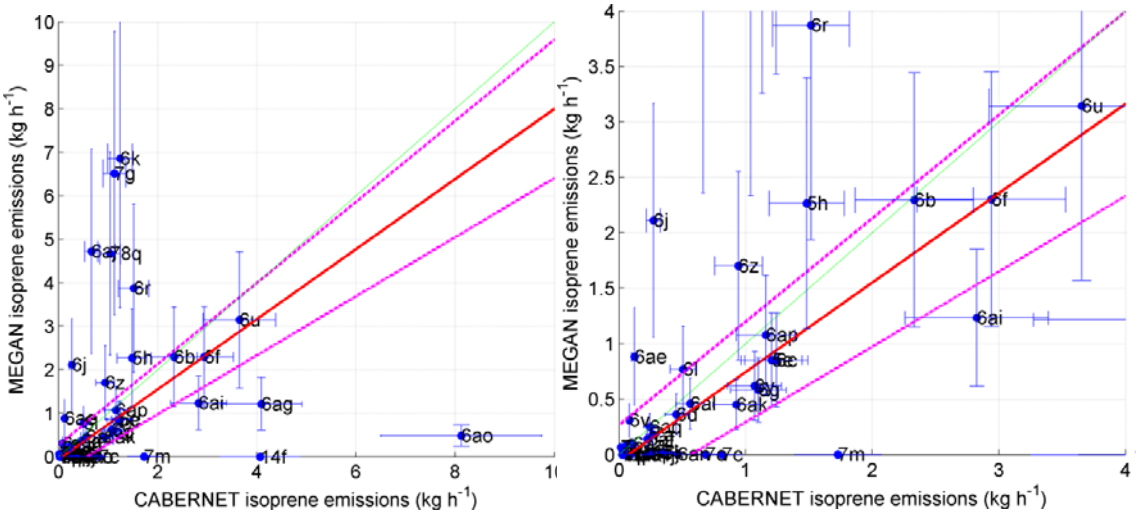

Figure 33. Scatter plots for the ecoregion averaged emissions. The vertical error bars represent the 50% model uncertainty and the horizontal error bars represent the 20% uncertainty of the measurement.

Quantitative comparisons between measured and modeled fluxes including summary statistics for each ecoregion are presented in Table 3

*Table 3. Summary quantitative statistics for CABERNET and MEGAN emisisons (kg h^{-1})**

		CABERNET					MEGAN				
Ecoregion	*N*	Mean	Median	SD	Min	Max	Mean	Median	SD	Min	Max
Total	1746	1.38	0.416	2.74	0	26.2	1.64	0.360	4.34	0	59.9
Good agreement											
5e	29	1.21	0.992	1.22	0.000	4.36	0.852	0.622	0.842	0.000	3.83
5h	26	1.48	1.11	1.509	0.039	5.85	2.27	1.96	1.70	0.175	5.69
6aa	28	0.113	0.000	0.231	0.000	0.949	0.095	0.026	0.216	0.000	0.962
6al	44	0.562	0.381	0.730	0.000	3.13	0.460	0.215	0.848	0.000	4.82
6ap	31	1.16	0.749	1.15	0.006	4.51	1.08	0.720	1.18	0.049	5.31
6b	196	2.33	1.31	2.67	0.000	15.9	2.30	1.23	2.66	0.008	14.2
6c	181	1.24	0.647	1.65	0.000	11.3	0.851	0.383	1.13	0.000	6.62
6d	24	0.453	0.275	0.440	0.000	1.45	0.364	0.113	0.530	0.000	1.70
6l	22	0.505	0.346	0.569	0.000	2.43	0.770	0.326	1.26	0.000	5.14
6z	136	0.944	0.252	1.88	0.000	10.6	1.70	0.592	2.66	0.000	11.6
7a	27	0.266	0.130	0.365	0.000	1.36	0.182	0.074	0.262	0.000	0.857
Model underestimates											
6ac	36	0.073	0.037	0.093	0.000	0.345	0.000	0.000	0.000	0.000	0.000
6af	24	0.223	0.00	0.341	0.000	1.03	0.140	0.040	0.214	0.000	0.647
6ag	30	4.09	1.05	5.47	0.000	20.7	1.22	0.607	1.39	0.067	5.07
6ai	201	2.83	1.17	4.41	0.000	23.6	1.24	0.307	2.92	0.000	25.5
6ak	36	0.927	0.513	1.24	0.000	5.66	0.453	0.108	0.975	0.013	4.25
6g	20	1.10	0.297	1.68	0.000	6.20	0.582	0.247	0.918	0.067	4.19
7j	35	0.358	0.295	0.337	0.000	1.37	0.015	0.000	0.050	0.000	0.257
7m	23	1.73	0.234	2.65	0.000	7.58	0.000	0.000	0.000	0.000	0.000
7o	38	0.683	0.203	0.994	0.000	3.93	0.004	0.000	0.014	0.000	0.085
7p	22	0.053	0.026	0.129	0.000	0.619	0.000	0.000	0.000	0.000	0.000
7t	23	0.025	0.005	0.066	0.000	0.318	0.000	0.000	0.000	0.000	0.000
Model overestimates											
6aj	23	0.665	0.205	0.820	0.008	2.80	4.72	2.59	4.84	0.873	19.4
6j	41	0.272	0.148	0.382	0.000	1.73	2.11	0.884	5.46	0.031	35.2
6k	22	1.241	0.423	1.80	0.000	6.69	6.86	1.92	12.7	0.070	54.0
6r	204	1.516	0.388	3.06	0.000	20.7	3.87	0.854	6.80	0.000	39.9
78q	32	1.040	0.297	1.64	0.000	6.75	4.67	1.32	10.8	0.060	59.9

*Ecoregions with *N*<20 (<40 km) were omitted from this table

On average for the entire available flux dataset, we conclude that the model overestimates the emissions by only 19% and this seems driven by a few high episodic events in the simulations which were not observed in the measured emissions (see earlier Figure 27). Interestingly, when comparing the median values the model is also very close to the observation with only 16% underestimation by the model. This is excellent agreement which is much better than the predicted accuracy of either the modeled or measured values. The analysis points to the importance of regional assessments of the modeled emissions where in some cases discrepancies may occur. For example, the subecoregion which was most extensively covered (~400 km, RF2, RF3, RF4) was 6b (Northern Sierran Foothills) and exhibited almost identical quantitative statistics for the model (mean 2.30, median 1.23, s.d. 2.66, min 0.008 and max 14.2 kg h^{-1}), and measurements (mean 2.33, median 1.31, s.d. 2.67, min 0.000, and max 15.9 kg h^{-1}), and the qualitative correspondence suggests we should have high confidence in the combination of the wavelet flux measurement, footprint analysis, and the emission modeling approach. This ecoregion includes the most homogeneously distributed oak woodlands and is therefore perhaps easier to model correctly in terms of properly estimating isoprene emissions in CA. Subecoregion 6d (Camanche Terraces) covered in 50 km of tracks was neighboring to the east with 6b and to the west with 7a, and with much sparser oaks showed lower emissions but still had reasonable agreement between the model (mean 0.364, median 0.113, s.d. 0.530, min 0.000, and max 1.70 kg h^{-1}) and measurements (mean 0.453, median 0.275, s.d. 0.440, min 0.000, and max 1.45 kg h^{-1}). On the other hand there are regions where quantitative agreement is not as good, such as coastal 6ai (Interior Santa Lucia Range) represented in ~400 km of the flight tracks where on average the model underestimated the emissions by approximately a factor of two or 7m (San Joaquin Basin), where the model showed zero emissions (over ~50 km of tracks) and isoprene emissions were measured as high as 7.58 (mean 1.73) kg h^{-1}. An opposite example in a different region (6r, East Bay Hills/Western Diablo Range) where ~400 km were measured had model overestimation by about a factor of 2. This region suffered from fires with the most notable fire storm in 1991. Apart from the changes in landcover, the discrepancies may be caused by inaccuracies in meteorological driving inputs although probably to a lesser degree based on results from our sensitivity study. In cases where the footprint was near the boundary of the oaks the circular footprint approach may be responsible for poorer agreement. An example for a non-homogeneous situation when

this might happen is shown in Figure 34. The half-dome footprint approach is currently still being developed so for this report it has been assumed that the full-dome footprint should be a sufficiently good approximation for most areas, although this issue should be kept in mind.

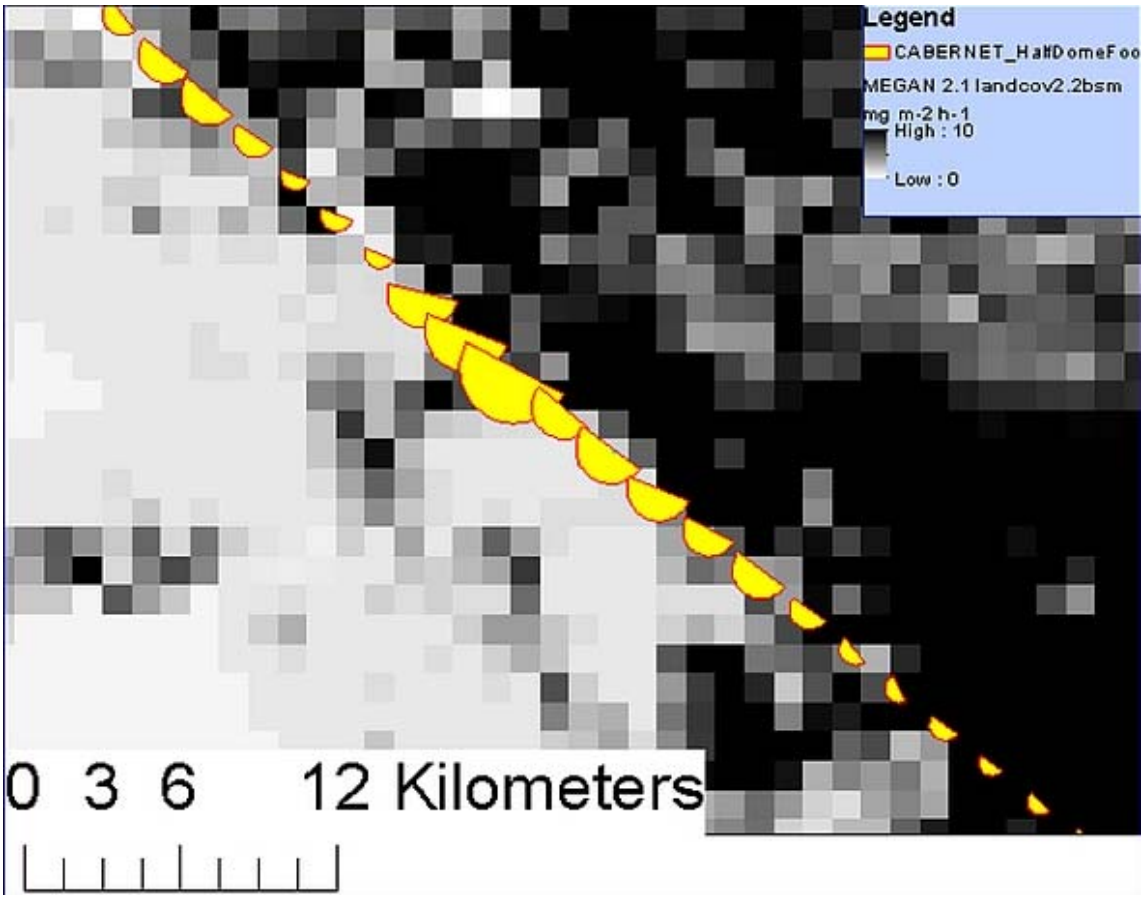

Figure 34. An example of a non-homogenous landcover where half dome footprint faced upwind would be superior to full-dome footprint of the same area.

6.2 Conclusions

Accurate prediction of isoprene emissions is crucial for air quality modeling and ozone forecasting in the state of California. We used direct airborne flux measurements over the

main regions in California where emissions are expected to be high to evaluate CARB's inventory based on MEGAN 2.1 that is used for simulation isoprene emissions of those areas. This is the model currently being considered for use by the state of California for simulating BVOC emissions important for development of the SIP for air quality. The approaches that were used in the comparison of the model with observation involved comparison of airborne and landcover BEFs and independently the emissions integrated over the same footprint areas. The agreement that was obtained was extremely good. Mean measured and modeled emissions agreed within 50% for half of the ecoregions, while for 21% of the ecoregions the model overestimated mean measured emissions and for 29% the model underestimated emissions. On average the agreement of model with measurement was within 19% over the whole dataset. The conducted sensitivity tests for a 20% change in temperature, 20% change in PAR and 50% change in LAI altered the total mean of the simulated fluxes by up to 43%, 21%, and 40%, respectively. Although the change in these input variables would not improve the overall agreement significantly, it could significantly impact specific regional agreements. The quality of the model output is directly tied to the input datasets and based on our analysis we conclude that the most important or uncertain input database is the landcover. The measurements were done in late spring, immediately after a period of relatively cold and cloudy weather, when the emission potentials were likely changing due to seasonally increasing temperatures. Similar aircraft flux measurements of BVOC emissions should be done again during the hotter part of the summer when isoprene emissions are expected to be highest in order to make sure maximum emissions are properly represented during periods when ozone pollution is the most problematic.

7 Additional Analyses

7.1 Methanol emissions from Dairies

Methanol was found to be the most abundant VOC in California with mean concentrations in CABERNET flights of 7.0 ppb (median 6.8 ppb). Maximum concentrations were found in the central valley and often exceeding 10 ppb. The spatial pattern of methanol concentrations was significantly different than that of isoprene and MVK+MAC. Methanol has a longer atmospheric lifetime of about a week which broadens the concentration distribution such that they are not as obviously representative of the spatial patterns of sources (see Sect. 3.4).

7.1.1 Methanol fluxes

The fluxes derived from wavelet analysis (Figure 35) point more accurately to methanol sources and sinks because their flux footprint is in the order of ~ 1 km while the concentration footprint is more than an order of magnitude larger. These differences in the spatial patterns explain high methanol concentrations (Figure 22c) over the oak bands which come with the upslope winds blowing towards the Sierra Nevada Mountains bringing methanol from the dairies in the Central Valley. Interestingly, these high-methanol concentrations downwind of the valley were often coincident with observations of a depositing flux. This is in contrast to the areas above the dairies which fall within the flux footprint with emissions exceeding 2 mg m^{-2} h^{-1}. The dominant source of methanol in California seems to be the dairies, although methanol emission hotspots were also found near growing conifers with elongating needles and around landfill facilities. Methanol flux was also high over a large beef cattle operation (denoted by a pink triangle in Figure 35) which was not previously included in the CARB emission database (dairy map 2004). Further analysis of the observed methanol concentrations and fluxes is beyond the scope of the current project, but we intend to use this data for more detailed analysis in the future.

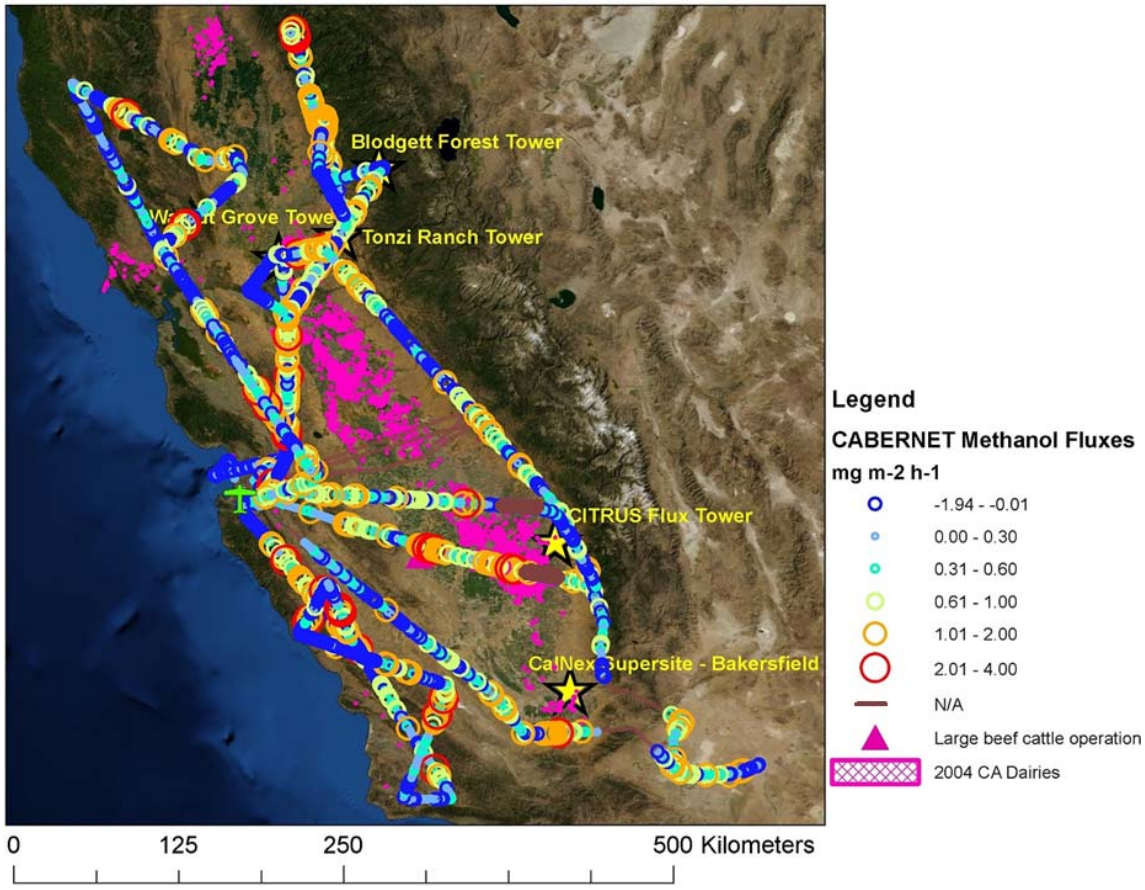

Figure 35. Methanol fluxes observed in CABERNET. [Preliminary data]

7.2 Fluxes of aromatics from oil fields

During RF 1 we included PTRMS measurements of benzene, toluene, and C-8 aromatic compounds while flying over the Central Valley. The track of this RF colored by concentration of these species is shown in Figure Figure 36. The highest concentrations of aromatics were found on transects through the Central Valley and near the south-eastern oak woodland band not far from Bakersfield. To check for their emissions from oil fields we selected an 80 km stretch for calculating fluxes on the returning leg closest to those areas. Concentrations, fluxes and wavelet cross spectra for toluene, benzene, and C-8 aromatics on an 80 km segment close to oil fields (RF1) are shown in Figure 37. Two events (event 1 and 2) occurred simultaneously in concentrations toluene, benzene and C8 aromatics, while a third event (event 3) had concentration enhancements of toluene and C-8 aromatics but no benzene. The wavelet fluxes show that the footprint area of event 1 was associated with a small

emission for all the aromatics measured; while the footprint of event 2 was associated with strong emission of all those aromatic compounds from nearby oil fields. Finally, event 3 showed clear emission of toluene and C-8 aromatics but no flux of benzene. We attribute event 2 to emission from an oil field with source strengths of 2.4, 1.7, and 2.8 mg m^{-2} h^{-1} for toluene, benzene and C-8 aromatics, respectively. Event 3 occurred close to an industrial facility. Further analysis of the observed aromatics from oil fields is beyond the scope of the current project, but again we intend to use this data for more detailed analysis in the future. We also believe it demonstrates the potential to measure emissions of a much wider range of VOCs using wavelet analysis eddy covariance from aircraft.

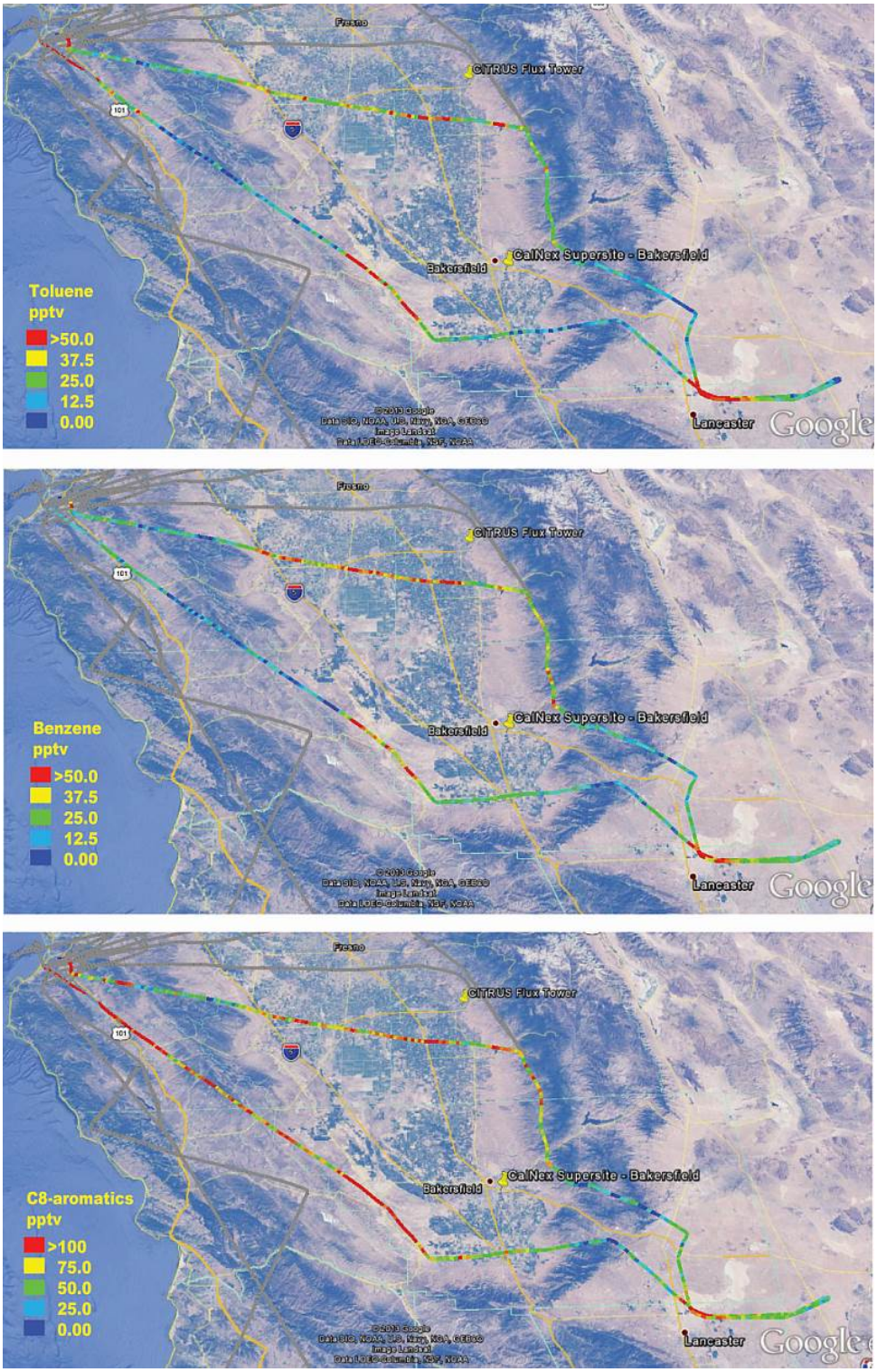

Figure 36. Toluene, benzene and C-8 aromatics concentration distributions on the RF 1 track.

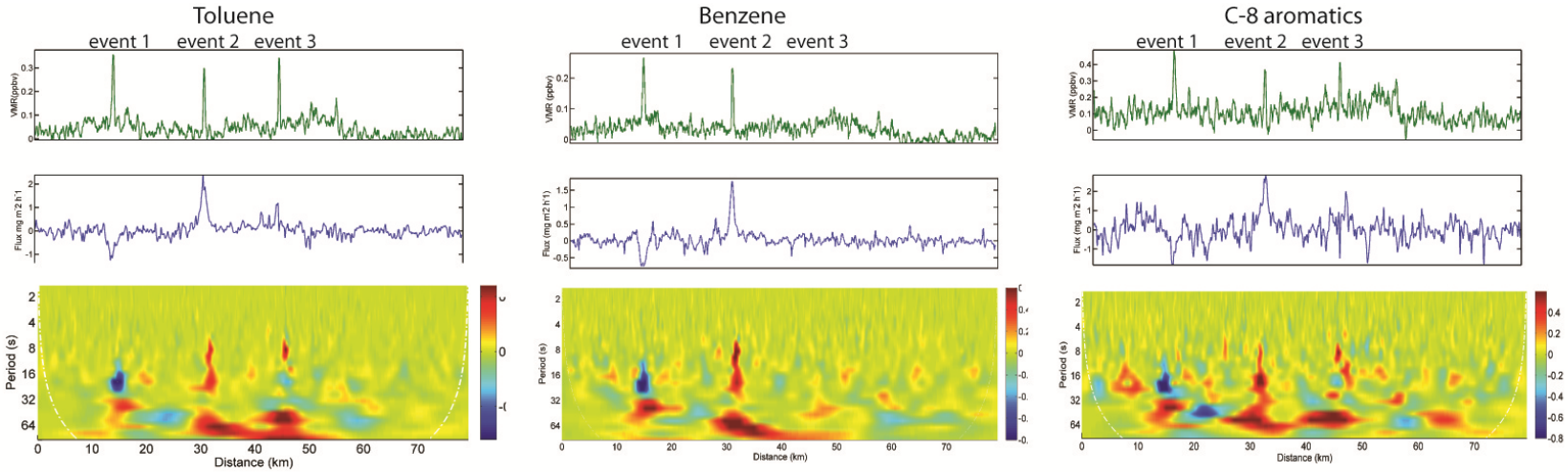

Figure 37. Concentrations, Fluxes and Wavelet cross spectra shown for toluene, benzene, and C-8 aromatics on a 80 km segment close to oil fields (RF1). The wavelet fluxes and their cross spectra deliver more information on the source/sink profile of the encountered aromatics.

7.3 Early modeling efforts

7.3.1 Comparison of BEIGIS and MEGAN 2.0 emission factors for California

Prior to the campaign the emission factors from MEGAN 2.0 (Guenther et al., 2006) and BEIGIS (Scott and Benjamin, 2003) were compared and a map showing the differences was constructed in order to guide measurement flights towards areas where these models indicated high emissions were likely, or where the models disagreed.

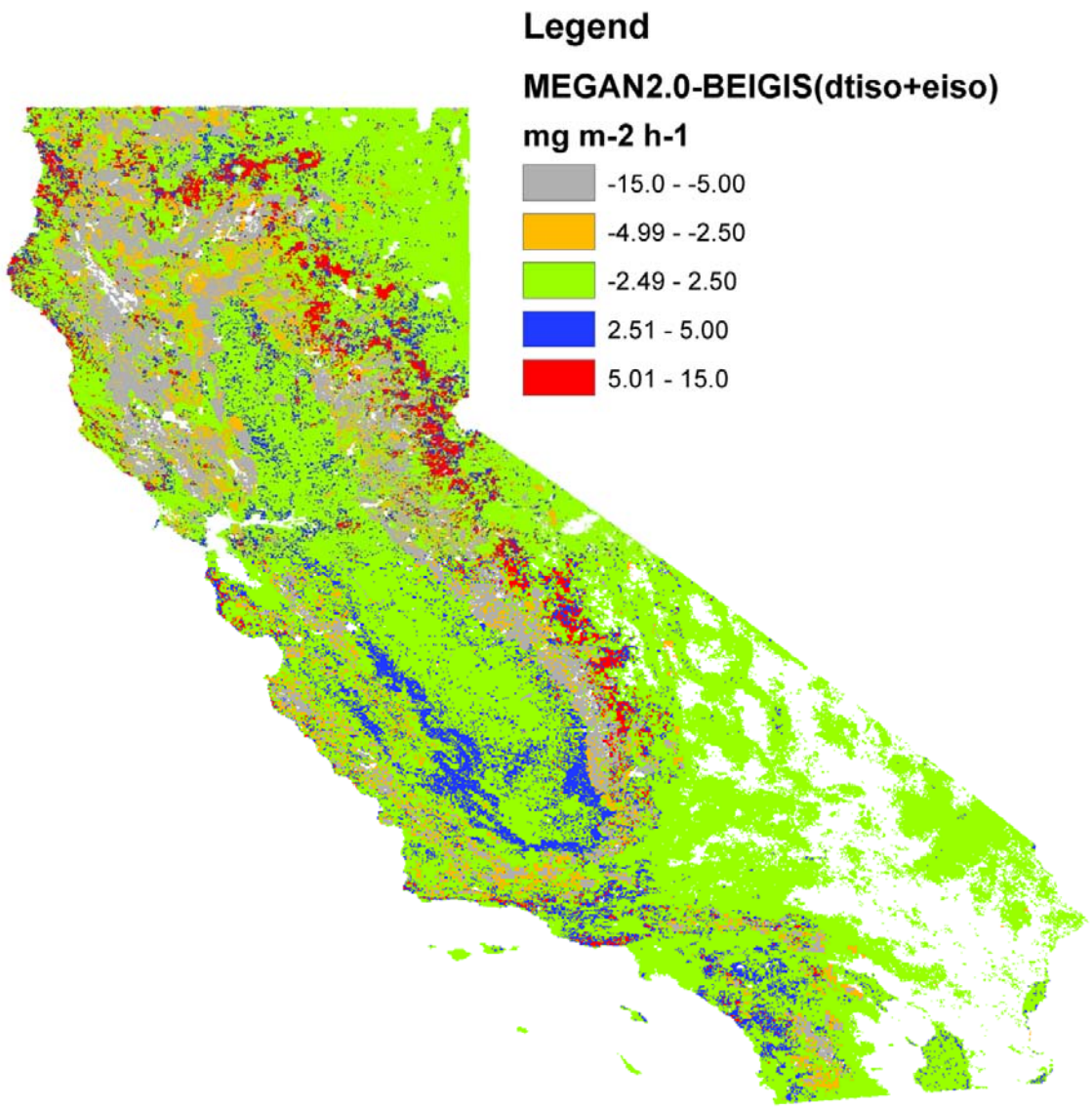

Figure 38. Map showing a difference between MEGAN2.0 and BEIGIS (eiso+dtiso) emission factors. The BEIGIS emission factors were roughly converted to land area units my multiplying mg g^{-1} h^{-1} by LAI 5.

The green areas show where the difference in MEGAN and BEIGIS emission factors was less than 2.5 mg m^2 h^{-1}. Some areas between the Sierra foothills and the Central Valley are shown in red where BEIGIS suggested higher emission factors than MEGAN. These areas correspond to oak woodlands and became the focus for many of the research flight tracks. For the areas higher into the Sierra Nevada Mountains, the opposite was the case (MEGAN>BEIGIS) but these areas were not selected for the flight tracks because of the very hilly terrain which were considered difficult areas for the flux measurements and because of the limits of the range of the Twin Otter for the available flight-time. The Western Coastal side off the Central Valley also showed interesting differences with MEGAN>BEIGIS in the Central Coast and BEIGIS>MEGAN in the Northern Coast. These areas were also used to guide the flight planning.

7.4 Application of reverse G06 algorithm to the airborne fluxes

Comparison of the measured fluxes to the model emission potentials was done after calculating BEF's from the measurements. The raw data undergoes the following workflow to obtain airborne BEFs from the airborne fluxes:

1) Application of wind corrections from "Lenschow maneuvers"
2) Derivation of airborne concentrations from daily calibrations
3) Wavelet and FFT flux derivation at aircraft altitude
4) Interpolation of fluxes at aircraft altitude to the surface fluxes using coefficients from racetracks, and (z/z_i) (i.e. accounting for flux divergence)
5) Spatial averaging of surface fluxes to 2 km resolution
6) Derivation of BERs by normalization of the surface fluxes using surface temperature and PAR according to MEGAN algorithm which accounts for previous temperature and PAR history (equation from Misztal et al., 2011):

$$F_{G06} = \mathrm{BER} \cdot \underbrace{\mathrm{b}_3 \cdot \exp\left[\mathrm{b}_2 \cdot (P_{24} - P_0)\right] \cdot (P_{240})^{0.6} \cdot \frac{\left[\mathrm{b}_1 - \mathrm{b}_2 \ln(P_{240})\right] \cdot \mathrm{PAR}}{\sqrt{1 + \left[\mathrm{b}_1 - \mathrm{b}_2 \ln(P_{240})\right]^2 \cdot \mathrm{PAR}^2}}}_{\gamma_P} \cdot \underbrace{\mathrm{b}_5 \cdot \exp\left[\mathrm{b}_6 \cdot (T_{24} - 297)\right] \cdot \exp\left[\mathrm{b}_6 \cdot (T_{240} - 297)\right] \cdot \frac{\mathrm{C}_{T2} \cdot \exp\left[\mathrm{C}_{T1} \cdot \left(\frac{1}{T_{\mathrm{opt}}} - \frac{1}{T}\right) \cdot \frac{1}{0.00831}\right]}{\mathrm{C}_{T2} - \mathrm{C}_{T1} \cdot \left[1 - \exp\left(\mathrm{C}_{T2} \cdot \left(\frac{1}{T_{\mathrm{opt}}} - \frac{1}{T}\right) \cdot \frac{1}{0.00831}\right)\right]}}_{\gamma_T}$$

8 Summary and conclusions

Direct AvDEC fluxes of isoprene and several other VOCs were measured by a PTR-MS aboard a CIRPAS Twin Otter aircraft on almost 10,000 km of flight tracks covering most of California's oak woodlands and many nearby landscapes. The aircraft measurements were made on June 8, 9, 10, 14, 15, 16, 20, and 31 as part of the CABERNET project which was the first regional airborne flux study focused on isoprene. The acquired airborne data were processed into concentrations, fluxes, emission factors and grid area emissions and were used to evaluate the landcovers and predictions of the model simulating biogenic VOC emissions in California.

8.1 Refinement of AEC approach for BVOC flux measurements

Homogenous oak woodland areas were selected for vertical characterization of fluxes in racetrack profiles. These vertically resolved measurements showed that first order chemistry can describe the decrease of isoprene fluxes throughout the PBL under typical atmospheric conditions with experimentally determined Dahmköhler numbers in the range of 0.3 to 0.9. We demonstrated that the eddy covariance measurements of volatile organic compounds can be used to characterize heterogeneous surface emissions using wavelet analysis. In addition we demonstrated that flux divergence measurements can be used to provide estimates of OH.

8.2 Oak woodlands major isoprene source in California

The survey flight products were comprised of 2-km spatially resolved fluxes which were used to map out horizontally varying source distributions of isoprene emissions for the

dominant oak emitting ecosystems in California. High concentrations (up to 8 ppbv) and high surface emissions of isoprene ranging from several to more than ten mg m^{-2} h^{-1} were observed from the oak woodlands in the foothills of the Sierra Nevada and Coastal Ranges. Consistent with other studies we showed that in the Central Valley isoprene emissions are typically undetectably small at aircraft level except for some areas of Eucalyptus trees planted near the highways from which emissions were detected.

8.3 Evaluation of input landcovers and model performance

Airborne emission factors derived as measured fluxes normalized for temperature and PAR using Guenther et al., 2006 activity factors were directly compared with emission factors from the MEGAN2.1 model landcover used by CARB. Subsequently, grid area averaged emissions for corresponding aircraft footprints were compared with emissions simulated by CARB using an adaptation of the MEGAN2.1 model for the entire CA domain and averaged for specific California ecoregions. Measured BEFs showed generally good correspondence with the landcover and quantitative agreement with the modeled emissions was remarkable over the majority of ecoregions. On average for all ecoregions the model and measurement were within 19% agreement. Regional discrepancies were identified and pointed to some inaccuracies in the landcover. A sensitivity analysis showed that 20% change in temperature, 20% change in PAR or 50% change in LAI could have a significant influence on regional agreement and could alter the overall mean flux by up to 43%, 21% and 40%, respectively. The wide range of temperatures encountered in the CABERNET campaign following a significantly cooler period pointed to the need for using the past history of temperature and PAR in the model to adjust the basal emission potentials. A study in a warmer season would

be useful to confirm the full emission capacity of Oak ecosystems during the peak ozone season.

We conclude that CARB's modeling approach provides accurate simulations of isoprene for use in modeling ozone formation. Further work on landcover database improvements and more accurate representations of the measurement footprint using a half-dome footprint approach is continuing in collaboration with CARB.

9 Recommendation for future research

We have demonstrated the capability for direct VOC flux measurements from an aircraft using PTRMS. The application of this capability to isoprene flux measurements was demonstrated for the first time in this project. More airborne measurements are required to achieve better statistics for measurement-model intercomparisons, and for including more urban areas or Eucalyptus dominated regions for isoprene. A Time-of-Flight version of the PTR-MS (PTR-ToF-MS) with high sensitivity suitable for airborne flux measurements is now available which does not require limiting the number of VOCs measured and thus would enable simultaneous measurements of a full range of VOC fluxes and could therefore contribute observations for a much more complete emission inventory. Additional potential foci for future work include:

1) Use PTR-ToF-MS to measure a full suite of VOC concentrations and fluxes from aircraft (not limited to a few masses by the quadrupole MS).

2) Measure fluxes from a much broader variety of sources to test the ARB's anthropogenic and biogenic emissions inventories for VOC.

3) Further modeling with the current data set should focus on optimization of the flux footprint analysis for more accurate spatial comparisons between fluxes measured from aircraft and modeled fluxes.

4) Expand the scope of measurements to include GHG's CH_4, CO_2, and possibly N_2O. Could also include NOx/NOy, or other species for which fast measurements are available and emission inventories may be uncertain.

5) A measurement program is needed to focus on sources of oxygenated VOC in the San Joaquin Valley, particularly methanol and associated compounds from dairy emissions, and a suite of VOC's from agricultural management operations (pruning, harvesting, flowering, composting organic material).

6) An airborne flux study focused on VOC fluxes in urban areas is needed to determine biogenic VOC contributions from urban vegetation and compare them to VOC emissions from anthropogenic sources.

10 Literature Cited

Apel, E., Riemer, D., Hills, A., Baugh, W., Orlando, J., Faloona, I., Tan, D., Brune, W., Lamb, B., and Westberg, H.: Measurement and interpretation of isoprene fluxes and isoprene, methacrolein, and methyl vinyl ketone mixing ratios at the PROPHET site during the 1998 Intensive, Journal of Geophysical Research, 107, 4034, 2002.

Arey, J., A.M. Winer, R. Atkinson, S.M. Aschmann, W.D. Long, C.L. Morrison, and D.M. Olszyk. 1991. Terpenes emitted from agricultural species found in California's Central Valley. J. Geophys. Res., 96: 9329–9336.

Arey, J., D.E. Crowley, M. Crowley, M. Resketo, and J. Lester. 1995. Hydrocarbon emissions from natural vegetation in California's South Coast Air Basin. Atmos. Environ. 29: 2977-2988.

Arey, J., Winer, A. M., Atkinson, R., Aschmann, S. M., Long, W. D., and Lynn Morrison, C.: The emission of (Z)-3-hexen-1-ol,(Z)-3-hexenylacetate and other oxygenated hydrocarbons from agricultural plant species, Atmospheric Environment. Part A. General Topics, 25, 1063-1075, 1991.

Baker, B., A. Guenther, J. Greenberg, A.H. Goldstein, and R. Fall. 1999. Canopy fluxes of 2-methyl-3-buten-2-ol over a ponderosa pine forest by relaxed eddy accumulation: Field data and model comparison. J. Geophys. Res. 104: 26107-26114.

Baldocchi, D. D.: Assessing the eddy covariance technique for evaluating carbon dioxide exchange rates of ecosystems: past, present and future, Global Change Biol, 9, 479-492, 2003.

Baldocchi, D., and Ma, S.: How will land use affect air temperature in the surface boundary layer? Lessons learned from a comparative study on the energy balance of an oak savanna and annual grassland in California, USA, Tellus B, 65, 2013.

Baldocchi, D., Tang, J., and Xu, L.: How switches and lags in biophysical regulators affect spatial-temporal variation of soil respiration in an oak-grass savanna, Journal of Geophysical Research: Biogeosciences (2005–2012), 111, 2006.

de Gouw, J., Warneke, C., Karl, T., Eerdekens, G., van der Veen, C. and R. Fall, 2003: Sensitivity and specificity of atmospheric trace gas detection by Proton-Transfer-Reaction Mass Spectrometry, Int. J. for Mass Spectrometry, 223, 365-382.

Desjardins, R. L., Hart, R. L., Macpherson, J. I., Schuepp, P. H., and Verma, S. B.: Aircraft-Based and Tower-Based Fluxes of Carbon-Dioxide, Latent, and Sensible Heat, J Geophys Res-Atmos, 97, 18477-18485, 1992.

Desjardins, R. L., MacPherson, J. I., Mahrt, L., Schuepp, P., Pattey, E., Neumann, H., Baldocchi,

EPA, Ecoregions of California, CA poster, ftp resource (accessed 1/31/2014): ftp://ftp.epa.gov/wed/ecoregions/ca/CA_poster-front_Dec2010_DRAFT_v7.2.pdf.

Faloona, I., Lenschow, D.H., Campos, T., Stevens, B., van Zanten, M., Blomquist, B., Thornton, D., Bandy, A. and H. Gerber, 2005: Observations of entrainment in eastern Pacific marine stratocumulus using three conserved scalar. J. Atmos. Sci., 62, 3268-3285.

Griffith, G.E., Omernik, J.M., Smith, D.W., Cook, T.D., Tallyn, E., Moseley, K., Sleeter, B., and Johnson,C.B., 2011(draft), Ecoregions of California: U.S. Geological Survey, Open File Report 2011-xxxx, xx p.

Fares, S., Gentner, D. R., Park, J. H., Ormeno, E., Karlik, J., and Goldstein, A. H.: Biogenic emissions from Citrus species in California, Atmospheric Environment, 45, 4557-4568, DOI 10.1016/j.atmosenv.2011.05.066, 2011.

Fares, S., Park, J. H., Gentner, D. R., Weber, R., Ormeno, E., Karlik, J., and Goldstein, A. H.: Seasonal cycles of biogenic volatile organic compound fluxes and concentrations in a California citrus orchard, Atmos Chem Phys, 12, 9865-9880, DOI 10.5194/acp-12-9865-2012, 2012.

Fuentes, J. D., and Wang, D.: On the seasonality of isoprene emissions from a mixed temperate forest, Ecological Applications, 9, 1118-1131, Doi 10.2307/2641382, 1999.

Goldstein, A. H., and Galbally, I. E.: Known and unexplored organic constituents in the earth's atmosphere, Environmental Science & Technology, 41, 1514-1521, 2007.

Goldstein, A. H., Goulden, M. L., Munger, J. W., Wofsy, S. C., and Geron, C. D.: Seasonal course of isoprene emissions from a midlatitude deciduous forest, Journal of Geophysical Research: Atmospheres (1984–2012), 103, 31045-31056, 1998.

Goldstein, A., Hultman, N., Fracheboud, J., Bauer, M., Panek, J., Xu, M., Qi, Y., Guenther, A., and Baugh, W.: Effects of climate variability on the carbon dioxide, water, and sensible heat fluxes above a ponderosa pine plantation in the Sierra Nevada (CA), Agr Forest Meteorol, 101, 113-129, 2000.

Goldstein, A.H., and Schade, G.W.: Quantifying biogenic and anthropogenic contributions to acetone mixing ratios in a rural environment, Atmospheric Environment, 34, 29-30, 4997-5006, 2000.

Greenberg, J. P., Guenther, A., Zimmerman, P., Baugh, W., Geron, C., Davis, K., Helmig, D., and L.F. Klinge: 1999, Tethered balloon measurements of biogenic VOCs in the atmospheric boundary layer. Atmos. Environ., 33, 855–867.

Guenther, A. B., Jiang, X., Heald, C. L., Sakulyanontvittaya, T., Duhl, T., Emmons, L. K., and Wang, X.: The Model of Emissions of Gases and Aerosols from Nature version 2.1 (MEGAN2.1): an extended and updated framework for modeling biogenic emissions, Geosci Model Dev, 5, 1471-1492, DOI 10.5194/gmd-5-1471-2012, 2012.

Guenther, A. B., Zimmerman, P. R., Harley, P. C., Monson, R. K., and Fall, R.: Isoprene and monoterpene emission rate variability - model evaluations and sensitivity analyses, J Geophys Res-Atmos, 98, 12609-12617, 1993.

Guenther, A., Greenberg, J., Harley, P., Helmig, D., Klinger. L, Vierling, L., Zimmerman, P., and C. Geron, 1996: Leaf, branch, stand and landscape scale measurements of volatile organic compound fluxes from US woodlands. Tree Physiology, 16, 17-24.

Guenther, A., Karl, T., Harley, P., Wiedinmyer, C., Palmer, P. I., and Geron, C.: Estimates of global terrestrial isoprene emissions using MEGAN (Model of Emissions of Gases and Aerosols from Nature), Atmos Chem Phys, 6, 3181-3210, 2006.

Hamba, A., 1993: Modified K Model for Chemically Reactive Species in the Planetary Boundary Layer. J. Geophys. Res., 98, 5173–5182.

Hegg, D. A., Covert, D. S., Jonsson, H., and Covert, P. A.: Determination of the transmission efficiency of an aircraft aerosol inlet, Aerosol Sci Tech, 39, 966-971, Doi 10.1080/02786820500377814, 2005.

Hofzumahaus, A, Rohrer, F., Keding, L, Bohn, B., Brauers, T., Chang, C.C., Fuchs, H., Holland, F., Kita, K., Yukata, K., Xin, L., Shengrong, L., Shao, M., Zeng, L., Wahner, A., and Y. Zhang, 2009: Amplified trace gas removal in the troposphere. Science, 324, 1702-1704, DOI: 10.1126/science.1164566

Hong, S.Y., Noh, Y., Dudhia, J., Korea, S., and M.M Division, 2006: A New Vertical Diffusion Package with an Explicit Treatment of Entrainment Processes. Monthly Weather Review, 2318–2341.

Horst, T., and Weil, J.: Footprint estimation for scalar flux measurements in the atmospheric surface layer, Boundary-Layer Meteorology, 59, 279-296, 1992.

Jeong, S., Zhao, C., Andrews, A. E., Dlugokencky, E. J., Sweeney, C., Bianco, L., Wilczak, J. M., and Fischer, M. L.: Seasonal variations in N2O emissions from central California, Geophys Res Lett, 39, 2012.

Karl, T. G., Spirig, C., Rinne, J., Stroud, C., Prevost, P., Greenberg, J., Fall, R., and Guenther, A.: Virtual disjunct eddy covariance measurements of organic compound fluxes from a subalpine forest using proton transfer reaction mass spectrometry, Atmos Chem Phys, 2, 279-291, 2002.

Karl, T., A. Guenther, R. J. Yokelson, J. Greenberg, M. Potosnak, D. R. Blake, and P. Artaxo, 2007: The tropical forest and fire emissions experiment: Emission, chemistry, and transport of biogenic volatile organic compounds in the lower atmosphere over Amazonia. J. Geophys. Res., 112, D18302, doi:10.1029/2007JD008539.

Karl, T., Apel, E., Hodzic, A., Riemer, D. D., Blake, D. R., and Wiedinmyer, C.: Emissions of volatile organic compounds inferred from airborne flux measurements over a megacity, Atmos Chem Phys, 9, 271-285, 2009.

Karl, T., Guenther, A., Turnipseed, A., Patton, E. G., and Jardine, K.: Chemical sensing of plant stress at the ecosystem scale, Biogeosciences, 5, 1287-1294, 2008.

Karl, T., Misztal, P. K., Jonsson, H. H., Shertz, S., Goldstein, A. H., and Guenther, A. B.: Airborne flux measurements of BVOCs above Californian oak forests: Experimental

investigation of surface and entrainment fluxes, OH densities and Dahmköhler numbers, J Atmos Sci, 10.1175/jas-d-13-054.1, 2013.

Karlik, J. F., and McKay, A. H.: Leaf area index, leaf mass density, and allometric relationships derived from harvest of blue oaks in California oak savanna, USDA Forest Service General Technical Report Number PSW-GTR-184, 2002.

Karlik, J. F., and Winer, A.M.: Measured isoprene emission rates of plants in California landscapes: comparison to estimates from taxonomic relationships, Atmospheric Environment, 35, 1123-1131, 2001.

Kristensen, L., Andersen, C. E., and H.E. Jørgensen, 1997: First-Order Chemistry in the Surface-Flux Layer. J. Atmos. Chem., 2, 249–269.

Kuhn, U., Rottenberger, S., Biesenthal, T., Wolf, A., Schebeske, G., Ciccioli, P., Brancaleoni, E., Frattoni, M., Tavares, T., and Kesselmeier, J.: Isoprene and monoterpene emissions of Amazonian tree species during the wet season: Direct and indirect investigations on controlling environmental functions, Journal of Geophysical Research, 107, 8071, 2002.

Kurpius, M.R., and Goldstein, A.H.: Gas-phase chemistry dominates O3 loss to a forest, implying a source of aerosols and hydroxyl radicals to the atmosphere. Geophys. Res. Let. 30: 1371 doi:10.1029/2002GL016785, 2003.

Lamb, B., Westberg, H., and Allwine, G.: Isoprene Emission Fluxes Determined by an Atmospheric Tracer Technique, Atmospheric Environment, 20, 1-8, Doi 10.1016/0004-6981(86)90201-5, 1986.

Langford, B., Misztal, P. K., Nemitz, E., Davison, B., Helfter, C., Pugh, T. A. M., MacKenzie, A. R., Lim, S. F., and Hewitt, C. N.: Fluxes and concentrations of volatile organic compounds from a South-East Asian tropical rainforest, Atmos. Chem. Phys., 10, 8391-8412, 10.5194/acp-10-8391-2010, 2010.

Lelieveld, J., Butler, T. M., Crowley, J. N., Dillon, T. J., Fischer, H., Ganzeveld, L., Harder, H., Larwence. M.G., Martinez, M., Taraborrelli, D., and J. Williams, 2008: Atmospheric oxidation capacity sustained by a tropical forest. Nature, 452, 737–40. doi:10.1038/nature06870

Lenschow, D. H., Cullian, C. A., Friese, R. B. and E. N. Brown, 1978: The status of air motion measurements on NCAR aircraft. Proc., AMS 4th Symposium on

Meteorological Observations and Instrumentation, 10-14 April 1978, Denver, Colorado, 433- 438.

Lenschow, D. H., Mann, J., and Kristensen, L.: How Long Is Long Enough When Measuring Fluxes and Other Turbulence Statistics, J Atmos Ocean Tech, 11, 661-673, 1994.

Lenschow, D. H., Pearson, R., and Stankov, B. B.: Estimating the Ozone Budget in the Boundary-Layer by Use of Aircraft Measurements of Ozone Eddy Flux and Mean Concentration, J Geophys Res-Oc Atm, 86, 7291-7297, 1981.

Lenschow, D., Delany, A., Stankov, B., and Stedman, D. H.: Airborne measurements of the vertical flux of ozone in the boundary layer, Boundary-Layer Meteorology, 19, 249-265, 1980.

Lenschow, D.: Probing the Atmospheric Boundary Layer, Probing the Atmospheric Boundary Layer, American Meteorological Society, 1986.

Lenschow, D.H., and L. Kristensen, 1984: Uncorrelated noise in turbulence measurements. J. Atmos. Oceanic Techn., 2, 68-81.

Lenschow, D.H., Mann, J., and L Kristensen, 1994: How long is long enough when measuring fluxes and other turbulence statistics. Journal of Atmospheric and Oceanic Technology, 11, 661-673.

Lin, Y.L., and I.C. Jao, 1995: A numerical study of flow circulations in the Central Valley of California and formation mechanisms of the Fresno Eddy, Monthly Weather Review, 123, 3227-3239.

Liu, Y., San Liang, X., and R.H. Weisberg, 2007: Rectification of the Bias in the Wavelet Power Spectrum. Journal of Atmospheric and Oceanic Technology, 24, 2093–2102. doi:10.1175/2007JTECHO511.1

Loreto, F., and Sharkey, T. D.: A gas-exchange study of photosynthesis and isoprene emission inQuercus rubra L, Planta, 182, 523-531, 1990.

Mauder, M., Desjardins, R. L., and MacPherson, I.: Scale analysis of airborne flux measurements over heterogeneous terrain in a boreal ecosystem, Journal of Geophysical Research: Atmospheres (1984–2012), 112, 2007.

Mauldin III, R.L., Berndt, T., Sipilä, M., Paasonen, P., Petäjä, T., Kim, S., Kurtén, T., Stratmann, F., Kerminen, C.M., and M. Kulmala, 2012: A new atmospherically relevant oxidant of sulphur dioxide. Nature, 488,193–196, doi:10.1038/nature11278.

Metzger, S., Junkermann, W., Mauder, M., Butterbach-Bahl, K., Trancón y Widemann, B., Neidl, F., Schäfer, K., Wieneke, S., Zheng, X., and Schmid, H.: Spatially explicit regionalization of airborne flux measurements using environmental response functions, Biogeosciences, 10, 2193-2217, 2013.

Misztal, P.K., Karl T., Jiang, X., Avise, J., Scott, K., Guenther, A.B., and A.H. Goldstein, 2013: Characterization of isoprene emission factors from oak woodlands derived from airborne eddy covariance over California. in preparation.

Moeng, C.H. and P. Sullivan, P.: 1994, A Comparison of Shear and Buoyant Driven Planetary Boundary Layer Flows. J. Atmos. Sci., 51, 999–1022.

Moore, C.: Frequency response corrections for eddy correlation systems, Boundary-Layer Meteorology, 37, 17-35, 1986.

Niinemets, Ü., Tenhunen, J., Harley, P., and Steinbrecher, R.: A model of isoprene emission based on energetic requirements for isoprene synthesis and leaf photosynthetic properties for Liquidambar and Quercus, Plant, Cell & Environment, 22, 1319-1335, 1999.

Nordbo, A., and Katul, G.: A Wavelet-Based Correction Method for Eddy-Covariance High-Frequency Losses in Scalar Concentration Measurements, Boundary-Layer Meteorology, 146, 81-102, 10.1007/s10546-012-9759-9, 2013.

Pankratz, D., and Bush, D.: Study of temporal and vertical ozone patterns at selected locations in California. Final report, AeroVironment, Inc., Monrovia, CA (United States), 1993.

Panofsky, H. A., and Dutton, J. A.: Atmospheric turbulence: models and methods for engineering aplications, 1984.

Park, J.-H., Goldstein, A. H., Timkovsky, J., Fares, S., Weber, R., Karlik, J., and Holzinger, R.: Active Atmosphere-Ecosystem Exchange of the Vast Majority of Detected Volatile Organic Compounds, Science, 341, 643-647, 10.1126/science.1235053, 2013.

Pattey, E., Strachan, I., Desjardins, R., and Massheder, J.: Measuring nighttime CO2 flux over terrestrial ecosystems using eddy covariance and nocturnal boundary layer methods, Agr Forest Meteorol, 113, 145-158, 2002.

Patton, E.G., Sullivan, P.P. and C.H. Moeng, 2005: The Influence of Idealized Heterogeneity on Wet and Dry Planetary Boundary Layers Coupled to the Land Surface. J. Atmos. Sci., 62, 2078–2097.

Peischl, J., Ryerson, T. B., Holloway, J. S., Trainer, M., Andrews, A. E., Atlas, E. L., Blake, D. R., Daube, B. C., Dlugokencky, E. J., Fischer, M. L., Goldstein, A. H., Guha, A., Karl, T., Kofler, J., Kosciuch, E., Misztal, P. K., Perring, A. E., Pollack, I. B., Santoni, G. W., Schwarz, J. P., Spackman, J. R., Wofsy, S. C., and Parrish, D. D.: Airborne observations of methane emissions from rice cultivation in the Sacramento Valley of California, Journal of Geophysical Research: Atmospheres, 117, D00V25, 10.1029/2012jd017994, 2012.

Petersen, A. C., and A. M. Holtslag, 1999: A First-Order Closure for Covariances and Fluxes of Reactive Species in the Convective Boundary Layer. J. Appl. Meteor., 38, 1758–1776.

Pierce, T., Geron, C., Bender, L., Dennis, R., Tonnesen, G., and Guenther, A.: Influence of increased isoprene emissions on regional ozone modeling, J Geophys Res-Atmos, 103, 25611-25629, Doi 10.1029/98jd01804, 1998.

Rasmussen, R. A.: Isoprene: Identified as a forest-type emission to the atmosphere, Environmental Science & Technology, 4, 667-671, 1970.

Reid, J. S., Jonsson, H. H., Smith, M. H., and Smirnov, A.: Evolution of the vertical profile and flux of large sea-salt particles in a coastal zone, J Geophys Res-Atmos, 106, 12039-12053, Doi 10.1029/2000jd900848, 2001.

Reissell, A., and Arey, J.: Biogenic volatile organic compounds at Azusa and elevated sites during the 1997 Southern California Ozone Study, Journal of Geophysical Research: Atmospheres (1984–2012), 106, 1607-1621, 2001.

Rinne, H., Guenther, A., Greenberg, J., and Harley, P.: Isoprene and monoterpene fluxes measured above Amazonian rainforest and their dependence on light and temperature, Atmospheric Environment, 36, 2421-2426, 2002.

Rowe, M. D., Fairall, C. W., and Perlinger, J. A.: Chemical sensor resolution requirements for near-surface measurements of turbulent fluxes, Atmos. Chem. Phys., 11, 5263-5275, 10.5194/acp-11-5263-2011, 2011.

Schade, G.W. and Goldstein, A.H.: Fluxes of oxygenated volatile organic compounds from a ponderosa pine plantation, J. Geophys. Res. 106 (D3), 3111, 2001.

Schade, G.W., Goldstein, A.H. and Lamanna, M.S.: Are monoterpene emissions influenced by humidity? Geophys. Res. Lett. 26: 2187-2190, 1999.

Schade, G.W., Goldstein, A.H., Gray, D.W. and Lerdau, M.T.: Canopy and leaf level 2-methyl-3-butene-2-ol fluxes from a ponderosa pine plantation. Atmos. Environ. 34: 3535-3544, 2000.

Schumann, U., 1989: Large-eddy simulation of turbulent diffusion with chemical reactions in the convective boundary layer. Atmos. Environ., 23, 1713–1727, Doi:10.1016/0004-6981(89)90056-5.

Scott, K. I., and Benjamin, M. T.: Development of a biogenic volatile organic compounds emission inventory for the SCOS97-NARSTO domain, Atmospheric Environment, 37, S39-S49, Doi 10.1016/S1352-2310(03)00381-9, 2003.

Serca, D., Guenther, A., Klinger, L., Vierling, L., Harley, P., Druilhet, A., Greenberg, J., Baker, B., Baugh, W., and BOUKA-BIONA, C.: EXPRESSO flux measurements at upland and lowland Congo tropical forest site, Tellus B, 53, 220-234, 2001.

Sharkey, T. D., Singsaas, E. L., Lerdau, M. T., and Geron, C. D.: Weather effects on isoprene emission capacity and applications in emissions algorithms, Ecological Applications, 9, 1132-1137, 1999.

Spirig, C., Guenther, A., Greenberg, J.P., Calanca, P., and V. Tarveinen, 2004: Tethered balloon measurements of biogenic volatile organic compounds at a Boreal forest site. Atmos. Chem. Phys., 4, 215-229.

Steiner, A., Pressley, S., Botros, A., Jones, E., Chung, S., and Edburg, S.: Analysis of coherent structures and atmosphere-canopy coupling strength during the CABINEX field campaign, Atmos Chem Phys, 11, 11921-11936, 2011.

Stoy, P. C., Richardson, A. D., Baldocchi, D. D., Katul, G. G., Stanovick, J., Mahecha, M. D., Reichstein, M., Detto, M., Law, B. E., Wohlfahrt, G., Arriga, N., Campos, J., McCaughey, J. H., Montagnani, L., Paw U, K. T., Sevanto, S., and Williams, M.: Biosphere-atmosphere exchange of CO2 in relation to climate: a cross-biome analysis across multiple time scales, Biogeosciences, 6, 2297-2312, 10.5194/bg-6-2297-2009, 2009.

Thomas, C., and Foken, T.: Detection of long-term coherent exchange over spruce forest using wavelet analysis, Theor Appl Climatol, 80, 91-104, 2005.

Thomas, C., and Foken, T.: Flux contribution of coherent structures and its implications for the exchange of energy and matter in a tall spruce canopy, Boundary-Layer Meteorology, 123, 317-337, 2007.

Torrence, C., and Compo, G. P.: A practical guide to wavelet analysis, B Am Meteorol Soc, 79, 61-78, 1998.

Troen, I., and L. Mahrt, 1986: A simple model of the atmospheric boundary layer sensitivity to surface evaporation. Boundary Layer Meteorology, 37, 129–148.

Vargas, R., Detto, M., Baldocchi, D. D., and Allen, M. F.: Multiscale analysis of temporal variability of soil CO2 production as influenced by weather and vegetation, Global Change Biol, 16, 1589-1605, 2010.

Vilà-Guerau de Arellano, J., Patton, N., Karl, T., van den Dries, K., Barth, M.C., and J.J. Orlando, 2011: The role of boundary layer dynamics on the diurnal evolution of isoprene and the hydroxyl radical over tropical forests, J. Geophys. Res., 116, D07304, doi: 10.1029/2010JD014857.

Vinuesa, J., and J. Vilà-Guerau de Arellano, 2003: Fluxes and (co-)variances of reacting scalars in the convective boundary layer. Tellus Series B: Chemical and Physical Meteorology, 55, 935 - 949.

Weil, J.C., and T.W. Horst, 1992: Footprint estimates for atmospheric flux measurements in the convective boundary layer, In: Precipitation Scavenging and Atmosphere-Surface Exchange, Vol. 2, 717-728, Editors: S.E. Schwartz and W.G.N. Slinn, Hemisphere Publishing.

Westberg, H., Lamb, B., Hafer, R., Hills, A., Shepson, P., and Vogel, C.: Measurement of isoprene fluxes at the PROPHET site, Journal of Geophysical Research: Atmospheres (1984–2012), 106, 24347-24358, 2001.

Williams, J., Crowley, J., Fischer, H., Harder, H., Martinez, M., Petäjä, T., Rinne, J., Bäck, J., Boy, M., Dal Maso, M., Hakala, J., Kajos, M., Keronen, P., Rantala, P., Aalto, J., Aaltonen, H., Paatero, J., Vesala, T., Hakola, H., Levula, J., Pohja, T., Herrmann, F., Auld, J., Mesarchaki, E., Song, W., Yassaa, N., Nölscher, A., Johnson, A.M., Custer, T., Sinha, V., Thieser, J., Pouvesle, N., Taraborrelli, D., Tang, M.J., Bozem, H., Hosaynali-Beygi, Z., Axinte, R., Oswald, R., Novelli, A., Kubistin, D., Hens, K., Javed, U., Trawny, K., Breitenberger, C., Hidalgo, P.J., Ebben, C.J., Geiger, F.M., Corrigan, A.L., Russell, L.M., Ouwersloot, H., Vilà-Guerau de Arellano, J.,

Ganzeveld, L., Vogel, A., Beck, M., Bayerle, A., Kampf, C.J., Bertelmann, M., Köllner, F., Hoffmann, T., Valverde, J., González, D., Riekkola, M.L., Kulmala, M. and J. Lelieveld, 2011: The summertime Boreal forest field measurement intensive (HUMPPA-COPEC-2010): an overview of meteorological and chemical influences. Atmos. Chem. Phys., 11, 10599–10618.

Winer, A.M., J. Arey, R. Atkinson, S.M. Aschmann, W.D. Long, C.L. Morrison, and D.M. Olszyk.: Emission rates of organics from vegetation in California's Central Valley, Atmos. Environ. Part A, 26: 2647–2659, 1992.

Wofsy, S., Fitzjarrald, D., McCaughey, H., and D.W. Joiner, 1997: Scaling up flux measurements for the boreal forest using aircraft-tower combinations. J. Geophys. Res., 102, 29125–29133, doi:10.1029/97JD00278.

Wyngaard, J. C., and Brost, R. A.: Top-down and bottom-up diffusion of a scalar in the convective boundary layer, J Atmos Sci, 41, 102-112, 1984.

Yver, C. E., Graven, H. D., Lucas, D. D., Cameron-Smith, P. J., Keeling, R. F., and Weiss, R. F.: Evaluating transport in the WRF model along the California coast, Atmos. Chem. Phys., 13, 1837-1852, doi:10.5194/acp-13-1837-2013, 2013.

Appendix A: Supplemental Figures

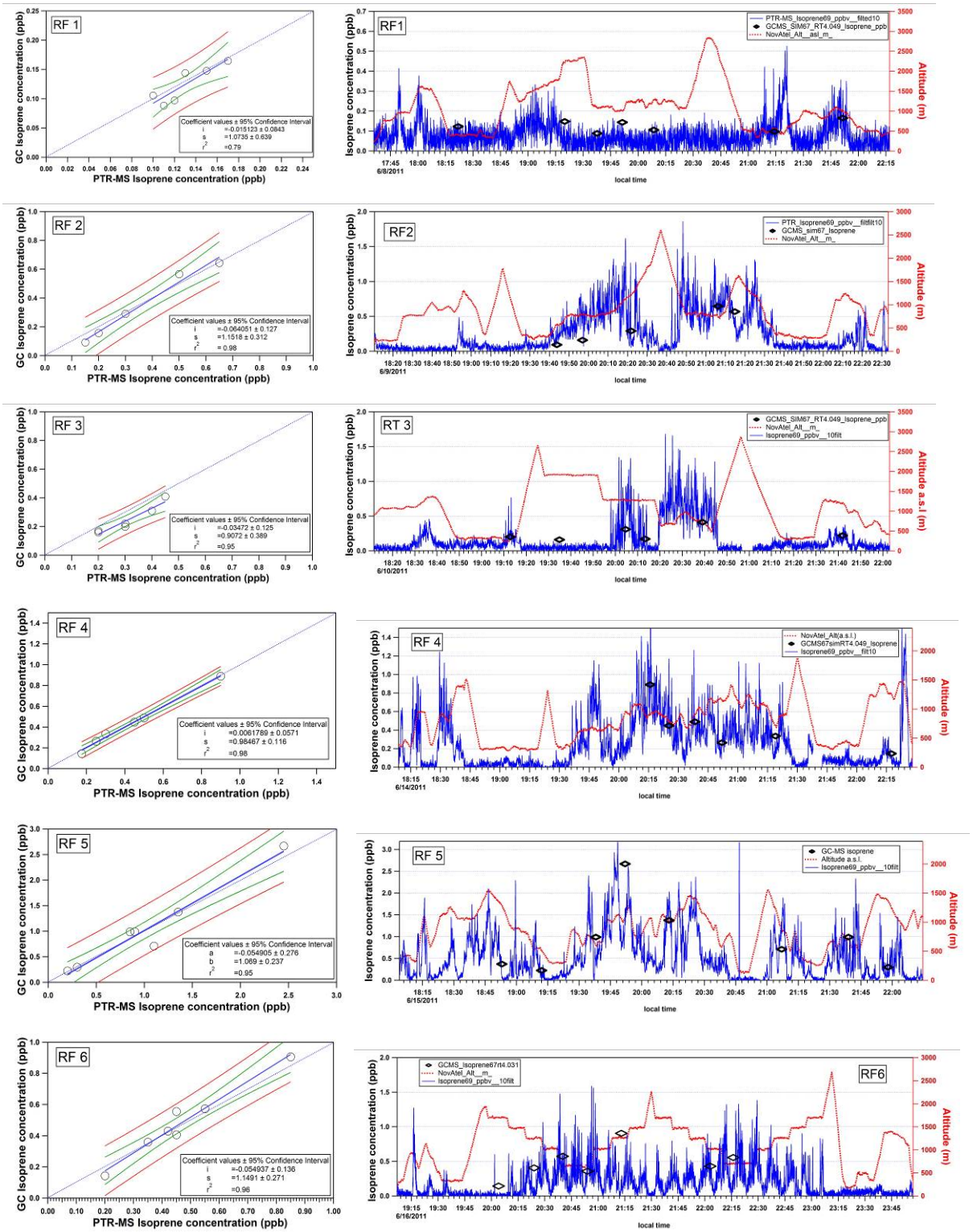

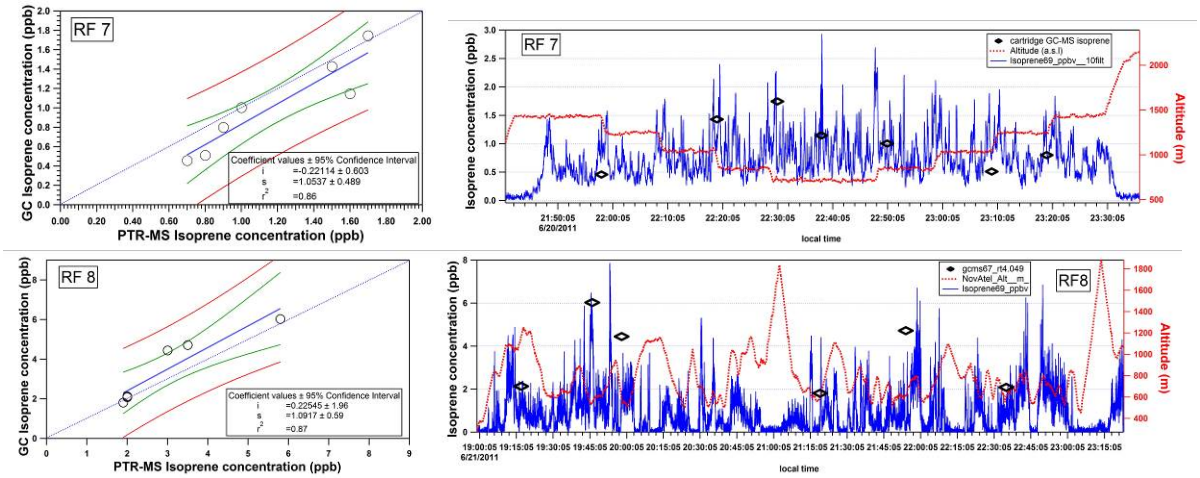

Figure B.1. Comparison of isoprene concentrations between PTR-MS and GC cartridges.

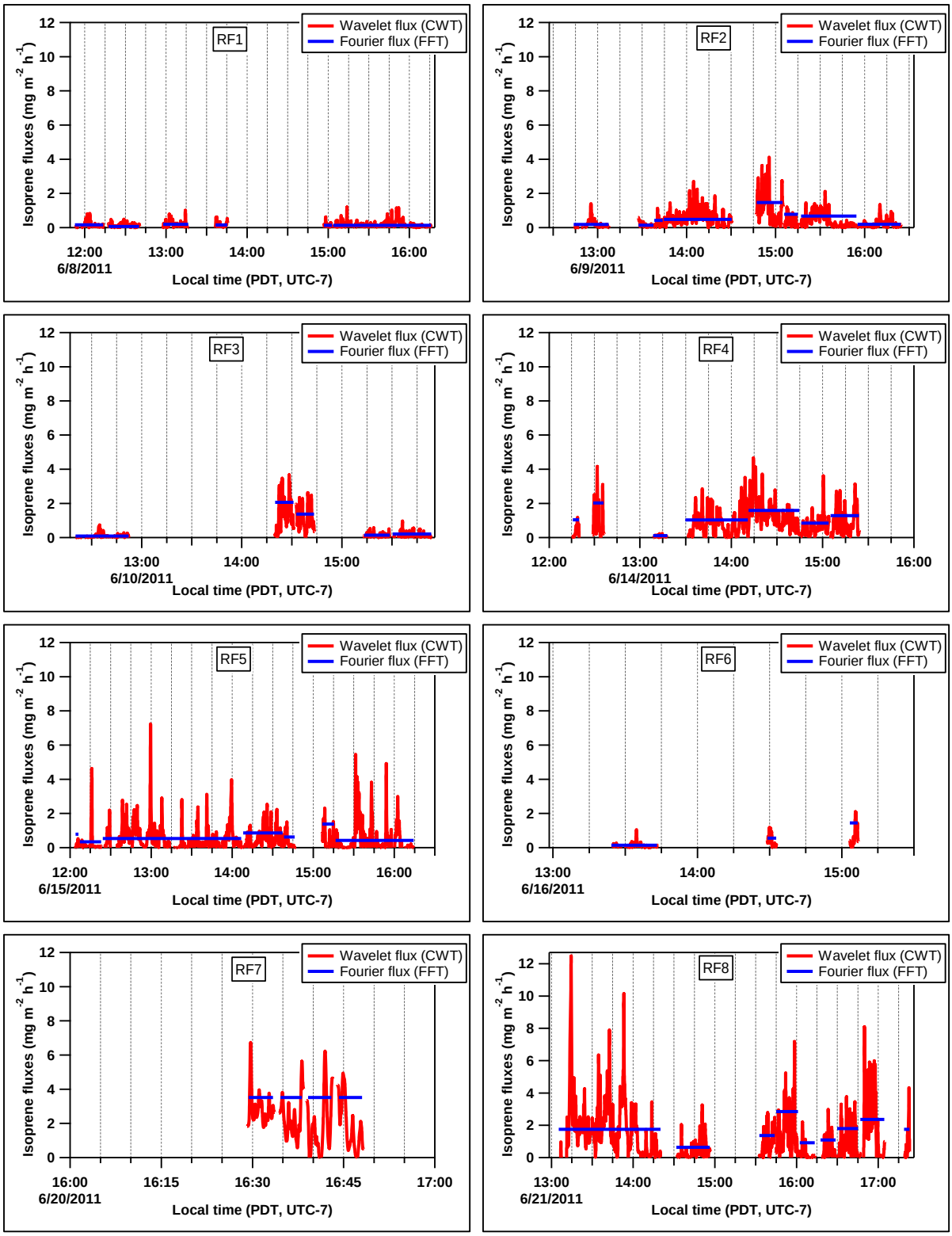

Figure B.3. Fluxes of isoprene on survey transects (only the lowest racetrack segments shown here) showing good agreement between FFT and CWT methods. Wavelet fluxes typically offered spatial resolution smaller than 1 km (here shown at 200 m resolution) before averaging to 2 km.

Appendix B: Abstracts of Associated Published Papers

1) Karl, T., Misztal, P. K., Jonsson, H. H., Shertz, S., Goldstein, A. H., and Guenther, A. B.: Airborne flux measurements of BVOCs above Californian oak forests: Experimental investigation of surface and entrainment fluxes, OH densities and Dahmköhler numbers, J Atmos Sci, 10.1175/jas-d-13-054.1, 2013. Available online: May 7, 2013

Abstract

Airborne flux measurements of isoprene were performed over the Californian oak belts surrounding Central Valley. We demonstrate for the first time (1) the feasibility of airborne eddy covariance measurements of reactive biogenic volatile organic compounds, (2) the effect of chemistry on the vertical transport of reactive species, such as isoprene, and (3) the applicability of wavelet analysis to estimate regional fluxes of biogenic volatile organic compounds. These flux measurements demonstrate that instrumentation operating at slower response times (e.g. 1-5s) can still be used to determine eddy covariance fluxes in the mixed layer above land, where typical length scales of 0.5-3 km were observed. Flux divergence of isoprene measured in the planetary boundary layer (PBL) is indicative of OH densities in the range of 4-7 x 10^6 molecules / cm^3, and allow extrapolation of airborne fluxes to the surface with Dahmköhler numbers (ratio between the mixing timescale to the chemical timescale) in the range of 0.3-0.9. Most of the isoprene is oxidized in the PBL with entrainment fluxes of about 10% compared to the corresponding surface fluxes. Entrainment velocities of 1-10 cm/s were measured. We present implications for parameterizing PBL schemes of reactive species in regional and global models.

[submitted 1/29/2014]

2) Misztal, P.K., T. Karl, R. Weber, H. H. Jonsson, A. B. Guenther, and A. H. Goldstein
Airborne flux measurements of Biogenic Volatile Organic Compounds over California

Biogenic Volatile Organic Compound (BVOC) fluxes were measured onboard the CIRPAS Twin Otter aircraft as part of the California Airborne BVOC Emission Research in Natural Ecosystem Transects (CABERNET) campaign during June 2011. The airborne virtual disjunct eddy covariance (AvDEC) approach used measurements from a PTR-MS and a wind radome probe to directly determine fluxes of isoprene, MVK+MAC, methanol, monoterpenes, and MBO over ~10,000-km of flight paths focusing on areas of California predicted to have the largest emissions of isoprene. The Fast Fourier Transform (FFT) approach was used to calculate fluxes over long transects of more than 15 km, most commonly between 50 and 150 km. The Continuous Wavelet Transformation (CWT) approach was used over the same transects to also calculate "instantaneous" fluxes with localization of both frequency and time independent of non-stationarities. Vertical flux divergence of isoprene is expected due to its relatively short lifetime and was measured directly using "racetrack" profiles at multiple altitudes. It was found to be linear and in the range 5% to 30% depending on the ratio of aircraft altitude to PBL height (z/zi). Fluxes were generally measured by flying consistently at 400 m ±50 m (a.g.l.) altitude, and extrapolated to the surface according to the determined flux divergence. The wavelet-derived surface fluxes of isoprene averaged to 2 km spatial resolution showed good correspondence to Basal Emission Factor (BEF) landcover datasets used to drive biogenic VOC (BVOC) emission models. The surface flux of isoprene was close to zero over Central Valley crops and desert shrublands, but was very high (up to 15 mg m-2 h¬-1) above oak woodlands, with clear dependence of emissions on temperature and oak density. Isoprene concentrations of up to 8 ppb were observed at aircraft height on the hottest days and over the dominant source regions.

While isoprene emissions from agricultural crop regions, shrublands, and coniferous forests were extremely low, high concentrations of methanol and monoterpenes were found above some of these regions.

These observations demonstrate the ability to measure fluxes from specific sources by eddy covariance from an aircraft, and suggest the utility of measurements using fast response chemical sensors to constrain emission inventories and map out source distributions for a much broader array of trace gases than was observed in this study.

This paper reports the first regional direct eddy covariance fluxes of isoprene. The emissions of VOCs measured from aircraft with 2 km spatial resolution can quantify the distribution of major sources providing the observations required for testing statewide emission inventories of these important trace gases. These measurements will be used in a future study to assess BVOC emission models and their driving variable datasets.

Appendix C: PTR-MS sensitivities and settings during CABERNET

Table C1. PTR-MS sensitivities and settings during CABERNET

	6/8/2011 RF1	6/9/2011 RF2	6/10/2011 RF3	6/14/2011 RF4	6/15/2011 RF5	6/16/2011 RF6	6/20/2011 RF7	6/21/2011 RF8
Normalized sensitivities (ncps ppbv^{-1})								
M79	19.816	22.124	19.622	21.913	20.788	18.842	24.852	23.559
M93	18.000	20.097	17.824	19.905	18.883	17.115	22.575	21.401
M105	14.108	13.588	10.719	14.059	13.779	11.146	17.496	15.551
M107	10.155	14.142	11.899	13.096	12.917	11.023	15.783	14.964
M113	10.570	15.216	12.546	13.665	13.224	11.669	16.476	15.435
M121			8.4953	11.468	12.061	9.5474	15.166	14.011
M147	2.4690	3.0201	2.5351	4.4609	4.5862	2.8743	7.4852	6.5489
M181	0.0533	0.1434	0.0836	0.0944	0.1333	0.0783	0.1722	0.1793
M41	1.5316	2.1000	1.5369	2.3115	2.4218	1.9551	2.4882	2.4709
M69	12.303	14.838	12.040	14.309	15.182	12.922	15.322	16.566
M81*	7.0856	7.5255	7.0029	7.8044	8.4026	7.4407	8.6862	9.1489
M137*	7.2781	7.0122	7.2037	6.9632	7.2211	6.9476	7.5266	8.0743
Isoprene	13.835	10.800	13.577	16.6202	17.603	14.877	17.810	19.037
MVK+MACR*	22.014	24.578	21.798	24.343	23.093	20.932	27.609	26.172
Monoterpenes*	14.364	14.538	14.207	14.768	15.624	14.388	16.213	17.223
M33*	15.916	15.916	15.916	15.916	15.916	15.916	15.916	15.916
M45*	25.017	25.017	25.017	25.017	25.017	25.017	25.017	25.017
M87 (MBO)*	3.6625	4.4172	3.5844	4.2596	4.5195	3.8467	4.5613	4.9316
Settings								
p_d (mb)	2.3	2.3	2.3	2.3	2.3	2.3	2.3	2.3
U_d	560	540	560	560	560	560	560	560
T (ºC)	50	50	50	50	50	50	50	50
H_2O flow (sccm)	6.4	6.4	6.4	6.4	6.4	6.4	6.4	6.4
M21 (cps)	19,123,000	24,000,000	20,900,000	20,000,000	18,000,000	19,200,000	19,100,000	19,100,000
SEM (V)	2335	2404	2435	2496	2510	2518	2626	2626

*derived from daily sensitivity curves and post-campaign calibrations

Appendix D: Data Set Description

Electronic datasets containing processed concentrations, fluxes and footprints will be enclosed with the final version of the report. In addition a dataset containing meteorology and other relevant parameters (coordinates, altitudes, etc.) will be provided.

These data have already been shared with the modeling team at CARB (Jeremy Avise and Klaus Scott).